PREPARATION AND CHARACTERIZATION OF CROSS-LINKED GRAPHENE OXIDE-BASED COMPOSITES FOR ADSORPTION-BASED APPLICATIONS

A Thesis Submitted to the College of

Graduate and Postdoctoral Studies

In Partial Fulfillment of the Requirements

For the Degree of Doctor of Philosophy

In the Department of Mechanical Engineering

University of Saskatchewan

Saskatoon

By

MINA SABZEVARI

PERMISSION TO USE

In presenting this thesis in partial fulfillment of the requirements for a Postgraduate degree from the University of Saskatchewan, I agree that the Libraries of this University may make it freely available for inspection. I further agree that permission for copying of this thesis in any manner, in whole or in part, for scholarly purposes may be granted by Professor Duncan Cree and Professor Lee Wilson who supervised my thesis work or, in their absence, by the Head of the Department or the Dean of the College in which my thesis work was done. It is understood that any copying or publication or use of this thesis or parts thereof for financial gain shall not be allowed without my written permission. It is also understood that due recognition shall be given to me and to the University of Saskatchewan in any scholarly use which may be made of any material in my thesis.

Requests for permission to copy or to make other uses of materials in this thesis/dissertation in whole or part should be addressed to:

Head of the Department of Mechanical Engineering
57 Campus Drive
University of Saskatchewan
Saskatoon, Saskatchewan S7N 5A9
Canada

OR

Dean
College of Graduate and Postdoctoral Studies
University of Saskatchewan
116 Thorvaldson Building, 110 Science Place
Saskatoon, Saskatchewan S7N 5C9
Canada

ABSTRACT

Increasing activities in industry have resulted in wastewater generation that contains contaminants. Therefore, several methodologies have been developed to manage wastewater pollutants in which adsorption technology using graphene-based materials may offer an approach for efficient wastewater remediation. This Ph.D. thesis describes the synthesis and characterization of graphene oxide (GO)-based composites for adsorption-based applications. In the present study, chitosan (CTS) and aluminum ions (Al^{3+}) as cross-linkers were utilized to enhance physical properties, mechanical performance and adsorption properties of GO by use of a solution-based method. The adsorption properties of samples were studied in solution and in the gas phase. Also, structural, morphological, physical, ion permeability, and mechanical properties of the GO and GO-based composites were studied using Fourier transform infrared spectroscopy (FTIR), Raman spectroscopy, X-ray diffraction (XRD), scanning electron microscopy (SEM), thermogravimetric analysis (TGA), ion permeability determination and dynamic mechanical analysis (DMA), respectively. Mechanical properties of GO upon addition of cross-linkers were analyzed statistically by means of analysis of variance (ANOVA). Interaction of CTS and Al^{3+} ions with functional groups of GO sheets were supported by changes in surface charge of the GO sheets and spectroscopy techniques. SEM results showed that cross-linking of GO changes its porosity and layered morphology. The TGA results revealed that the GO-based composites exhibited a gradual weight loss which started at higher temperatures as compared with GO due to cross-linking effects. In addition, it was found that the swelling degree of GO reduced and was demonstrated to be more stable in water upon cross-linking. The sorption properties of GO in solution and the gas phase were found to remarkably improve upon formation of a GO-based composite. The results of Ion permeability tests indicated that GO composites had variable ion transport characteristics according to the changes in inter-layer spacing of GO sheets upon cross-linking. Additionally, the use of cross-linkers led to an increase in the mechanical properties of GO-based composites as compared with pure GO. ANOVA revealed that GO-based composites have a statistically significant enhancement in mechanical properties over pure GO. Therefore, GO-based composites prepared via cross-linking GO sheets have great potential for use as an alternative adsorbent and/or membrane for adsorption-based applications.

ACKNOWLEDGMENTS

I would like to express my thanks to my supervisors, Prof. Duncan Cree and Prof. Lee Wilson, for all their support through my PhD study. I also would like to extend my appreciation to my advisory committee members: Prof. Anastasia Elias, Prof. Lope G. Tabil, Prof. Jerzy A. Szpunar, and Prof. Ike Oguocha for their constructive criticisms and useful suggestions. My special thanks go to Dr. Leila Dehabadi, Dr. Bahar Vafakish, Dr. Inimfon Udeotok, and Michael Danquah for their assistant in the experiments. I am also very thankful to Dr. Vivek Maheshwari, Department of Chemistry, and his student Hua Fan at University of Waterloo for permission to use their instrument for the diffusion tests. I am also grateful to Dr. Raghavan Jayaraman and his master student, Jardel Nobrega Dos Santos, Department of Mechanical Engineering, University of Manitoba for their technical assisting with DMA analysis.

Financial supports of this work by the University of Saskatchewan (U of S), the Government of Saskatchewan (GOS) and Natural Sciences and Engineering Research Council of Canada (NSERC) Discovery Grants (RGPIN 418729-2012 and RGPIN 2016-06197) are gratefully acknowledged. The Saskatchewan Structural Sciences Centre (SSSC) is also acknowledged for providing facilities to conduct part of the research.

DEDICATION

To my beloved parents and fiancé

My dear sisters Saba and Shagha

and Nesa

Thanks for your unconditional love

TABLE OF CONTENTS

PERMISSION TO USE i
ABSTRACT ii
ACKNOWLEDGMENTS iii
DEDICATION iv
TABLE OF CONTENTS v
LIST OF TABLES ix
LIST OF FIGURES xi
LIST OF ABBREVIATIONS AND SYMBOLS xv
CHAPTER 1: INTRODUCTION 1
1.1 Overview of chapter 1 1
1.2 Research motivations 1
1.3 Research objectives 3
1.4 Thesis overview 3
CHAPTER 2: LITERATURE REVIEW 5
2.1 Overview of chapter 2 5
2.2 Sorption (adsorption and absorption) 5
2.3 Adsorption in solution and gas media 6
2.4 Types of adsorption isotherms 6
2.5 Equilibrium adsorption isotherms 8
2.5.1 Langmuir isotherm 8
2.5.2 Freundlich isotherm 9
2.5.3 Sips isotherm 10
2.6 Kinetic isotherm adsorption models 10
2.6.1 Pseudo-first order (PFO) model 11
2.6.2 Pseudo-second order (PSO) model 11
2.7 SA and porosity analysis model 11
2.7.1 Brunauer-Emmett-Teller (BET) isotherm model 11
2.8 Graphene-based adsorbents 12

2.9 Graphene oxide (GO) 12
2.9.1 Synthetic approaches for preparation of GO 13
2.9.2 Structure of GO 14
2.9.3 Diffusion (permeation) characteristics of GO sheets 15
2.9.4 Properties and applications of GO 16
2.9.5 Mechanical properties of GO 17
2.9.6 Mechanical properties of GO-based composites 18
2.9.7 Environmental applications of GO materials and its composites 22
2.9.8 Gas uptake properties of GO materials and its composites 23
2.9.9 Mechanism of metal ions and cationic species adsorption 25
2.10 Modification of GO 29
2.10.1 Chemical cross-linking of GO sheets 29
2.10.2 Cross-linking with metal ions 32
2.10.3 Cross-linking with CTS 35
2.11 GO-based membranes 37
2.12 Summary 37
CHAPTER 3: MATERIALS AND EXPERIMENTAL PROCEDURE 39
3.1 Overview of chapter 3 39
3.2 Materials 39
3.3 Synthesis of GO powder 40
3.4 Preparation of GO-based cross-linked composite powders 40
3.5 Preparation of GO-based cross-linked composite membranes 42
3.6 Characterization techniques 44
3.6.1 Surface charge (ζ-Potential) measurement 44
3.6.2 Fourier transform-infrared (FTIR) spectroscopy 44
3.6.3 Scanning electron microscopy (SEM) 44
3.6.4 Raman spectroscopy 45
3.6.5 X-ray diffraction (XRD) 47
3.6.7 Thermogravimetric analysis (TGA) 48
3.6.8 Equilibrium swelling properties (solvent swelling properties) 48
3.7 Dye-based adsorption properties 49

3.7.1 Equilibrium dye uptake 49
3.7.2 Kinetic dye uptake 50
3.7.3 Regeneration study 51
3.8 Water vapour adsorption isotherms 51
3.9 Nitrogen adsorption-desorption isotherms 52
3.10 Ion permeability test properties 53
3.11 Mechanical properties 55
3.12 Statistical analysis 55
CHAPTER 4: RESULTS AND DISCUSSION 57
4.1 Overview of chapter 4 57
4.2 Characterization of GO and GO-based composites 57
4.2.1 Surface charge (ζ-Potential) measurement 57
4.2.2 Fourier transform-infrared (FTIR) spectroscopy 59
4.2.3 Microstructure 61
4.2.4 Raman spectroscopy 63
4.2.5 X-ray diffraction (XRD) 64
4.2.6 Thermogravimetric analysis (TGA) 65
4.2.7 Equilibrium swelling properties (solvent swelling properties) 67
4.2.8 Equilibrium dye uptake 68
4.2.9 Kinetics of dye uptake 71
4.2.10 Regeneration study 73
4.2.11 Water vapour adsorption isotherms 73
4.2.12 Nitrogen adsorption-desorption isotherms 76
4.2.13 Membrane ion permeation properties 78
4.2.14 Mechanical properties 81
4.2.15 Statistical analysis 85
CHAPTER 5: CONCLUSIONS, FUTURE WORK AND CONTRIBUTIONS 87
5.1 Conclusions 87
5.2 Recommendations for future work 89
5.3 Contributions to original knowledge 90
5.3.1 Synthesis of GO-based composites 94

5.3.2 Characterization of GO-based composites membranes 95
REFERENCES 96
APPENDIX A 125
APPENDIX B 135

LIST OF TABLES

Table 2.1.	Summary of different metal ion removal studies using GO and GO-based composites as adsorbent (at pH ~ 6-7) ……..	26
Table 2.2.	Summary of various organic compounds removal studies using GO and GO-based composites as adsorbent (at pH ~ 6-7) …….	28
Table 2.3.	Fabricated GO-CTS composites with various applications…….…...…	36
Table 3.1.	The prepared samples with different cross-linker types and concentrations	42
Table 4.1.	Water swelling properties of graphite, GO and GO-based composites ……	68
Table 4.2.	The adsorption isotherm parameters obtained from Sips model for GO and GO-based composites with MB ……	71
Table 4.3.	Kinetic parameters for GO-based composites with MB obtained using the PSO model …….……..…..	73
Table 4.4.	Adsorption isotherm parameters for GO and GO-based composites with water vapour.……	76
Table 4.5.	Adsorption isotherm parameters for GO and GO-based composites with nitrogen (equation 2.6) ……..……	78
Table 4.6.	Membranes prepared for permeation test .……	79
Table 4.7.	Literature comparison of mechanical properties of GO produced in different forms ……...…...	82
Table 4.8.	ANOVA results at a 0.05 level of significance for tensile strength, tensile modulus, elongation at break and fracture strength based on the addition of CTS in a GO-based composite.……	86

Table 4.9. ANOVA results at a 0.05 level of significance for tensile strength, tensile modulus, elongation at break and fracture strength based on the addition of Al^{3+} in a GO-based composite …..…… 86

Table 5.1. Current membranes characteristic use for wastewater treatment…….. 91

Table 5.2. Literature comparison of the mechanical properties of available membranes and GO-based composite membranes. 92

LIST OF FIGURES

Figure 2.1.	(a) Volume-driven absorption vs. (b) surface-driven adsorption processes	5
Figure 2.2.	Sorption isotherm types based on IUPAC classification [19] ……..……	8
Figure 2.3.	Langmuir (a) and Freundlich (b) isotherms [21] ……..…	10
Figure 2.4.	Synthesis methods for preparation of GO using graphite and oxidation agents	14
Figure 2.5.	Proposed molecular structure for a fragment of GO [46] ……...…..	15
Figure 2.6.	Schematic image of possible permeation through GO sheets where L denotes the size of a crystal in a GO sheet, and d represents spacing between GO layers [60] ...…….……..…….	16
Figure 2.7.	Various potential applications of GO and GO-based materials [75] ……..…..	17
Figure 2.8.	Molecular structure of the glucosamine units of CTS, where n denotes the degree of polymerization [20]……..…	19
Figure 2.9.	Proposed GOF material formation from connected GO layers [116] …..…....	24
Figure 2.10.	Adsorption mechanism of metal cations on surface of GO [114] ……..…..	26
Figure 2.11.	Structure of (a) GO and (b) cross-linked GO membranes (GO-EDA, GO-BDA, and GO-PPD) with diamine monomers [180] ……..	31
Figure 2.12.	Proposed model for interactions between GO sheets and metal cations [8] …	33
Figure 3.1.	Synthesis process for preparation of GO ……	41
Figure 3.2.	Experimental procedure for GO-based composite preparation ……..	43
Figure 3.3.	Fabrication of GO-based composite membranes ……..……..	43
Figure 3.4.	Bio-Rad FTS-40 IR spectrophotometer used in this work …….	45
Figure 3.5.	The Jeol JSM-6010LV SEM instrument used in this work ……	46

Figure 3.6. Renishaw model 2000 Raman spectrometer used in this research ……. 46

Figure 3.7. PANalytical Empyrean powder XRD instrument used in this work …….. 47

Figure 3.8. TA Instruments Q50000IR TGA instrument used in this work …….. 48

Figure 3.9. Chemical structure of methylene blue (MB) [220] …….. 49

Figure 3.10. IGA-002 system used for water vapour adsorption analysis …….. 52

Figure 3.11. Micromeritics ASAP 2020 instrument used for nitrogen adsorption analysis 53

Figure 3.12. (a) Permeability test set up and (b) conductivity determination used for the study of the membrane materials ……..……. 54

Figure 3.13. Schematic view of the permeation cell used in this work ……... 54

Figure 3.14. DMA analyzer used in this work …… 56

Figure 4.1. The ζ-potential for GO at variable pH …… 58

Figure 4.2. The ζ-potential for GO and GO-cross-linked composites at ambient pH ……. 59

Figure 4.3. FTIR spectra obtained for (a) graphite, (b) GO, (c) CTS, (d) GO-CTS and (e) GO-AL cross-linked composites ……..…….. 60

Figure 4.4. Proposed structural changes after oxidation of graphite and after cross-linking of GO with two types of cross-linkers (Al^{3+} ions and CTS) to form GO-based composite materials ……..…. 61

Figure 4.5. SEM micrographs of (a) as-received graphite and (b) synthesized GO …….. 62

Figure 4.6. SEM micrographs of GO-based materials: (a) GO-CTS and (b) GO-AL ….. 62

Figure 4.7. SEM micrographs of cross-sections of GO and the GO-based composites membranes: (a) GO (b) GO-CTS and (c) GO-AL ……..….. 63

Figure 4.8. Raman spectra obtained for (a) graphite, (b) GO, (c) GO-CTS and (d) GO-AL cross-linked composites ……... 64

Figure 4.9. XRD pattern of (a) graphite, (b) GO, (c) GO-CTS and (d) GO-AL cross-linked composites ……..….. 65

Figure 4.10. TGA curves obtained for (a) GO, (b) GO-CTS and (c) GO-AL cross-linked composites from room temperature up to 500 °C …….……... 66

Figure 4.11. Swelling test of GO and GO-based composite materials in water. a) After 24 h, and b) 72 h……..….. 68

Figure 4.12. Equilibrium isotherm sorption results obtained for MB with GO and GO-based composites, where the solid lines correspond to the best-fit results obtained using the Sips model …….…….. 70

Figure 4.13. Decolorization of MB before and after the sorption process with GO-CTS composite …….. 70

Figure 4.14. Kinetic uptake profile obtained for MB by the GO-based composites, where the fitted lines correspond to the PSO model (see equation 2.5) …… 72

Figure 4.15. Adsorption−desorption cycles obtained for GO and GO-based composites (GO-CTS and GO-AL) for MB systems ……. 73

Figure 4.16. Water vapour adsorption isotherms obtained for (a) GO and GO-based composites: (b) GO-CTS, (c) GO-AL ……..... 75

Figure 4.17. Nitrogen adsorption isotherms obtained for (a) GO and GO-based composites: (b) GO-CTS, (c) GO-AL ……...…….. 77

Figure 4.18. Stability tests of GO and GO-based composites …… 79

Figure 4.19. Permeation of (a) NaCl solution and (b) $CaCl_2$ solution through GO and GO-based composites at room temperature ……..…… 81

Figure 4.20. Tensile stress versus strain curves: (a) unmodified synthetic precursors (GO and CTS) and, (b) GO-based composite membranes (GO-AL and GO-CTS) 84

Figure 4.21. a) Tensile strength and b) tensile modulus for GO and GO-based composites 84

Figure 4.22. A conceptual structural model for GO-based composites upon cross-linking to account for changes in tensile strength. CL indicates cross-linker (CTS or Al^{3+} ions) and F is the force or load applied to the composite membrane……. 85

LIST OF ABBREVIATIONS AND SYMBOLS

3D	Three dimensional
AA	Acetic acid
AC	Activated carbon
AFM	Atomic force microscope
Al	Aluminum
Al^{3+}	Aluminum ion
ANOVA	Analysis of variance
B	Boron (element)
BB	Brilliant blue
BDA	Butylenediamine
BET	Brunauer-Emmett-Teller
BF	Basic fuchsin
BSA	Bovine serum albumin
BSE	Backscattered electrons
CA	Calcium alginate
ca.	Approximately
Ca^{2+}	Calcium (II) cation
CH_4	Methane
CO_2	Carbon dioxide
CTS	Chitosan
Cu^{2+}	Copper (II) cation

DI	Deionized
DMA	Dynamic mechanical analyzer
DMF	N,N-dimethylformamide
EDA	Ethylenediamine
EPD	Electrophoretic deposition
FL	Fluoranthene
FTIR	Fourier-transform infrared spectroscopy
GLA	Glutaraldehyde
GO	Graphene oxide
GOF	Graphene oxide framework
GPU- ONCE	Gas permeation unit
h	Hour (s)
H	High
H_2O	Water
H_2O_2	Hydrogen peroxide
H_2SO_4	Sulfuric acid
IGA	Intelligent gravimetric analyzer
IUPAC	International Union of Pure and Applied Chemistry
$KMnO_4$	Potassium permanganate
L	Low
LbL	Layer-by-layer
MB	Methylene blue
MCDFT	Monte Carlo density functional theory

Mg^{2+}	Magnesium cation
MV	Methyl violet
N_2	Nitrogen
$NaNO_3$	Sodium nitrite
NR	Neutral red
O_2	Oxygen
OTR	Oxygen transmission rate
PAH	Poly allylamine hydrochloride
PAI	Polyamideimide
PD	Poly-dopamine
PEI	Polyethyleneimine
PES	Polyethersulfone
PFO	Pseudo first order
PI	Polyimide
PPD	*p*-phenylenediamine
PS	Pore size
PSO	Pseudo second order
PV	Pore volume
PZC	Point of zero charge
rGO	Reduced GO
SA	Surface area
SE	Secondary electrons
SEM	Scanning electron microscopy

SSSC	Saskatchewan structural sciences center
S_w	Water swelling
TA	Texture analyzer
TGA	Thermogravimetric analysis
TMC	1,3,5-Benzenetricarbonyl trichloride
W_d	Dry weight
W_s	Weight of the swollen samples
XRD	X-ray diffraction

CHAPTER 1: INTRODUCTION

1.1 Overview of chapter 1

In this chapter, the motivations for this research and the importance of improving the adsorption properties and mechanical performance of graphene oxide (GO)-based composite materials are discussed. The main goal of this Ph.D. study and specific objectives are also presented in this chapter.

1.2 Research motivations

The growth in generating toxic pollutants and various contaminants in bodies of water originating from industrial and agricultural activities have motivated researchers to adopt more efficient materials and technologies for water treatment in order to remove dissolved contaminants from freshwater.

Efforts from scientists to control water dissolved contaminants has led to the development of various technologies including filtration, electrolysis, chemical precipitation, adsorption and membrane filtration technologies [1]. Among the available techniques mentioned, adsorption and membrane filtration methods are known to be more efficient compared to other methods due to their simplicity in design, operation and wide applicability. However, the efficiency of these methods depends on the nature of the adsorbent and membrane material employed. Among the conventional types of available adsorbents and membranes for water treatment, graphene and its derivative materials have attracted much attention.

More recently, diverse applications of graphene have motivated scientists to develop other related graphene-based materials such as GO. Both graphene and GO, in the form of adsorbents and membranes have emerged as the next generation materials for treatment of water dissolved contaminants [2]. GO is an oxidized form of graphene produced by a chemical oxidation method and is an important precursor to obtain bulk scale graphene [3]. GO is functionalized with oxygen-containing groups and has been found to have a large surface area (SA) and high solubility in many solvents and matrices. These properties make GO a potential candidate for applications in water

treatment as an adsorbent and a membrane material [4,5]. Several studies have shown the feasibility of using GO to remove different compounds from contaminated water, such as heavy metal ions and charged species (anionic and cationic dyes) [4,6].

Although GO has been has widely studied and successfully tested for a number of applications, it was found that existence of functional groups on the surface and edges of GO sheets result in electrostatic separation when submerged in water [7]. This results in the loss of structural stability and mechanical performance which limits their applications in water-based media.

In 2008, the novel work done by Park et al. [8] indicated that modification of GO sheets with a metal ion as a cross-linking agent led to significant enhancement of the mechanical properties (e.g., tensile strength) of GO sheets. In 2015, Yeh et al. [7] similarly discovered aluminum ions (Al^{3+}) found in a nanopore disk used for vacuum filtration of GO solutions, were able to stabilize GO sheets in water. This allowed the resulting material to be tested in solution-based applications. Besides metal ions, chitosan (CTS) was found to cross-link effectively with the functional groups of GO to improve its mechanical properties and stability in aqueous media [9,10]. In a recent study conducted in 2017, Turgut et al. [11] found the SA of GO sheets was remarkably enhanced through cross-linking with aluminum ions (Al^{3+}) for flame retardant applications. However, no further investigation on adsorption properties of modified GO with Al^{3+} cations have been reported to date.

Oxygen-containing functional groups present on GO sheets allow them to bind with other species and to provide the opportunity of modification of GO to enhance its properties for specific applications. Preliminary results for GO-based composite materials confirmed cross-linking GO is a promising approach to improve its properties such as adsorption, mechanical performance, antimicrobial properties, etc. compared to pristine GO [8,12,13]. Although several studies have been carried out on the modification of GO, a cost-effective, facile and scalable technique is still required for large scale production of GO-based composite materials. This technique could overcome scalability and stability limitations of these materials and enhance their properties for use in practical applications.

1.3 Research objectives

The main aim of this Ph.D. study is to develop a facile technique for scalable production of GO-based composites suitable for sorption-based applications in solution and gas media. The hypothesis is to use CTS and/or multivalent metal ions (Al^{3+}) as cross-linking agents to yield GO-based composites (GO-CTS and GO-AL, respectively). Both composites were shown to possess greater SA and structural stability in solution with improved mechanical performance. Specifically, novel GO-AL composites were prepared and investigated for their adsorption properties in aqueous media and with gas phase systems.

The cross-linking approach enables GO to potentially be feasible for future commercial applications. Therefore, the specific objectives of this Ph.D. study are defined as follows:

- To synthesize GO-based composite materials by individually cross-linking GO with CTS and GO with Al^{3+} ions for evaluation of adsorption properties.
- To determine the effect of cross-linking GO by obtaining the physiochemical properties of GO-based composite materials.
- To evaluate adsorption properties of fabricated materials in aqueous solution and with gas phase species.
- To evaluate mechanical properties and ion permeability performance of GO and GO-based composite membranes.

1.4 Thesis overview

In this thesis, preparation and characterization of GO-based cross-linked composites for adsorption-based applications in solution and gas media are discussed. The thesis consists of five chapters as listed below.

In chapter 1 a brief introduction of the research project is provided along with research motivation, objectives, and organization of the thesis.

Chapter 2 presents a comprehensive literature review on the principles of sorption and graphene-based materials, followed by their properties and applications in environmental protection applications. Improvements in the properties of GO-based composite materials using the cross-

linking method is reviewed. Afterwards, the focus is on the relevant research associated with two main types of cross-linkers (e.g., CTS and metal ions).

In chapter 3 the materials and experimental process to synthesize the GO-based composites are introduced. Also, the characterization techniques applied in this research are explained including spectroscopy techniques, thermal gravimetric analysis, swelling tests, adsorption tests in solution and gas media, ion permeability tests and mechanical tests.

In chapter 4 the obtained results from tests conducted in the previous chapter are presented and discussed in detail.

Finally, conclusions drawn from the analysis of the tests results, suggestions for future work and major contributions are summarized in chapter 5.

CHAPTER 2: LITERATURE REVIEW

2.1 Overview of chapter 2

In this chapter, the principle of sorption in solution and gas phase is firstly introduced. Secondly, the structure, properties and applications of graphene oxide (GO) as a potential adsorbent in liquid and gas phase media is presented. An overview of previous research related to novel GO-based composite materials with enhanced physiochemical, adsorption and mechanical properties for a variety of applications is presented. Additionally, important knowledge gaps are presented from the literature that provide support for the thesis research objectives are highlighted in this chapter.

2.2 Sorption (adsorption and absorption)

The term sorption is generally defined as the processes in which a substance (sorbate) is adsorbed to and/or absorbed within a substrate [14], as illustrated in Figure 2.1. This term is a combination of two combined phenomena, absorption and adsorption. In the adsorption process, the adsorbate species are bound onto the surface of the adsorbent, while absorption occurs within the inner phase of the sorbent [15]. In other words, adsorption is considered a surface-driven phenomenon while absorption is a volume-driven phenomenon. Generally, increasing the adsorption capacity involves increasing exposed SA of adsorbent to the adsorbate species [15].

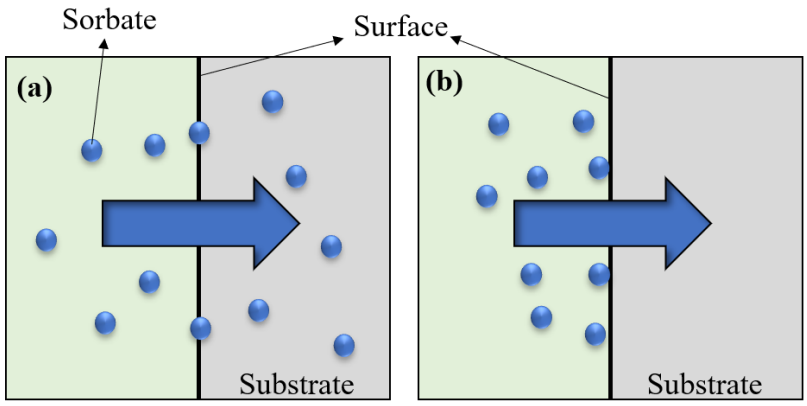

Figure 2.1. (a) Volume-driven absorption vs. (b) surface-driven adsorption processes.

Adsorption is considered as one of the most attractive and facile techniques for various applications including liquids purification, pollution control and gas separation [14]. This is mainly due to the simplicity of the equipment required for this method and its low energy consumption requirements [16]. Commercial adsorbents mostly have large SA and are either highly porous or comprise fine pores of materials such as activated carbons, zeolites, aluminophosphates silica gel desiccants, catalysts, clays, ceramics and membranes [16]. Nowadays, a great interest is being shown in the development of novel materials with well-defined pore structures, sizes and shapes.

2.3 Adsorption in solution and gas media

The liquid-phase adsorption process involves occupancy of the adsorbent sorption sites by either solvent or solute species [16]. The adsorption process is accompanied by a decrease of the adsorbate concentration in the bulk solution in accordance with localization at the adsorbent interface when it comes into contact with the adsorbate. The adsorption process can be monitored by measuring the concentration of species in the bulk or at the adsorbent interface. On the other hand, in solid-gas adsorption, the gas species are adsorbed to vacant sorption sites on the adsorbent surface through non-covalent bonding in the case of physisorption and chemical bonding in the case of chemisorption. Therefore, the adsorbent sorption capacity can be evaluated as the amount of adsorbate species bonded to the adsorbent surface [17].

2.4 Types of adsorption isotherms

The adsorption results can be studied by measurement of adsorption isotherms. An adsorption isotherm provides information on the amount of sorbate a material that can be adsorbed for a given set of pressure variables. Moreover, the adsorption isotherm shape can provide an estimation of pore size (PS) on the adsorbent's surface. The adsorption isotherms are well-stablished according to International Union of Pure and Applied Chemistry (IUPAC) classification system [18]. Based on this classification, the adsorption isotherms are categorized into six types as shown in Figure 2.2. The PS is defined as the internal pore width for slit-like pores and pore diameter in the case of cylindrical and spherical pores as follows:

1. Micropore possess PS below 2 nm.

2. Mesopores possess PS between 2 to 50 nm.

3. Macropores possess PS larger than 50 nm [19].

The following discussion summarizes the adsorption isotherm categories in more detail.

Type I: This type of isotherm represents a gradual increase in adsorption followed by reaching a maximum in the sorption capacity as indicated by the plateau region for the amount adsorbed with increasing pressure. Adsorbents in this type are typically microporous with small cross-sectional areas.

Type II: This type of isotherm shows unlimited monolayer-multilayer adsorption where point B indicates completion of the monolayer coverage for the amount adsorbed and the start of multilayer adsorption with increasing pressure. This isotherm type is given by a macroporous adsorbent.

Type III: This isotherm type is governed by strong adsorbate-adsorbate interactions compared with adsorbate-adsorbent interactions. The isotherm in this type of adsorption is convex to the relative pressure axis.

Type IV: This type of isotherm suggests multilayer adsorption and shows a hysteresis loop as a result of occurrence of capillary condensation taking place in mesopores. In this isotherm, the low pressure region has similar adsorption mechanisms to the type II isotherm as mentioned above.

Type V: This isotherm type is similar to type III; however, the adsorbate-adsorbate interactions are weaker in this type. The hysteresis loop suggests desorption of the agglomerated particles as a collective group.

Type VI: This type of isotherm signifies a step-wise multilayer adsorption in which one sorption site is initially occupied and another sorption site will be filled afterward. This isotherm type suggests the required energy to adsorb at different sorption sites varies for favored occupation of sites to occur.

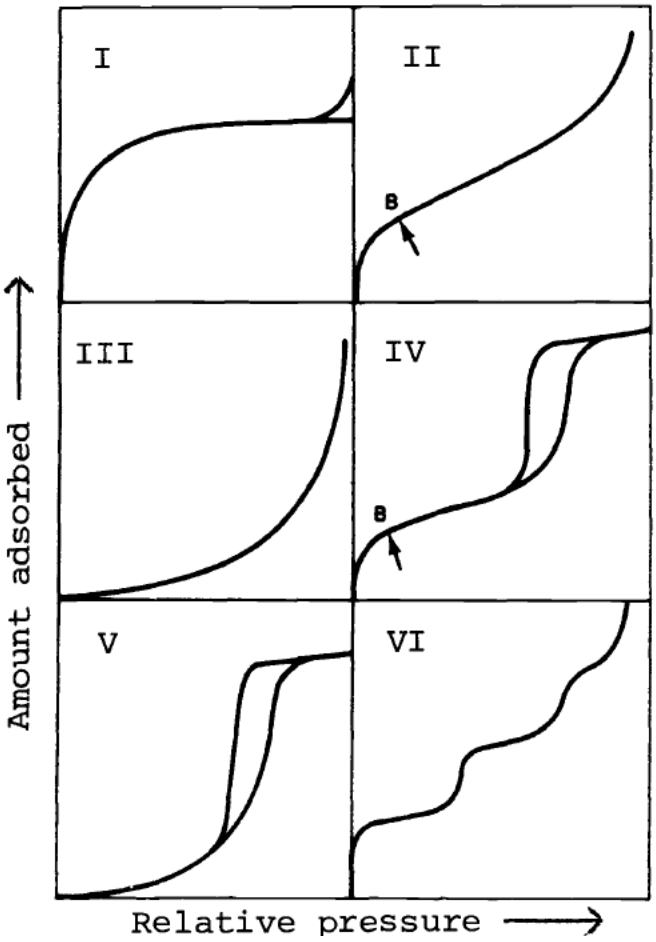

Figure 2.2. Sorption isotherm types based on IUPAC classification [19].

2.5 Equilibrium adsorption isotherms

Well-known isotherm models such as monolayer or multilayer isotherms that account for variable surface heterogeneity are generally used to correlate adsorption data in equilibrium and kinetic adsorption processes for characterization of sorbent materials. A brief overview of basic isotherm adsorption models is discussed below.

2.5.1 Langmuir isotherm

The Langmuir isotherm was initially established to explain the adsorption behavior of a specific gas (e.g., hydrogen) on a solid surface [20]. The use of this model involves three assumptions. Firstly, it is assumed that the adsorbent has a homogeneous surface. In other words, sorption sites available on the surface of the sorbent are equivalent (e.g., same adsorption energy). Secondly,

monolayer coverage is assumed for adsorption onto the adsorbent surface. Lastly, the adsorbate gas is assumed to be an ideal gas such that lateral interactions between the gas molecules within the monolayer can be neglected. Considering these assumptions, the model can be described in equation 2.1:

$$Q_e = Q_m \frac{K_L C_e}{1 + K_L C_e} \tag{2.1}$$

In this equation, Q_e (mmol/g or mg/g), is the amount of adsorbate species adsorbed per unit mass of the adsorbent at equilibrium, Q_m (mmol/g or mg/g) is the maximum adsorption capacity of the material at saturation, C_e (mmol/L) represents the equilibrium concentration of adsorbate and K_L (L/mmol) is defined as the Langmuir affinity constant for the adsorption process. The values of this constant, are related to the affinity of the adsorbate species to the adsorbent sites, where higher K_L values suggests a larger affinity of the adsorbate species to the adsorbent.

2.5.2 Freundlich isotherm

The Freundlich isotherm model is an alternative isotherm model to describe adsorption data. This model assumes that an infinite amount of adsorbate can be adsorbed by the adsorbent. This model can be described in equation 2.2:

$$Q_e = K_F C_e^{1/n} \tag{2.2}$$

In this equation, Q_e (mmol/g or mg/g), is the amount of adsorbate adsorbed per unit mass of the adsorbent at equilibrium, and C_e (mmol/L) represents the equilibrium concentration of adsorbate. K_F (L/g) represents the Freundlich constant attributed to the adsorption affinity, and 1/n is defined as an isotherm constant which is a measure of adsorption intensity. Generally, $0.1 < 1/n < 1.0$ designates a favorable adsorption, while; $1/n > 1$ specifies unfavorable adsorption. Figure 2.3 shows the first two models.

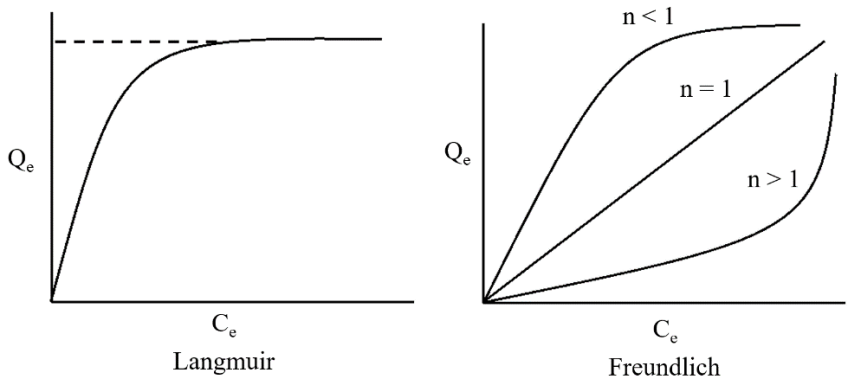

(a) (b)

Figure 2.3. Langmuir (a) and Freundlich (b) isotherms [21].

2.5.3 Sips isotherm

The Sips model shares features of both the Langmuir and Freundlich models. The Sips model can be described by equation 2.3.

$$Q_e = Q_m \frac{K_s C_e^{n_s}}{1 + K_s C_e^{n_s}} \quad (2.3)$$

In equation (2.3), Q_e (mmol/g or mg/g), is the amount of adsorbate adsorbed per unit mass of the adsorbent at equilibrium, Q_m (mmol/g or mg/g) is the maximum adsorption capacity of the material at concentration conditions of saturation, C_e (mmol/L) represents the equilibrium concentration of adsorbate. K_s (L/g) represents the Sips isotherm constant attributed to the affinity between the adsorbent and the adsorbate. A large K_s value specifies accessible sites and favored adsorption. Also, n_s is the heterogeneity parameter of the sorbent surface. When the value of n_s is close to unity, the Sips model provides a convergent description of that by the Langmuir adsorption isotherm. On the other hand, as this value diverges from unity, the equation converges to the Freundlich isotherm model. Since Sips model has the ability of describing both Langmuir and Freundlich isotherm behavior, this model is valuable for the study of solution phase adsorption.

2.6 Kinetic isotherm adsorption models

Similar to the equilibrium models, the kinetic adsorption profiles can be well described using two general types of kinetic models; namely, the pseudo-first-order (PFO) and pseudo-second-order (PSO) discussed as follows.

2.6.1 Pseudo-first order (PFO) model

This model was introduced by Lagergren [22] as a first example describing the adsorption rate according to the adsorption capacity as given by equation 2.4.

$$Q_t = Q_e\,[1 - \exp(-k_1 t)] \tag{2.4}$$

In this equation, Q_t (mg/g) and Q_e (mg/g), represent the adsorption capacities at time t (min) and at equilibrium, respectively, while k_1 (1/min) is defined as the rate constant of the PFO model. This equation has been extensively used to investigate the kinetics of adsorption that describes various contaminants from aqueous solutions within the last decade [23].

2.6.2 Pseudo-second order (PSO) model

Another model to describe kinetic adsorption parameters is the PSO model which was initially developed to represent adsorption of divalent metals onto a solid sorbent [24]. The PSO model is described by equation 2.5.

$$Q_t = \frac{Q_e^2\ k_2\ t}{1 + Q_e^2\ k_2\ t} \tag{2.5}$$

In this equation, Q_t (mg/g) and Q_e (mg/g) represent the adsorption capacities at time t (min) and at equilibrium, respectively, where k_2 represents the rate constant according to the PSO adsorption model.

2.7 SA and porosity analysis model

2.7.1 Brunauer-Emmett-Teller (BET) isotherm model

BET theory was developed to describe gas molecules adsorption onto a surface. The concept of this model is an extension of the Langmuir model. While the Langmuir model describes monolayer adsorption, the BET model accounts for multilayer adsorption coverage. Multilayer adsorption occurs when several layers are stacked on top of each other due to adsorbate-adsorbate interactions [17]. Specifically, this model enables the adsorption process to be correlated to physical properties of a material including the SA, distribution of PS, and porosity. The use of the BET model requires three main assumptions, as follows: firstly, physical adsorption of gas molecules on the solid

surface. Secondly, no interaction between layers that are adsorbed on the surface, and thirdly, the utility of applying the Langmuir theory to monolayer systems. Therefore, using these assumptions, the BET equation can be described by equation 2.6.

$$\frac{n_a}{n_m} = \frac{C\ (^{P}/_{p_0})}{(1-^{P}/_{p_0})(1+(C-1)(\left(^{P}/_{p_0}\right))} \tag{2.6}$$

In this equation, n_a is the adsorbed gas quantity, n_m is the monolayer capacity, P and P_0 represent the equilibrium pressure and the saturation pressure of adsorbates, respectively and C is the BET constant associated with the affinity of the solid sorbent with the adsorbate (gas molecules). Moreover, use of the BET model affords determination of the SA ($S_{BET,\ Total}$) can be determined by the amount of gas that is adsorbed at a specific pressure according to equation 2.7.

$$S_{BET,Total} = \frac{n_m N_S A}{V} \tag{2.7}$$

Where n_m is the monolayer adsorption capacity, N_s is Avogadro's number, A represents adsorbate cross-sectional area, and V is the molecular volume of the adsorbate.

2.8 Graphene-based adsorbents

An effective adsorbent must have favourable properties such as high SA with accessible adsorption sites, porosity (e.g. PS distribution and pore volume (PV)), chemical and thermal stability, affinity to the targeted adsorbate (e.g. anionic or cationic), presence of suitable chemical functional groups on the surface of the adsorbent, and capability of regeneration in multiple adsorption cycles [1,25–27]. Graphene materials and its modified forms have potential as adsorbents in wastewater treatment applications for a wide range of contaminants in water, such as organic, inorganic, and heavy metal species [27–31]. Graphene is a two-dimensional form of carbon consisting of a single layer of carbon atoms arranged in a honeycomb crystalline structure. Graphene possesses high thermal conductivity, high SA, unique physiochemical, and mechanical properties [32].

2.9 Graphene oxide (GO)

Graphene is a single layer of graphite. A layer of sp^2-hybridized carbon atoms that are covalently bonded in a honeycomb lattice. Graphene is known as the thinnest, yet the strongest material with

numerous potential applications including structural composites, battery electrodes, supercapacitors, transport barriers and biomedical technologies [2]. The oxide derivative form of graphite is commonly known as graphite oxide which has a multi-layered structure and its product is brown in color. Exfoliation of graphite oxide in a solvent using sonication converts it into highly stabilized individual layers referred to as graphene oxide (GO) which appears as a dark yellow color [33]. GO is functionalized with a variety of reactive oxygen-containing functional groups that would not be stacked together due to repulsive forces between their sheets. This group confers various ways for chemical functionalization of GO. Oxidation of graphite results in increasing the interlayer spacing between GO sheets due to the introduction of the oxygen functional groups [4,29]. As well, this results in dispersibility of GO in various solvents. The remarkable adsorption properties reported for GO indicate its effective use as an adsorbent in numerous applications including the treatment of wastewater [34,35].

2.9.1 Synthetic approaches for preparation of GO

GO has been conventionally prepared through the Brodie, Staudenmaier, or Hummer's methods, or variations upon these methods [36–39]. Brodie was the first to investigate the structure of graphite and the preparation of GO in 1859 [36]. He proved that GO could be made through oxidizing a graphite structure when treated using oxidizing agents such as potassium perchlorate and concentrated mixtures of nitric acid. In 1898, Staudenmaier made a slight change in the oxidation process of GO by increasing the activity of the graphite mixture through heating. This modification resulted in an increase in the degree of GO oxidation [37]. In 1958, Hummers presented an alternative method to generate GO which has been used as the most convenient route for preparation of GO in a powdered form until the present [38]. A summary of the synthesis methods for the preparation of GO using graphite and oxidizing agents is presented in Figure 2.4. The preparation of GO involves chemical oxidation of graphite by strong oxidants such as concentrated sulfuric acid (H_2SO_4), sodium nitrate ($NaNO_3$) and potassium permanganate ($KMnO_4$) [40]. These oxidizing agents react with aromatic carbon of graphite to introduce oxygen functional groups to the basal planes and the edges of graphene sheets [41]. This consequently extends the inter-layer distance of graphite sheets from 0.34 nm to 0.80 nm [42,43]. Fabrication of GO via chemical oxidation is not only a technique for large-scale preparation of graphene, but also a significant feature for application of GO in many fields including composites, coatings, paints,

and energy storage [33]. This is due to the reactive functional groups responsible for binding with other species to form robust layered-structures [44]. These functional groups also make a significant contribution to remarkable adsorption properties of GO toward various adsorbates such as organic dyes and dissolved metals [45].

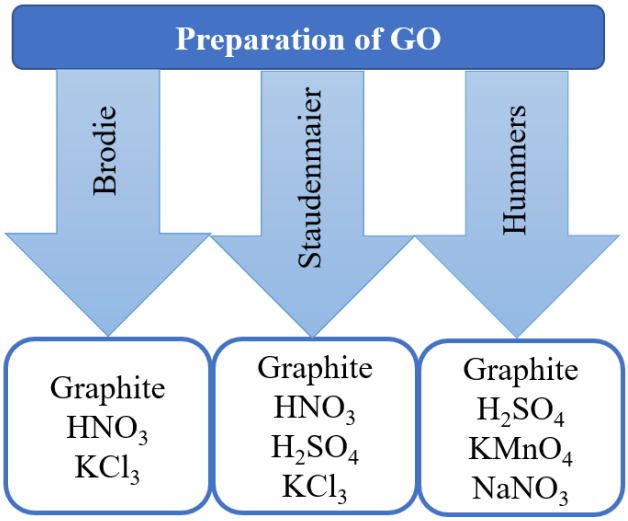

Figure 2.4. Synthesis methods for preparation of GO using graphite and oxidation agents.

2.9.2 Structure of GO

The structure of GO is proposed as graphene sheets including sp^2-hybridized-carbon atoms that are bonded with numerous oxygen atoms in the form of epoxy, hydroxyl, carboxyl (as shown in Figure 2.5) [46]. Furthermore, the distribution of oxygen functional groups was investigated and shown that epoxy and hydroxyl groups are present in the basal planes, while carboxyl groups are mainly at the edges [47]. The reactive functional groups presented on GO are responsible for its negative charge density [4,48]. Therefore, GO sheets can be dispersed homogeneously and are able to resist aggregation in solvents as a result of their strong electrostatic repulsion between sheets [49]. Furthermore, the negative surface charge of GO has a significant contribution to adsorption of metal ions, anion and cation species [4,6,50]. Parameters such as the type of graphite used to prepare GO, synthesis method and obtained degree of oxidation, as well as purification process can cause variations in the GO structures which influence the properties of GO [51]. A homogeneous suspension of GO can be prepared through exfoliating of GO powder in a suitable solvent with mechanical stirring or sonicating methods [52]. Although the thickness of a single

layer graphene sheet is about 0.3 nm, the thickness of GO sheets obtained by sonication or stirring is approximately 0.7–1.2 nm [53,54] as a result of the presence of functional groups on the GO sheet [41,42]. The functional groups present on GO can be precisely verified by techniques such as Fourier-transform infrared spectroscopy (FTIR) [55].

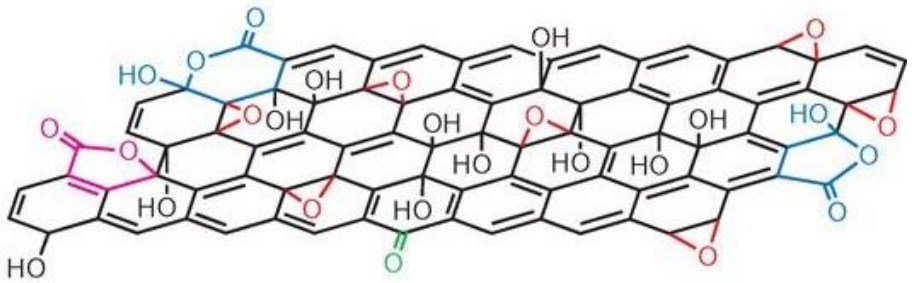

Figure 2.5. Proposed molecular structure for a fragment of GO [46].

2.9.3 Diffusion (permeation) characteristics of GO sheets

Compared to graphene, GO sheets possess vacant spaces (due to defects arising from the oxidation process) and large inter-layer distances between sheets due to existence of functional groups. This leads to the formation of nano-capillary networks between the GO sheets which enables permeation of different chemical species, depending on their relative size, through the GO sheets as shown in Figure 2.6 [56]. The permeability, selectivity and molecular sieving properties of GO sheets using various species in solvent media and gas media (CO_2, CH_4, H_2, and N_2) have been examined by several researchers through experimental and simulation methods [57–61]. GO sheets reveal fast permeation of water molecules and CO_2 species, while they can be impermeable to other species including helium [62–65]. For example, permeability of water molecules through GO laminates for separation and filtration techniques were investigated by Nair et al. [60], where they prepared GO suspensions according to the Hummer's method. The GO laminates were fabricated with a variable thickness in the range of 0.1-10 μm using a spin coating method. The permeation properties of prepared GO laminates were tested toward different species by filling a sealed-container with different gases under a small pressure (below 100 mbar). The changes in pressure of gases and the weight of sample was detected and recorded over a time period as an indication of permeation of gas molecules. The prepared GO laminates showed unrestricted water vapor permeation with high permeation rates compared to the other gases (e.g., He, H_2, N_2, and

Ar). The results also showed permeation of water species was significantly altered upon changes in the structure and inter-layer spacing of GO laminates. Modifying the inter-layer distance of GO sheets led to a fast transport of molecules through GO layers ascribed by low friction water vapor molecules through inter-layer spaces of GO sheets. Other studies have shown GO to be an efficient material in the field of pervaporation, air dehumidification, desiccant applications and in water transport devices [66–68]. In a related study, Stampfer et al. [69] fabricated nanostructured-graphene from graphite using a mechanical exfoliation technique. The surface charge of the prepared material was investigated, where it was observed that negatively charged functionalized nanopores facilitated passage of cations, while positively charged nanopores enabled anions to permeate through the graphene sheets.

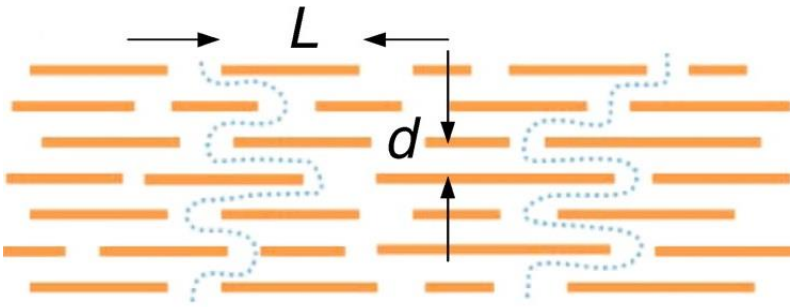

Figure 2.6. Schematic image of possible permeation through GO sheets where L denotes the size of a GO sheet, and d represents spacing between GO layers [57].

It can be concluded the selective permeation properties of GO sheets depend on the formation of nano-capillaries within the GO structure, porosity properties (PS, PV) and surface charge of the GO sheets. Several approaches have been used to tune the permeation properties of GO membranes, including reduction of GO, oxidative etching, and cross-linking [70–72].

2.9.4 Properties and applications of GO

GO offers remarkable properties including high SA, chemical and mechanical stability, tunable surface chemistry and optical properties. Therefore, GO and GO-based materials have become one of the promising materials for versatile applications as shown in Figure 2.7. For example, they have been used in environmental protection applications (including removal of air pollutants,

greenhouse gases capture, wastewater treatment and purification), energy conversion, hydrogen storage, batteries, sensors, catalysis and devices for biomedical applications [3,73–75].

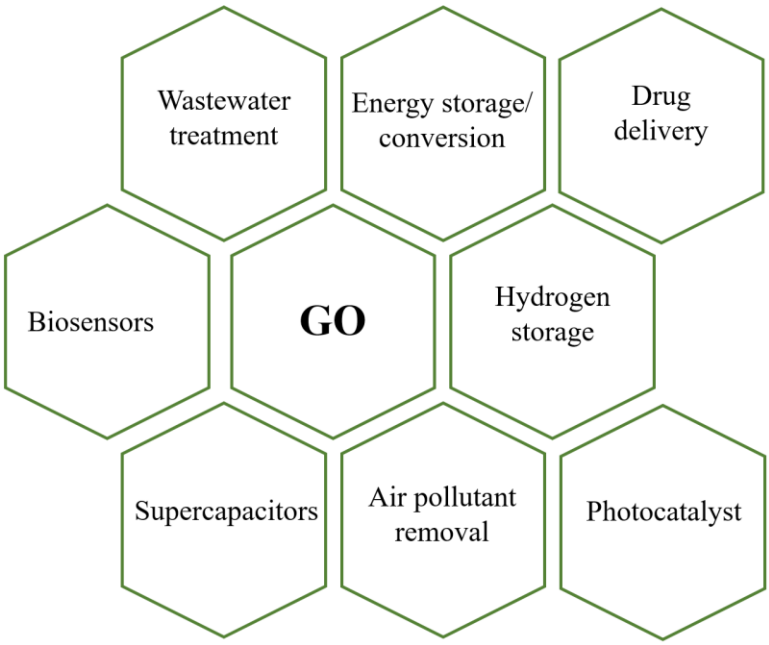

Figure 2.7. Various potential applications of GO and GO-based materials [73].

Although GO materials show promising properties, there are numerous methods to improve the properties of GO. As a flexible yet robust material with several types of functional groups on its surface, there are unlimited possibilities for functionalization or modification of GO's structure to fabricate GO-based materials at low cost and large scale [76–78]. GO powder yields a homogeneous dispersion in various solvents and matrices owing to the existence of its oxygen functional groups. This advantage makes GO a great candidate for coordinating with other matrices or reagents for the preparation of GO-based composites [79,80].

2.9.5 Mechanical properties of GO

The mechanical properties (e.g. tensile strength, Young's modulus, elongation at break and fracture strength) of GO and GO-based composite materials in the form of monolayer sheets, paper, membranes, fibers, and thin films prepared from Hummer's method have been studied experimentally and computationally (e.g., molecular dynamics simulations) [8,81–87].The

reported mechanical properties of GO have shown to be dependent on the degree of oxidation and coverage of functional groups on the GO surface arising from synthetic processes, thickness of samples and test conditions (e.g., strain rate) [84,88,89]. The tensile strength and Young's modulus of GO sheets (with thickness of 1.1-1.2 nm) have been reported in the range of 76-293 MPa and 6-42 GPa, respectively. The values are dependent on the final shape of the GO (sheet, membrane, film) and synthesis process [73,90]. For example, early in 2007, Dikin et al. [82] prepared GO according to Hummer's method and evaluated the mechanical properties of GO paper (with thickness in the range of 1-30 μm). The GO paper was prepared through a directed-flow assembly (filtration) method and was tested using a dynamic mechanical analyzer with a force ramp rate of 0.02 N/min. The tensile strength and Young's modulus were reported as 74.5 MPa and 32.1 GPa, respectively. These relatively high values were attributed to the strong interactions of GO sheets that enabled the sheets to distribute the load across the entire sample effectively. In 2010, another study by Suk et al. [81], produced an ultrathin GO paper (contained one to three layers of GO) by depositing a GO suspension (prepared by Hummer's method) on a carbon film substrate. The mechanical properties of GO papers (with thicknesses in the range of 0.7-2.1 nm) were measured using an atomic force microscope (AFM). It was found that a GO paper containing one layer of GO with a thickness of 0.7 nm had a Young's modulus of 207.6 GPa. However, in a different study, the mechanical properties of GO films were studied using an MTS nano-indentation instrument with a diamond probe having radius of 100 nm [91]. Free-standing GO films with 50-60 nm thicknesses, were produced by an electrophoretic deposition (EPD) technique. Nano-indentation measurements were conducted at a load of 85 μN and held for 10 s. The tensile strength and Young's modulus of the GO films were reported in the range of 8-11 N/m and 695-697 GPa, respectively. Recently, GO films (with average thickness of ~23 μm) were fabricated through a dispersion-evaporation technique, where 7.4 mg/ml of GO solution were cast-dried on a polystyrene petri dish and dried at 25 °C for 3 days [92]. The mechanical properties were measured using an Instron 3342 universal testing machine with strain rate of 5×10^{-4} s^{-1}. The tensile strength and Young's modulus of the GO films were found to be 206 MPa and 10.6 GPa, respectively [92]. The literature suggests that the Young's modulus of GO sheets increases dramatically when the thickness of the GO sheet is reduced. Therefore, a monolayer of GO shows a larger Young's modulus value compared to a GO sheet with a larger thickness.

2.9.6 Mechanical properties of GO-based composites

The mechanical performance of GO sheets can be enhanced by different methods such as reduction, introduce bonding between individual GO sheets by chemically cross-linking [8,88,93,94]. However, only a few studies have used metal ions and polyallylamine as cross-linkers [8,80]. Also, the mechanical properties of GO sheets can be improved by combining GO with another material to produce GO-based composites. The composite will be described as matrix-reinforcement where the matrix (GO) is the higher weight percentage. Among different GO-based composites, much progress has been made toward the preparation of GO-CTS composites. CTS is a product of deacetylation of chitin and is one of the most abundant natural biopolymers. CTS is a protonated biopolymer as it contains hydrophilic groups such as amino and carboxyl groups on its structure (Figure 2.8) [95]. Owing to the excellent biological properties of CTS such as biodegradability and biocompatibility, it has been extensively used in different technologies such as medicinal development, molecular separation, food packaging, artificial skin, wastewater treatment, electrochemical sensors and antibacterial agents [96–100].

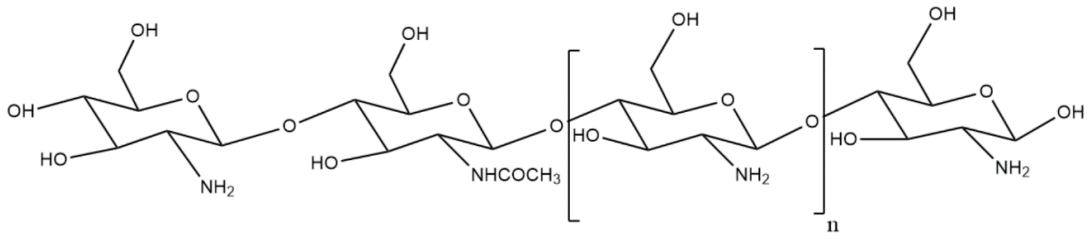

Figure 2.8. Molecular structure of the glucosamine units of CTS, where n denotes the degree of polymerization.

In 2010, Pan et al. [101] reported on the preparation and characterization of CTS-GO composite films through a solution casting technique. In the reported method, 1 wt. % CTS solution was prepared and different amounts of GO (0, 0.25, 0.5, 0.75, 1 wt. %) (prepared from Hummer's method) were added to a CTS solution. The films were oven-dried at 50 °C for 2 h and cut into 20 mm by 5 mm rectangular samples before performing the mechanical test using an Instron Model 5543 mechanical tester at a strain rate of 5.0 mm/min. The tensile strength, tensile modulus and elongation at break of the films increased from 87.5 MPa to 133.1 MPa, 3.45 GPa to 4.42 GPa and 22.9 % to 31.6 % with increasing GO content from 0.25 to 1 wt. %, respectively. This enhancement of mechanical properties was related to the formation of robust interfacial adhesion between GO and CTS. In a similar study in 2014 [102], CTS-GO composite films were prepared by a solution

mixing method and their mechanical properties were investigated. The GO material was prepared according to Hummer's method and then added to the CTS solution (1 g dissolved in 30 mL acetic acid) in different loading amounts (0.05, 0.5, 1 wt. %). The mixture was poured into a petri dish and dried at ambient condition to obtain the composite films. The mechanical performance of the obtained composite films was evaluated by means of a Shimadzu Autograph AG-X universal tester with an extension rate of 5 mm/min. It was found with the addition of GO to CTS the mechanical properties were substantially improved as a result of dispersion of GO in the CTS matrix and the robust interaction between GO's functional groups and CTS. The tensile strength of composites was reported in the range of 39-65 MPa, while elongation at break was (9-14) %, respectively. Which shows an enhancement of 51 % and 56 % in tensile strength and elongation at break, respectively compared to pure CTS. Similar to previous approaches, Zuo et al. [9] reported preparation of GO-CTS composites by a solution casting method. In their process, GO was prepared according to Hummer's method. About 50 mg of GO powder and 1 g of CTS powder were added into 50 mL of DMF (N,N-dimethylformamide) solution and sonicated. Subsequently, 0.45 g of DCC (N,N'-dicyclohexylcarbodiimide) and 0.3 g of DMAP (4-dimethylaminopyridine) were added to the solution and stirred for 48 h. Finally, the mixture was dried at 60 °C for 24 h to obtain composite films. The final GO-CTS composite contained 0.25 wt. % GO and 2.25 wt. % CTS (GO: CTS mass ratio was 1:9). The mechanical performance of the GO-CTS composite films with specimen dimension of 75 mm by 4 mm were studied by mechanical analyzer (ZWICK ZO 20/TN2S, Germany) with an extension rate of 10 mm/min. The average tensile strength and Young's modulus of the films increased by 150 % and 366 %, respectively, as compared to CTS. Further advancements in preparing GO-based composites were made by Yan et al. [103] in 2016, who used borate ions for cross-linking CTS and GO in order to prepare CTS-GO composites. In their study, GO was made according to the Hummer's method. CTS-GO composite films were produced by the solution casting technique where different amounts of GO solutions (0, 0.25, 0.5, 1.0, 1.5, 2.0 wt. %) and 1.0 wt. % of boron element (B) were added to the 1 wt. % CTS solution. The films were obtained by vacuum drying the mixture at 90 °C for 50 min. The mechanical performance of the films was evaluated by means of a universal testing machine (Instron 3360) under extension rate of 5 mm/min. The addition of both GO and borate ions was found to increase the tensile strength and elongation at break of the composites by 160 % and 230 % compared to pure CTS, respectively. A recent study in 2017 [104] showed GO was synthesized according to a

modified method reported by Santos et al. [105]. The CTS-GO films were prepared using a solution mixing method where GO solution in different loading percentages (0.1, 0.2, 0.4, 0.6 wt. %) were dispersed in 1 % acetic acid (AA) and added to a 2 w/v % CTS solution. The mixture was vacuum-dried at 20 °C to thermally cross-link GO and CTS. The obtained films had thicknesses in the range of 48-52 µm. The films were cut into 165 mm by 20 mm strips and tested in a mechanical analyzer (Shimadzu EZ-LX, Japan) with an extension rate of 12 mm/min. The mechanical properties of composites were significantly enhanced with addition of GO due to formation of covalent bonds between CTS and GO as a result of thermal cross-linking between them. This bonding facilitated transferring load from CTS to GO under tension. The tensile strength, Young's modulus and elongation at break of composites were in the range of 52-69 MPa, 5.8-6.8 GPa and 0.9-3 %, respectively for different loading percentages of GO. The highest values obtained were for the composite containing 0.25 wt. % GO. In a comparable investigation by Ahmed et al. [106] CTS-GO composites were fabricated by mixing with 4 w/v % CTS solution with selected concentrations of GO solutions (0.5, 1 and 2 % w/w) and cast on a rimmed silicone resin plate for formation of films. The films with thicknesses in the range of 0.172-0.178 mm were tested for mechanical performance using a Texture Analyzer (TA) XT plus (Stable Micro Systems, UK) with a crosshead speed of 50 mm/min. It was found that while there was a remarkable enhancement in the tensile strength of the CTS films from 8.9 MPa to 15.3 MPa upon the addition of the GO, the elongation at break dropped from 69.8 % to 57.3 % for CTS films containing 2 % w/w GO. The enhancement in tensile strength of samples were found to be related to two main factors. Firstly, uniform dispersion of GO in the CTS matrix, along with covalent bond formation and hydrogen bonding between components. Secondly, the addition of GO can restrict CTS chain movement and hence enhance load transfer under stress. Similar observations were reported by Han et al. [94] and Shao et al. [107] in 2011 and 2013, respectively. In a more recent experiment in 2018, Zhang et al. [108] prepared CTS-GO films and evaluated their mechanical properties. First, the as-prepared GO sheets were functionalized using KH560 (3-glycidyloxypropyltrimethoxysilane). The GO solutions (0,1 ,3, 5 wt. %) were then added to 1 % w/w CTS to produce GO films by vacuum drying the solution at 50 °C for 72 h. Finally, the samples were irradiated with γ-rays in order to cross-link GO and CTS. The samples were then cut into 50 mm by 5 mm strips. To measure mechanical properties of the composite films, a tensile strength tester (DSA 502A, Sans, Minneapolis, MN, USA) was used under a loading speed of 2

mm/min. They determined the tensile strength of the composites to be in the range of 68-125 MPa where composites containing 3 wt. % GO had the highest tensile strengths. However, the elongation at break were in the range of 4-38 % which decreased with increasing GO content.

More recently, in a study done by Chen et al. [109] a flexible GO and nylon 6 (GO-nylon 6) membrane with thickness of 1.2-2.2 μm was prepared by a layer-by-layer assembly technique using an electrospinning processes. The mechanical performance of the prepared membranes was measured using an electronic universal testing machine (CMT4201, China) with crosshead speed of 3 mm/min. The membranes had tensile strengths in the range of 2.98-8.10 MPa and were dependent on the thickness of the samples. Although the effect of adding GO to a CTS matrix on mechanical properties of obtained composites was investigated, very few studies have evaluated the addition of CTS to a GO matrix.

Park et al. [8] were the first to report an enhancement in mechanical properties of GO modified with 1 wt. % metal ions such as magnesium (Mg^{2+}) and calcium (Ca^{2+}). In their study, GO was synthesized by Hummer's method and further cross-linked with 0.2 mM solution of either metal ion species. The papers were prepared by continuous filtration of a GO solution and metal ion solution and further dried for 1-2 days at ambient temperature. The mechanical performance of the films was obtained using a dynamic mechanical analyzer (2980 DMA, TA Instruments, New Castle, DE) with a force ramp rate of 0.05 N/min. The tensile strength was found to increase from 81.9 MPa for pristine GO, to a maximum of 125.8 MPa for cross-linked GO papers. In addition, Young's modulus and elongation at break enhanced from 5.8 GPa up to maximum 17.2 GPa and from 0.40 % up to maximum 0.50 %, respectively. The potential applications of the GO papers are anticipated to serve as adhesives and protective layers, chemical filters, supercapacitors, electronic components and materials in the food packaging industry [82,110,111].

2.9.7 Environmental applications of GO materials and its composites

GO has attracted much interest for environmental protection technologies. For instance, it has been shown that GO's functional groups can serve as effective and accessible sites for immobilization of different active species [112]. GO has been effectively used as an adsorbent for removal of various species including heavy metal ions, organic and inorganic species, both anionic and cationic dyes [4,113]. The remarkable sorption capacities of GO are evidenced by fast adsorption

rates and high adsorption affinity. More importantly, the use of GO-based adsorbents can facilitate the adsorbent-based separation after the adsorption process [114]. Although GO has strong adsorption affinity toward most metal ions (as the main type of water contaminant species) [113], the affinity depends on several parameters including the type of metal ion [114].

2.9.8 Gas uptake properties of GO materials and its composites

Generally, air pollutants purification process is divided into three categories: (1) decrease of gas emission directly, (2) capture and storage of the gas, and (3) final gas utilization. GO and GO-based materials possess layered-structures with expanded layer distances and tunable porosity which have attracted many studies for use as hydrogen storage materials and for air pollutant removal strategies [115–117]. For use as hydrogen storage materials, GO can store hydrogen molecules in between its layered framework structure, especially for expanded layers with porous properties [118]. Controlling the GO layer distance and PS has been observed to enhance the hydrogen storage capacity [119,120]. Fabricated GO sheets possess reduced SA (ca. 10 m^2/g) compared to graphene with its greater SA (ca. 2600 m^2/g) [121,122]. This reduction in SA can be due to the rearrangement of the graphitic structure during the synthesis process which leads to reduced inter-layer distances and limits the accessible SA for adsorption processes [34]. This problem has been addressed by use of methods such as thermal exfoliation, chemical reduction, and functionalization of GO layers in an effort to develop pillared layers of GO [122–125]. Burress et al. [115] showed a novel graphene oxide framework (GOF) material can be obtained by linking GO layers together using a proper linker to form a novel layered-structure as shown in Figure 2.9. GOFs are suitable for potential use as adsorbent and gas storage materials. Interestingly, the pore properties (such as pore widths and volumes) and bonding sites of GO can be modified according to variations in linker concentrations and linker types.

Nitrogen adsorption using GO and GO-based materials have been reported using both experimental (Brunauer–Emmett–Teller (BET) nitrogen (N_2) adsorption isotherm) and simulation (Monte Carlo Density Functional Theory; MCDFT) approaches [34,126]. In BET measurements, GO showed insignificant N_2 adsorption and low SA as a result of the filled inter-layer spaces of GO layers (due to presence of functional groups). In addition, reduced GO (rGO) materials

displayed negligible adsorption of N_2 due to elimination of oxygen functional groups and changes in the graphene structure.

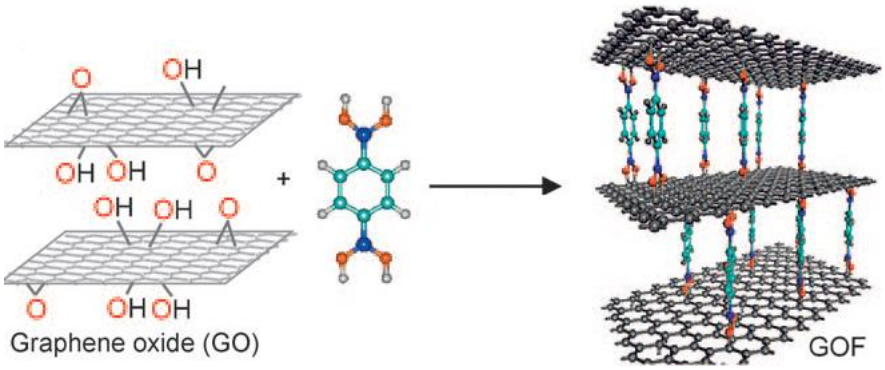

Figure 2.9. Proposed GOF material formation from connected GO layers [115].

Generally, the major N_2 uptake of GO occurred at a relatively low pressure which was indicative of a highly developed microporous structure [34]. Although GO showed insufficient N_2 adsorption, modification of GO was reported to enhance the SA and porosity properties of GO-based materials [34,126]. Wang et al. [127] prepared GO according to Hummer's method and fabricated 3D graphene by placing it into a glass bottle under vacuum at 150 °C for 45 min. The gas adsorption properties were measured using a Quantachrome Adsorb-1 pore and surface analyzer. The nitrogen and hydrogen isotherm properties were evaluated at 77 K, while carbon dioxide (CO_2), and water vapor at 273 K. The nitrogen adsorption-desorption analysis showed the BET SA of about 477 m^2/g, which was significantly greater than reported BET values for graphite (38 m^2/g) and carbon nanotubes (< 200 m^2/g) [128]. In addition, the measured total PV of the samples was reported as ~1.04 cm^3/g possibly due to the structural imperfections. The hydrogen storage capacity determined by hydrogen adsorption-desorption measurements at 77 K was found to be 1.40 wt. % at 106.6 kPa, while the adsorption-desorption isotherms of CO_2 showed the sorption capacity to be 2.98 wt. % at 106.6 kPa. Although the adsorption mechanisms were not investigated in depth, the CO_2 adsorption on the GO was different from nitrogen and hydrogen. This may be due to interactions occurring between functional groups of GO sheets with CO_2 molecules. Moreover, the water vapor sorption capacity obtained from adsorption-desorption isotherms was found to be 18.7 wt. % at 97.0 kPa. Although GO shows promising adsorption capacity toward various species, it has been demonstrated that GO's adsorption properties can be

improved through various functionalization approaches. For instance, there have been studies in which GO-CTS materials have been tested for gas adsorption properties. In a work performed by Yan et al. [103] GO was prepared from Hummer's method and 0.1 mg/ml GO solution was added to different solution concentrations of CTS (0, 0.25, 0.5, 1.0, 1.5, 2.0 wt. %) and stirred for 1 h. The barrier performance of prepared materials was tested by oxygen transmission rate (OTR) by a permeability meter (Extra solution, MULTIPERM) equipment. The GO-CTS materials were shown to possess improved oxygen barrier properties (the oxygen permeability decreased by 25-90 %) compared to pristine CTS for potential packaging applications.

2.9.9 Mechanism of metal ions and cationic species adsorption

Several studies have investigated the adsorption mechanisms using GO as an adsorbent. The relevant studies showed electrostatic attraction between the positively charged species (e.g., metal ions, cationic species (an ionic species with a positive charge)) and GO's negatively charged surface, was considered the main mechanism for adsorption (as shown in Figure 2.10) [129,130]. Therefore, compared to conventional carbonaceous adsorbents, GO is a superior adsorbent for metal ion and dye adsorption which arise from GO's oxygen groups accessible on its surface to interact with other species [30].

Numerous studies have used GO as an adsorbent model for remediation of water contaminants, as summarized in Table 2.1 and Table 2.2. Additionally, other parameters were observed to significantly affect the adsorption capacity of GO including pH, number of chemical functional groups on the GO surface, thickness of GO sheets, adsorbate species and experimental conditions [6,113,133]. For example, cationic dye adsorption (e.g., methylene blue (MB) and methyl violet) into GO took place within a wide range of pH values through electrostatic interactions [4].

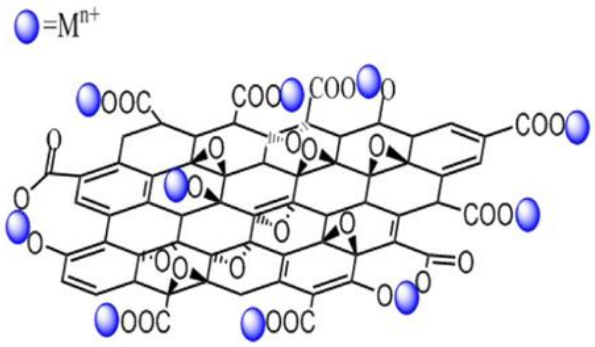

Figure 2.10. Adsorption mechanism of metal cations on surface of GO [114].

Table 2.1. Summary of different metal ion removal studies using GO and GO-based composites as adsorbent (at pH ~ 6-7).

Adsorbent	Metal Species (adsorbate)	Maximum adsorption Capacity (Q_{max}) mg (adsorbate) / g (adsorbent)	Ref
GO	Am(III)	8	[134]
GO	Au(III)	108	[135]
GO-CTS	Au(III)	990	[136]
GO	Co(II)	68	[6]
GO-Fe_3O_4	Co(II)	13	[137]
GO-NH_2	Co(II)	116	[138]
GO	Cd(II)	106	[6]
GO	Cd(II)	345	[113]
GO-CTS	Cr(VI)	34	[139]
GO	Cu(II)	47	[140]
GO	Cu(II)	294	[113]
GO	Cu(II)	118	[131]
GO-Fe_3O_4	Cu(II)	118	[141]
GO-CTS	Cu(II)	25	[142]
GO	Eu(III)	175	[143]
GO	Eu(III)	115	[134]

Adsorbent	Metal Species (adsorbate)	Maximum adsorption Capacity (Q_{max}) mg (adsorbate) / g (adsorbent)	Ref
GO	Ni(II)	38	[144]
GO-glycine (G)	Ni(II)	36	[144]
GO	Pb(II)	250	[145]
GO	Pb(II)	842	[132]
GO	Pb(II)	81	[135]
GO	Pb(II)	1119	[113]
GO	Pd(II)	98	[136]
GO-poly (acrylamide)	Pd(II)	1000	[146]
GO-CTS	Pd(II)	100	[147]
GO-CTS	Pd(II)	217	[136]
GO-SiO_2	Pd(II)	114	[148]
GO-Fe_3O_4-CTS	Pd(II)	77	[149]
CTS–gelatin/GO (CGGO)	Pd(II)	120	[150]
Polyacrylamide (PAM)-GO	Pd(II)	819	[151]
GO	Pt(IV)	71	[135]
GO	U(VI)	98	[152]
GO	U(VI)	299	[153]
GO	Th(IV)	411	[154]
GO	Zn(II)	345	[113]
GO	Zn(II)	246	[133]
GO	Au(III)	1077	[136]

Table 2.2. Summary of various organic compounds removal studies using GO and GO-based composites as adsorbent (at pH ~ 6-7).

Adsorbent	Organic compound (adsorbate)	Maximum adsorption capacity (Q_{max}) mg (adsorbate) / g (adsorbent)	Ref
GO	MB	244	[155]
GO	Tetracycline	313	[156]
GO-FeO.Fe_2O_3	Naphthalene	283	[157]
GO-FeO. Fe_2O_3	1-Naphthol	389	[157]
GO-FeO. Fe_2O_3	1-Naphthylamine	408	[157]
GO-Fe_3O_4	Bisphenol A	123	[158]
GO-SiO_2-Fe_3O_4	MB	111	[159]
GO- sodium alginate (SA)	MB	833	[160]
GO-CTS- Fe_3O_4	MB	181	[161]
GO-CTS- Fe_3O_4	MB	95	[44]
GO-B (β-cyclodextrin) -CTS-Fe_3O_4	MB	50	[162]
GO-calcium alginate (CA)	MB	182	[163]
GO- brilliant blue (BB)	Anthracenemethanol (AC)	349	[164]
GO-BB	Fluoranthene (FL)	447	[164]
GO-poly-dopamine (PD)	Methyl violet (MV)	2100	[165]
GO-PD	Basic fuchsin (BF)	1700	[165]
GO-PD	Coomassie brilliant blue (CBB)	2100	[166]
GO-PD	Malachite green oxalate (MGO)	2000	[166]
GO-PD	Neutral red (NR)	1400	[166]
GO-CTS	MB	402	[167]

2.10 Modification of GO

Chemically reactive functional groups present on GO sheets offer an opportunity for modification of GO. There are various approaches to modify GO based on reaction with or modification of the functional groups of GO with other suitable reagents. Generally, GO has been modified through either non-covalent or covalent bonding interactions or a combination [168]. While the electrical properties and surface charge of GO can be enhanced through non-covalent modification methods, the stability and mechanical properties can be enhanced via covalent methods. Non-covalent interactions of GO can be achieved through van der Waals interaction and hydrogen bonding. In non-covalent modification, the interactions are relatively weak compared to covalent interactions. However, multiple non-covalent bonds have been shown to yield a stable modification as well [168]. Moreover, these types of interactions can easily be achieved on the GO surface (while the GO's structure remains unaffected) and can be reversible in some cases [169]. Furthermore, GO is shown to be covalently modified by altering the surface functional groups by reaction with molecular or polymeric species with carboxyl or hydroxyl groups of GO [170,171]. Covalent functionalization of GO can be obtained by reaction with the epoxy groups of GO through ring-opening reactions [8,172,173].

2.10.1 Chemical cross-linking of GO sheets

A cross-linker can be used to enhance the structure and bonding between individual GO sheets through electrostatic interactions and covalent bonds between adjacent GO nanosheets [8,13,172,174–177]. Using this approach, the structural stability, adsorption, physicochemical and mechanical properties of GO sheets, papers, films, hydrogels and membranes can be improved [178]. GO sheets can be cross-linked together by means of various polymers, metal ions, aliphatic amines, amino acids, diaminoalkanes, boronates and acyl chloride [179–181]. Previous studies on cross-linked GO materials are outlined in the form of diverse studies in the following examples. Feng et al. [182] reported cross-linked GO membranes using polyimide (PI) as the linker. In their study, GO was prepared by the modified Hummer's method. The GO-PI was produced in a water coagulation bath method where 1.564 g of PI was added into the different concentrations of GO solutions (0, 0.5, 1, 2 wt. %) at 50 °C while stirring. Membranes with thicknesses of 100 mm were obtained by casting the solution onto a glass plate using a casting knife, followed by drying at 60

°C for 1 h. The prepared membranes were further characterized for desalination performance (water permeability and salt rejection performance) for 3.5 wt. % seawater. The results showed the GO-PI membranes had high permeation flux (36.1 kg/m h) and high ion rejection (around 99.9 %) which remained up to 120 h. The high flux and ion rejection of GO-PI membranes was attributed to the presence of hydrophilic sites on GO-PI membranes and electrostatic interactions between salt ions and pores in the membrane. The results were in good agreement with a previous study [183]. Using a similar approach, GO was prepared from Hummer's method and modified with the poly (amide-imide)–polyethyleneimine (PAI–PEI). In this study, the PAI hollow fiber substrate was fabricated and further modified with PEI. The GO sheets with negative surface charges were then deposited on the PAI–PEI membrane surface with positive charge via a dip coating method. The water and salt permeability of the membranes was studied by placing them into tube 3/8″ x 1/2″ (9.5 mm x 12.7 mm) containing deionized water and $MgCl_2$, $CaCl_2$ and NaCl in aqueous solutions. The water permeability performance of the samples was determined by applying a pressure of 1 bar and a cross flow rate of 600 ml/min for 1 h. Finally, the permeate volume was measured and water permeability coefficient of the membrane was estimated. It was found that depositing GO sheets on the membrane surface enhanced the rejection efficiency of the membrane by 15 % and water permeability up to 86 %. The improved properties arose from reducing PS of the membranes by depositing GO [184]. Hung et al. [180] developed GOF membranes which were cross-linked with diamine monomers with various inter-layer spacing between the GO sheets (Figure 2.11). In this study, GO was fabricated according to Hummer's method and cross-linked with three types of diamine monomers including ethylenediamine (EDA), butylenediamine (BDA), and *p*-phenylenediamine (PPD) via a solution mixing method. GO solution with a concentration of 400 ppm was mixed with 0.1 M solutions of diamine monomers to produce GO-EDA, GO-BDA, and GO-PPD composites. The composite membranes were produced through pressure-assisted self-assembly method on the cellulose acetate substrate. The membranes were oven-dried at 80 °C for 1 h and tested for water permeability in an ethanol/water mixture. The results indicated that GO membranes cross-linked with diamine monomers had high water permeation flux (2297 $g/m^2.h$) and high-water concentrations (99.8 wt. %) when tested for the separation of ethanol/water mixture at 80 °C. These changes were found to be due to formation of covalent bonds between GO and diamine monomers which led to increasing inter-layer spacing of GO sheets.

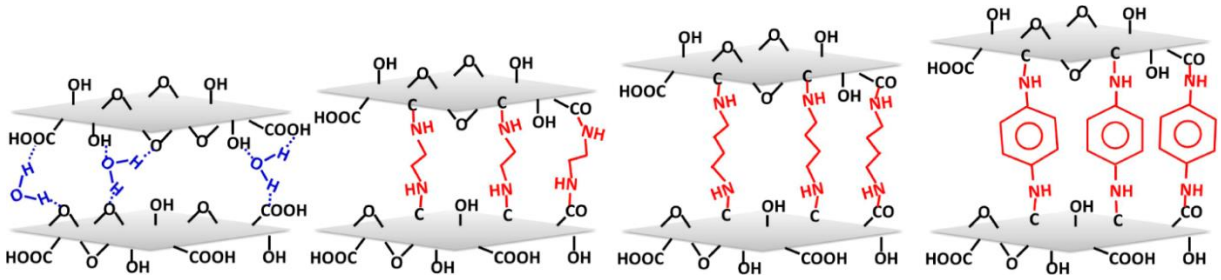

(a) (b)

Figure 2.11. Structure of (a) GO and (b) cross-linked GO membranes (GO-EDA, GO-BDA, and GO-PPD) with diamine monomers [180].

In two related studies, cross-linked GO membranes were prepared using 1,3,5-benzenetricarbonyl trichloride (TMC) and poly (allylamine hydrochloride) (PAH) as cross-linkers via a layer-by-layer assembly method to obtain a cross-linked GO membrane with a thicknesses of ca. 14-16.5 nm [72,185]. Flux and rejection rate of GO-TMC membranes were tested using a dead-end membrane filtration system and different feed solutions including NaCl, Na_2SO_4 and MB under 50 psi (0.34 MPa) transmembrane pressure. The flux of water for the cross-linked GO membranes decreased to 80 LMH/MPa, while the rejection rate toward NaCl, Na_2SO_4 and MB increased to a maximum of 19 %, 46 %, and 66 %, respectively. This performance was shown to be related to changes in inter-layer spacing of GO sheets and presence of surface charges on the membrane [72]. Also, membrane performance of cross-linked GO membranes by positively charged PAH was evaluated using a dead-end membrane system under 50 psi (0.34 MPa) hydraulic pressure. The water permeability of the GO-PAH membrane decreased from 88.4 LMH/ atm to 5.8 LMH/atm. In terms of gas phase species, Wang et al. [64] prepared a permeable borate cross-linked GO-polyethersulfone (PES) membrane with lateral size of 2 µm and thickness of about 8 nm by a vacuum-assisted filtration method followed by thermally treated them for cross-linking formation. The gas separation performances of the cross-linked membranes were tested using a constant volume-variable pressure method. The feed gases included N_2, CH_4 and CO_2 as well as gas mixtures (CO_2: N_2 50:50, CO_2:CH_4 50:50, O_2:N_2 50:50) under fixed gas pressures of 30-50 mL/min. The prepared membranes were found to be an effective carbon capture material with CO_2 permeability of 650 gas permeation unit (GPU). Also, this material can be used as a selective membrane in the separation process of a CO_2/CH_4 mixture with CO_2/CH_4 selectivity of 75. The

performance was attributed to changes in the inter-layer spaces between the GO sheets upon cross-linking which enabled adequate transport channels in the GO for gas molecules.

2.10.2 Cross-linking with metal ions

The other type of cross-linker for use in modification of GO sheets are metal ions. The work done by Park et al. [8] was the first successful example of developing a cross-linked GO membrane using divalent ions through a continuous filtration method. It was found that cross-linking GO sheets with less than 1 wt. % metal cations (e.g., Mg^{2+} and Ca^{2+}) significantly improved the mechanical properties of GO sheets. The interactions were shown to take place between the functional groups of GO sheets and the cations in two modes. One of them occurred via binding of the metal ions to the carboxylic acid groups of GO sheets, while the other one through introduction of the metal ions with the epoxide rings of the GO sheets. Figure 2.12 shows the proposed model for the reactions between metal cations and GO sheets. This approach has promoted several researchers to developed cross-linked GO sheets with metal ions. For example, in a systematic study performed by Bai et al. [178], GO was prepared from graphite powder using Hummer's method and used to fabricate GO hydrogels using various metal ions through a solution mixing method. The hydrogel formation was studied using a tube inversion method. Monovalent ions (e.g., K^{+}, Li^{+}, Ag^{+}) were observed to be incapable of producing GO hydrogels, while divalent and trivalent metal ions (e.g., Ca^{2+}, Mg^{2+}, Cu^{2+}, Pb^{2+}, Cr^{3+}, Fe^{3+}) were able to yield the formation of 3D networks of GO. The driving force for the formation of 3D networks are due to the coordination of the metal ions with hydroxyl and carboxyl groups within the GO sheets. Moreover, to support the cross-linking effect of metal ions in a 3D network of GO, Chithra et al. [186] added a chelating agent to the GO-metal ion mixture to further eliminate metal ions.

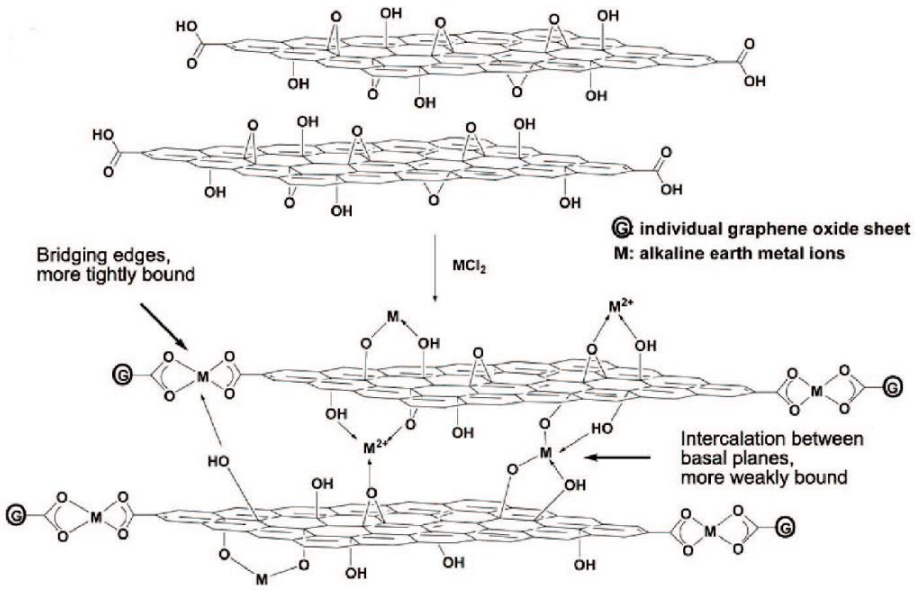

Figure 2.12. Proposed model for interactions between GO sheets and metal cations [8].

It was observed that the 3D GO-metal ion hydrogel disintegrated due to elimination of metal ions. Therefore, the cross-linking effect was found to promote the formation of 3D self-assembly of GO sheets due to the increase in bonding force between individual GO sheets. In a study by Yeh et al. [7], GO membranes were unintentionally found to be remarkably stable in water when they were cross-linked with metal cations (e.g., Al^{3+} and Mn^{2+}). In their study, GO was synthesized using Hummer's method where 1 mg/mL of GO was dispersed and vacuum-filtered through a porous AAO filter (Anodisc, 47 mm in diameter, 0.2 μm), followed by peeling off the filter and air-dried for 24 h. The mechanical performance of the membranes with a thickness of 18-20 μm were tested using a dynamic mechanical analyzer (2980 DMA, TA Instruments). The GO membranes had average tensile strengths and Young's modulus of 100.5 MPa and 26.2 GPa, respectively. The values were remarkably higher compared to GO membranes prepared without using AAO filter paper, which showed average tensile strengths of 86.9 MPa and Young's modulus of 7.6 GPa. In addition, the vacuumed-filtered membranes were found to be highly stable in water. Therefore, it was suggested that releasing metal ions (such as Al^{3+}) from the filter paper during the vacuum filtration process could effectively cross-link GO sheets together. Recently, in a similar approach, GO membranes were developed by cross-linking them with a range of metal cation (e.g., Na^{+}, Mg^{2+}, Ca^{2+} and Al^{3+}) [187]. GO was synthesized using Hummer's method and brought into an

aqueous solution with a GO concentration of 2 g/L and cross-linked using a solution mixing method. The mixture of GO solution and salt solutions were filtered through cellulose acetate membrane filters (47 mm in diameter, 0.2 µm PS). The membrane stability was evaluated by placing them into different test solutions (i.e. deionized (DI) water, NaCl, alginate solution and bovine serum albumin (BSA) solution) for different periods of time. Modified GO membranes were observed to offer greater integrity than unmodified GO. The monovalent cation such as Na^+ was not able to stabilize the GO layers, however incorporating multivalent cations such as Mg^{2+}, Ca^{2+} and Al^{3+} as cross-linkers were able to provide more stable membranes [187]. In a recent study in 2018, the thermal stability (open flame resistance) and SA of GO sheets were remarkably improved through cross-linking with Al^{3+} cations [11]. In this study, cross-linked GO membranes with Al^{3+} cations were prepared using a solution mixing method where 3 mg/ml of GO were added to 0.2 w/v % solution of $Al(NO_3)_3 \cdot 9H_2O$ under constant stirring. The membranes were produced by a drop-casting method using a polystyrene substrate. Thermal stability of prepared membranes was tested using thermogravimetric analysis (TGA) Q50 V20.10 under N_2 atmosphere and ramping speed of 15 °C/min. Aside from thermal stability, the MB adsorption method was used to estimate SA of GO before and after cross-linking. The cross-linked-GO samples showed a lower rate of mass loss starting at about 200 °C, which was higher compared to pure GO at 125 °C. Also, cross-linked GO samples were found to resist decomposition in a flame, while pure GO was burnt out in ~5 s. The higher thermal stability of cross-linked GO was found to be related to firstly, reduction of epoxide groups on GO surface as a result of cross-linking with Al^{3+} cations and secondly, shielding heat propagation between the cross-linked GO sheets. The SA of GO sheets increased by 90 m^2/g due to higher in-layer distance between GO sheets and hence accessibility of more MB molecules to available spaces between GO sheets. Along with improving thermal stability and flame resistance, it's been demonstrated that by cross-linking GO sheets with copper cations (Cu^{2+}) the conductivity of GO sheets increased significantly for applications in light-emitting diodes, displays and photovoltaics [188]. In this approach, GO was prepared by Hummer's method and 3 mg/mL GO solution was added to Cu^{2+} solutions of variable concentration (10, 20, 30, 40 and 50 mM). The solution was filtered through porous membranes using a vacuum filtration method in order to fabricate cross-linked GO films. Finally, the electrical conductivity of the GO films was evaluated using a low power xenon flash equipment. The results indicated cross-linked GO sheets with Cu^{2+} cations had lower electrical resistance (higher

electrical conductivity) (0.540 KΩ cm^2) compared to pure GO (11.35 KΩ cm^2). These changes were suggested to be related to the increased conduction channels within GO sheets upon addition of metal ions. As a conclusion, cross-linking was found to be a promising approach to tailor and enhance various GO properties in solution and dry-state for potential applications in many fields.

2.10.3 Cross-linking with CTS

CTS was shown to function as an effective cross-linker for cross-linking GO sheets through electrostatic interactions coupled with formation of amide bonds between functional groups of GO and CTS [10,189]. By combining the advantages of both GO and CTS, applications have led to formation of stable GO-CTS cross-linked framework materials, nanocomposites, hydrogels, films and membranes [104,117]. Table 2.3 lists the studies conducted on GO-CTS composites prepared for various applications.

Preliminary results on GO-CTS composite properties confirmed a promising material with improved properties such as adsorption, mechanical performance and antimicrobial properties compared to pristine GO or CTS. For instance, Travlou et al. [191] prepared GO-CTS composites through solution mixing. CTS solution with concentration of 2 % v/v was added to 0.3 g GO powder prepared from Hummer's method and 0.05 mol/L glutaraldehyde (GLA) solution. The mixture was stirred for 90 min and its pH was adjusted to pH 9. The adsorption properties of the obtained sorbent were investigated toward a commercial reactive dye. The GO-CTS sorbent had higher adsorption capacity toward targeted dyes compared to pure GO and pure CTS (205, 224, and 277 mg/g for pure GO, CTS, and GO-CTS, respectively). The improvement was suggested to be due to the increase in available adoption sites of GO-CTS. In another approach by same research group (Travlou et al.) [12] GO was functionalized with magnetic CTS in an effort to produce novel sorbents. Magnetic CTS was prepared by dissolving CTS in 2 % v/v acetic acid solution containing magnetic particles ($FeCl_2 \cdot 4H_2O$ (3.5 g), $FeCl_3 \cdot 6H_2O$ (9.5 g)) followed by addition of GLA. The GO powder obtained by Hummer's method was added to the mixture. The final sorbent was obtained by adjusting the pH of the solution, washing and drying the mixture. Adsorption properties were measured using batch adsorption experiments toward a reactive dye (reactive black 5), where 0.020 g of the prepared sorbents were added to different concentration of adsorbate solutions. Based on the adsorption results, GO-CTS adsorbent materials showed higher adsorption

capacities (368-425) mg/g) compared to pure GO (205-299 mg/g) between 25-65 °C. The proposed mechanisms for synthesis of GO-CTS composites was related to the formation of amides as a result of reactions between the GO's carboxyl groups and the amino groups of CTS. Additionally, enhancement of the adsorption properties contributed to formation of composites and increasing the available adsorption sites resulting from the disruptions of some of the material's interior bonds.

Table 2.3. Fabricated GO-CTS composites with various applications.

Material	Application	Ref
GO-CTS	Tissue engineering	[192]
GO-CTS-poly(vinyl alcohol)	Drug delivery	[193]
GO-CTS	Wastewater treatment Smart materials	[194]
GO-CTS	Supercapacitors	[195]
GO-CTS	Water purification (removal of various contaminants)	[142,196]

Other investigations on GO-CTS composites were performed by Kyzas et al. [197] who prepared GO-CTS for adsorption of toxic mercury ions. The preparation of GO-CTS composite was similar to a previous report [191] where uptake properties of the sorbents was evaluated using 1 g/L adsorbent with different concentrations of Hg (II) ranging from 0–500 mg/L at three different temperatures (25, 45, 65 ℃). The adsorption capacity results showed GO increased by 194 mg/g upon addition of CTS for all temperatures. Similar studies have indicated GO-CTS adsorbents to be stable and reusable in multiple adsorption-desorption cycles [44,149] (refer to Table 2.1 and 2.2 for more details on the adsorption capacity for GO-CTS materials). In other approaches, composites of GO and CTS were prepared, and their mechanical properties were measured. For instance, Syuhada et al. [102] fabricated CTS-GO through a solution mixing method using 1000 mg of CTS dissolved in 30 mL of acetic acid solution and added to 0.05, 0.5 and 1 wt. % of GO in a CTS solution. Mechanical property measurements were conducted on GO-CTS films with dimension of 60 mm by 10 mm using a Shimadzu Autograph AG-X universal tester at an extension

rate of 5 mm/min. The tensile stress and elongation at break of CTS-GO composites increased by about 18-50 % and 35-71 %, respectively compared to pure CTS. Similarly, GO powder prepared by Hummer's method was mixed with CTS powder in a ratio of 0.05:1 and dispersed in N,N-dimethylformamide (DMF) solution. The mixture was sonicated to obtain a well-dispersed solution, followed by drying on a flat surface to obtain CTS-GO films. The prepared films with dimension of 75 mm by 4 mm were tested for mechanical properties using a mechanical analyzer (ZWICK ZO 20/TN2S, Germany) under an extension rate of 10 mm/min. Based on the results, the tensile strength, and Young's modulus of CTS-GO films improved by 24 %, and 56 %, respectively compare to pure CTS [9].

2.11 GO-based membranes

GO-based membranes have been prepared in different forms such as self-assembly (free standing) GO sheets, modified and/or supported membranes and thin film composites [198–201]. Several techniques have been explored to prepare GO-based membranes such as filtration-assisted, casting-assembly, layer-by-layer (LbL) assembly, evaporation-assisted and templating [202]. It has been suggested the structure and properties of fabricated membranes can be significantly affected by the preparation method. Despite achievements in preparing GO membranes, resulting membranes are not stable frameworks due to their weak mechanical performance (e.g. for applications where high-pressure operation is required) and their tendency to dissociate in solvents (swelling effect). As mentioned earlier, mechanical performance and stability of GO membranes can be well-maintained and improved via several approaches including chemically cross-linking of GO sheets using polydopamine, metal ions, diamine monomers, glutaraldehyde and polymers [8,179,203,204].

2.12 Summary

The literature review demonstrated pure GO to have a unique structure and its remarkable properties have attracted great attention as a potential material for fabrication of GO-based composites. This chapter reviewed the chemical structure, properties and applications of GO and GO-based composites. Among the available reviews on GO-based materials, there were comprehensive studies lacking on the development of a scalable and stable GO-based composite membrane using readily available cross-linking agents. Also, there is a shortage of comprehensive

studies on the effects of the addition of Al^{3+} ions on the mechanical performance and adsorption properties of GO-based materials toward a model cationic dye such as MB. These redundant research gaps gave the motivation to study the preparation and characterization of GO-based composites for adsorption applications toward dye and gas phase species.

CHAPTER 3: MATERIALS AND EXPERIMENTAL PROCEDURE

3.1 Overview of chapter 3

In this chapter, the materials used and experimental methods followed to achieve the objectives of this research are discussed.

Firstly, the synthesis process of GO powder (from graphite flakes) as the precursor to prepare GO-based composite materials is described. Secondly, GO-based composites prepared using a cross-linking method will be presented. Finally, fabrication of GO-based membranes are explained. Additionally, the techniques used to characterize the fabricated materials are presented. The characterization methods discussed in this chapter are classified into five main categories including; structural properties, physical properties, adsorption studies in liquid and gas phase media, ion permeability test and mechanical properties.

Portions of this chapter have been previously published in the following journal articles:

Sabzevari, M., Cree, D. E., and Wilson, L. D. (2018). Graphene Oxide–Chitosan Composite Material for Treatment of a Model Dye Effluent. *ACS Omega*, 3, 13045-13054.

Sabzevari M, Cree D. E, Wilson L. D. (2019). Mechanical properties of graphene oxide-based composite layered-materials. *Materials Chemistry and Physics*, 234, 81-89.

My contributions to the papers include review of the related literature, design of experiments and data collection (including the preparation of GO and cross-linking GO using two types of cross-linkers), conduct tests, analysis and interpretation of test results for publication. The manuscripts were reviewed by my supervisors, Professor Duncan Cree and Professor Lee Wilson, prior to submission to the selected journals. The excerpts from this article have been used in accordance with the ACS Author Choice License terms of use and Elsevier journal (see Appendix B).

3.2 Materials

The following materials were obtained to prepare GO and its composites. Graphite flakes, 325 mesh, 99.8 % (metals basis) and filter paper (Ahlstrom grade 613, 7.5 cm) were obtained from Alfa Aesar Thermo Fisher Scientific. The graphite flakes were purified by Soxhlet extraction for

24 h using methanol, followed by drying in a vacuum oven at 60 °C for 12 h to remove impurities. Sodium nitrite ($NaNO_3$), potassium permanganate ($KMnO_4$), sulfuric acid (H_2SO_4), hydrogen peroxide (H_2O_2) (30 v/v %), low molecular weight CTS (M_w = 50,000 Da, 75−85 % deacetylation), MB (high purity, biological stain) and aluminum nitrate nonahydrate ($Al(NO_3)_3 \cdot 9H_2O$) were purchased from Sigma-Aldrich Canada Ltd. Methanol was obtained from Fisher Scientific, NJ, USA.

3.3 Synthesis of GO powder

GO powder was prepared using the Hummer's method [38], which is a well-established method for its synthesis. According to this method, the first stage involves intensive oxidation of graphite using oxidizing agents such as $KMnO_4$. To perform this, 4 g of graphite powder was mixed with 100 mL concentrated H_2SO_4 and added into a 500 mL flask contained in an ice bath (low temperature stage) until the graphite powder was mixed well. Then 2 g of $NaNO_3$ was added to the mixture and stirred continuously for 4 h. Approximately 12 g of $KMnO_4$ was gradually added while the mixture was stirred for 2 h and the temperature was maintained below 10 °C. In the next stage, the ice bath was removed, and the mixture temperature was increased to 35 °C using an oil bath (set to this temperature) and stirred for 30 min (medium temperature stage). Subsequently, 240 mL of distilled water was slowly added to the mixture. This reaction was vigorously exothermic and caused the temperature to rise to 90 °C (high temperature stage). After stirring for 30 min at this temperature, 160 mL of water and 30 v/v % H_2O_2 were added to terminate the reaction. To obtain a well-mixed oxidized solution, the mixture was stirred overnight. This stage yielded an oxidized form of graphite. The purification of the GO solution was conducted through multiple washings to remove residual chemicals, contaminants, metal ions and acids. The GO solution was washed using millipore water, HCl (30 %), and ethanol until it reached neutrality (pH 7). At each washing cycle, a centrifuge was used to collect the GO powder. Finally, the GO paste was vacuum-dried at 40 °C to obtain dried GO powder. The steps of the synthesis process are shown in Figures 3.1.

3.4 Preparation of GO-based cross-linked composite powders

In this research, two types of cross-linkers were used for preparation of the cross-linked GO-based composites. The structure and properties for these GO-based systems were explored. The first set

of samples were fabricated using CTS, while the second set of samples were prepared using Al^{3+} ions. The prepared cross-linked GO samples with variable precursors, cross-linker types and weight ratios are listed in Table 3.1.

To fabricate cross-linked GO-based composite materials, the GO solution with a concentration of 1 mg/mL, was initially prepared by dissolving 100 mg of GO powder in 100 mL millipore water.

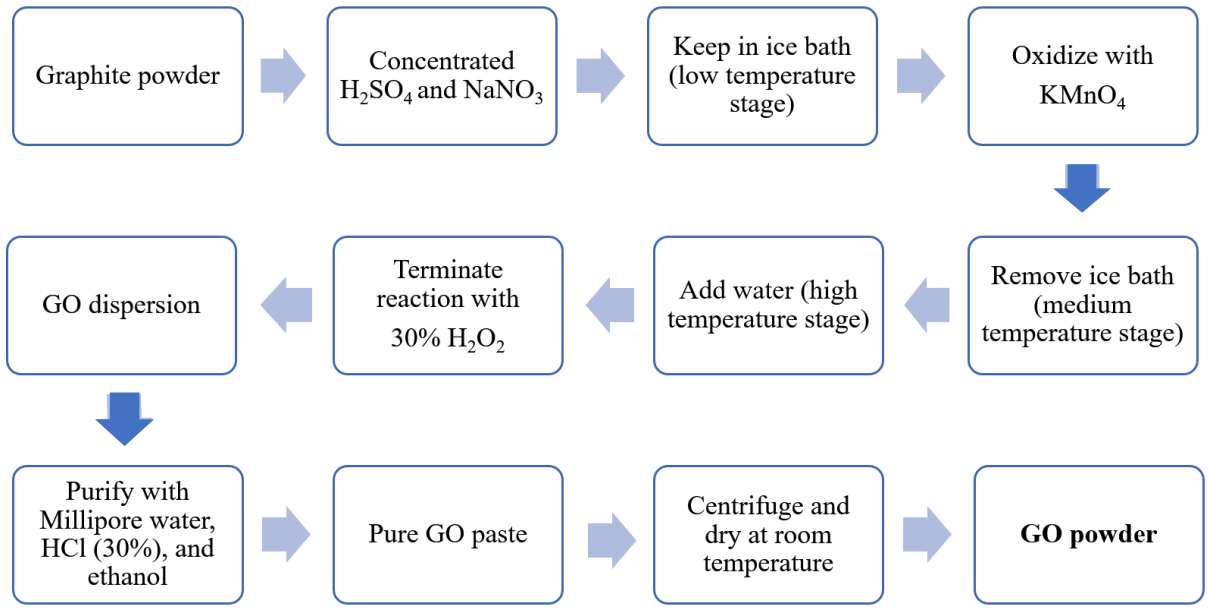

Figure 3.1. Synthesis process for preparation of GO.

For composite materials containing CTS, the CTS solutions were produced by dissolving 0.3 g and 0.6 g of CTS powder in 100 mL of 1 v/v % glacial acetic acid with constant stirring to obtain the 0.3 w/v% and 0.6 w/v% CTS solutions, respectively. Similarly, Al3+ ion solutions were prepared by dissolving 0.3 g and 0.6 g of aluminum nitrate powder in 100 mL millipore water to obtain 0.3 w/v% and 0.6 w/v% Al3+ solutions, respectively. Subsequently, the cross-linker solution was added drop-wise to the prepared GO solution by mean of a 1000 mL burette which was secured to a lab stand using a clamp with the rate of 20 drops/min under continuous stirring for 4 h. Finally, the resulting mixture was washed with millipore water followed by neutralizing the pH from approximately 4-5 to 7 using 1 M NaOH solution and stirring for 12 h. The solution was poured onto a polystyrene container (Fisherbrand medium hexagonal weighing dish,

diameter inner base 47 mm) and dried at ambient conditions for 48 h to obtain the GO and the GO-based composite powders. An outline of the experimental sequence is shown in Figure 3.2.

Table 3.1. The prepared samples with different cross-linker types and concentrations.

Sample ID	GO concentration (mg/mL)	Cross-linker concentration (w/v %)	GO/cross-linker (w/w) ratio	Note
Pure GO-L	1.0	0	0	Low concentration GO without cross-linker
Pure GO-H	3.0	0	0	High concentration GO without cross-linker
GO-CTS-L	1.0	0.3	1:3	GO cross-linked with low CTS concentration
GO-CTS-H	1.0	0.6	1:6	GO cross-linked with high CTS concentration
GO-AL-L	1.0	0.3	1:3	GO cross-linked with low concentration of Al^{3+} ions
GO-AL-H	1.0	0.6	1:6	GO cross-linked with high concentration of Al^{3+} ions

Note: -L and -H denote low and high levels of cross-linking, respectively. In the case of pure GO-L and -H, this refers to dilute and moderate concentrations of GO.

3.5 Preparation of GO-based cross-linked composite membranes

The obtained GO-based composite solutions were used to fabricate freestanding GO and GO-based composite membranes. First, the resulting GO and GO-based solutions were centrifuged and oven-dried at 60 °C for 12 h to initially remove water molecules in-between GO sheets. Then, the resulting paste was sonicated in 40 mL of millipore water to achieve a homogeneous solution. After that, the obtained solution was drop cast on a polystyrene substrate using a 100 mL burette and sonicated for 15 minutes to spread the solution uniformly. Finally, the substrate containing the solution was dried for 24 h at room temperature to obtain membranes with an average thickness ranging from 19.6 ± 1.5 µm to 33.7 ± 1.2 µm. To fabricate defect free membranes, several

substrates including polystyrene, glass, silicon wafer, polytetrafluoroethylene, and plastic paraffin were trial tested. The best method for preparation of robust freestanding membranes was obtained using polystyrene substrates. Figure 3.3 shows membranes prepared by the described method.

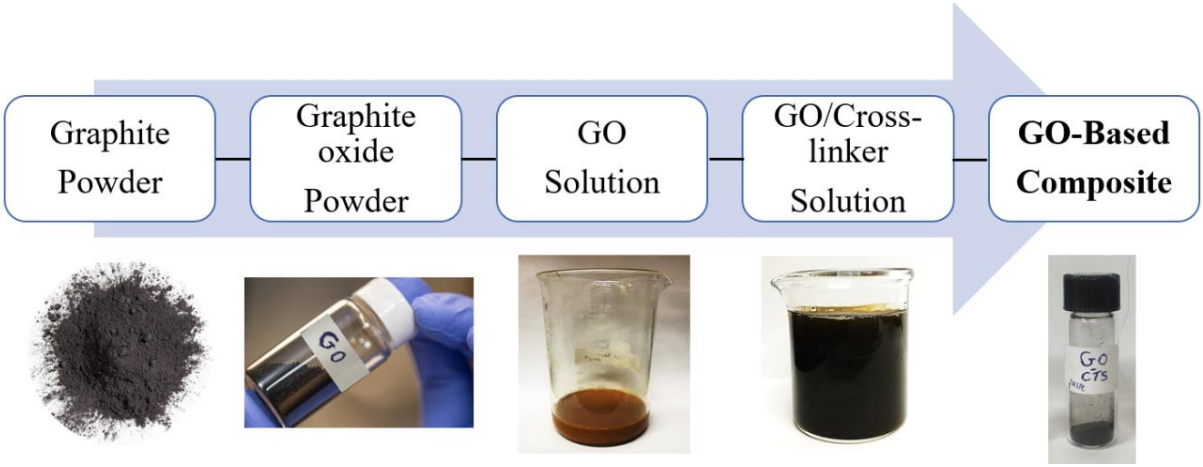

Figure 3.2. Experimental procedure for GO-based composite preparation.

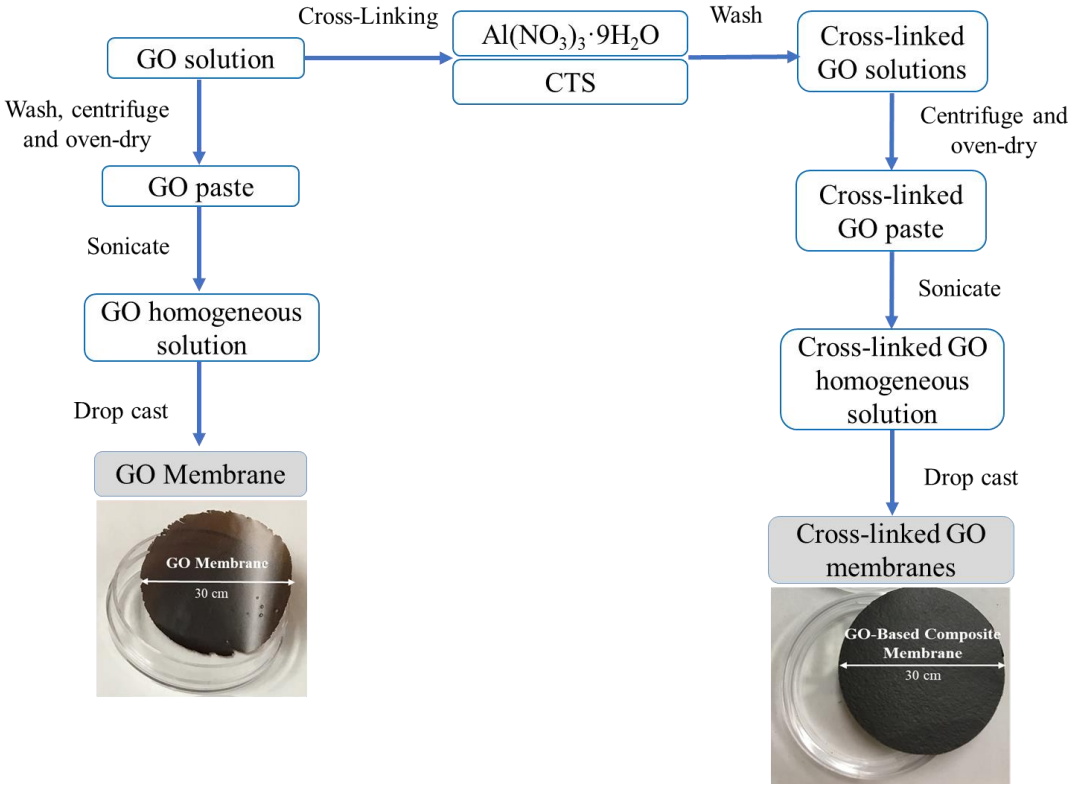

Figure 3.3. Fabrication of GO-based composite membranes.

3.6 Characterization techniques

3.6.1 Surface charge (ζ-Potential) measurement

Zeta potential values provide an estimate of the net charge on the surface of solid or dissolved particles. The point of zero charge (PZC) measurement of a material provides insight and understanding of the properties of colloidal systems such as their tendency to aggregate, adsorption of ions and molecules as well as interaction between particles in solution. In this work, Zetasizer Nano ZS (Nano ZS90, Malvern, UK) located in the Department of Health Science, University of Saskatchewan was used to measure the ζ-potential of the samples. All samples were diluted to 0.01 w/v % and measured in millipore water at different pH values (i.e.,4,5,6,7,8,9,10).

3.6.2 Fourier transform-infrared (FTIR) spectroscopy

FTIR spectroscopy is an analytical technique used to determine molecular components and structures as well as functional groups in molecules. FTIR spectroscopy has been widely used to investigate structure and functional groups present in GO [205–207]. In this work, A Bio-Rad FTS-40 IR spectrophotometer (Figure 3.4), located at the Saskatchewan Structural Sciences Centre (SSSC), University of Saskatchewan was used to obtain the IR spectra of the samples. Prior to performing the test, the powdered samples were mixed with pure spectroscopic-grade KBr (weight ratio: 1:10). The FTIR spectra were obtained in reflectance mode with a resolution of 4 cm^{-1} over a spectral range of 500−4000 cm^{-1}. The obtained spectral results were baseline-corrected and normalized using Origin 2018 peak fitting software by means of 5 points in the range of 500-4000 cm^{-1}.

3.6.3 Scanning electron microscopy (SEM)

SEM is a non-destructive technique used for high resolution imaging of surfaces morphology of materials. This technique can provide surface information over a wide range of magnification from 10× to 500,000×. In this thesis, the Jeol JSM-6010LV SEM (Figure 3.5) at accelerated voltage of 10-20 kV, located in the Department of Mechanical Engineering, University of Saskatchewan was used to observe surface morphology of samples and to measure the thickness of prepared membranes. The samples were gold coated using Edwards sputter coater S150B prior to SEM observation to improve the conductivity of the samples.

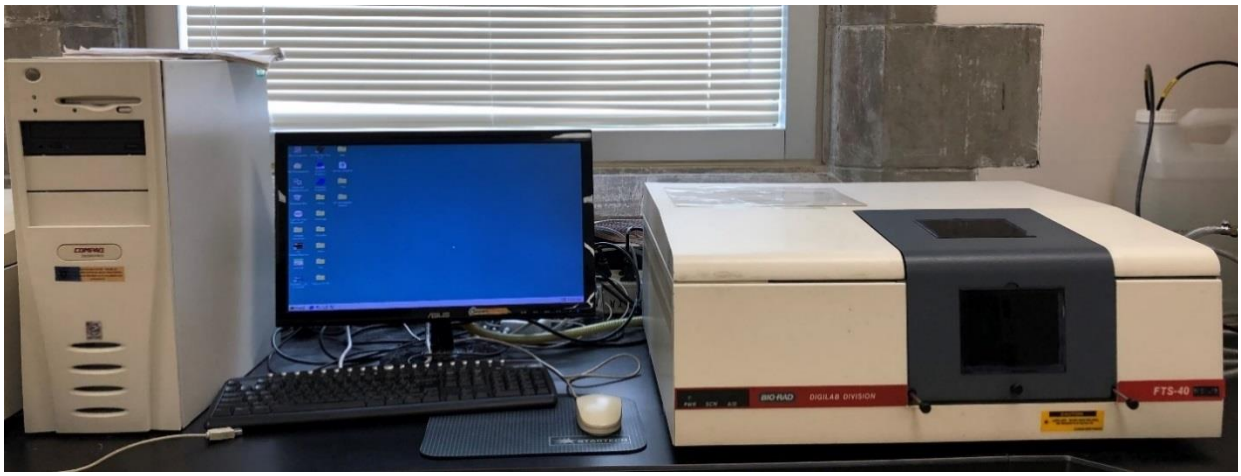

Figure 3.4. Bio-Rad FTS-40 IR spectrophotometer used in this work.

3.6.4 Raman spectroscopy

Raman spectroscopy is a suitable technique for the analysis of carbon-based materials including graphite, multilayer graphene, graphene oxide and carbon nanotubes [208,209]. Graphene derivative materials including GO have been widely studied by Raman spectroscopy to investigate the degree of order-disorder in the structure [210-211]. In this work, the Renishaw model 2000 Raman spectrometer equipped with an inVia reflex optical microscope and a laser excitation wavelength of 514.5 nm, located at SSSC, University of Saskatchewan was used to obtain Raman spectra of the samples (Figure 3.6). The scattering data was collected over the spectral range 3000−100 cm^{-1}. The acquired Raman results were baseline-corrected and normalized using Origin 2018 peak fitting software by means of 5 points in the range of 3000-100 cm^{-1}.

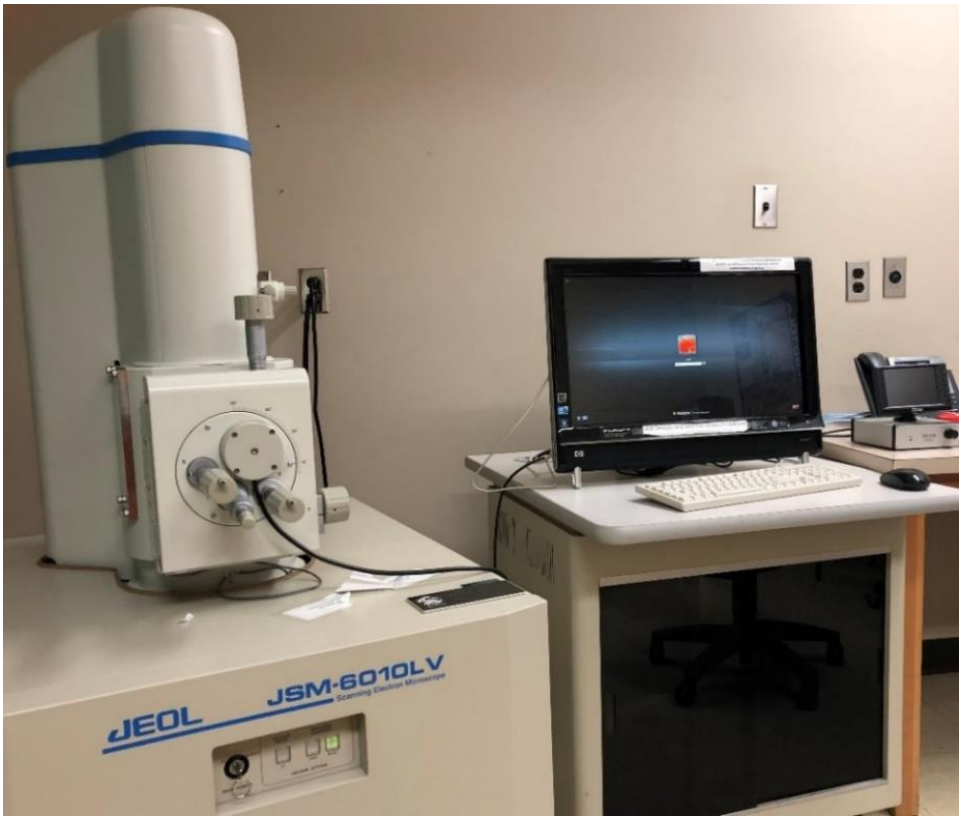

Figure 3.5. The Jeol JSM-6010LV SEM instrument used in this work.

Figure 3.6. Renishaw model 2000 Raman spectrometer used in this research.

3.6.5 X-ray diffraction (XRD)

XRD is a non-destructive characterization technique to obtain information on the crystallographic structure and parameters of materials. Specifically, XRD has been used to measure d-spacing of sheets of graphene derivative materials [212-213]. In this work, the samples were tested using a PANalytical Empyrean powder X-ray diffractometer equipped with a Co source (λ = 1.789 Å, operating at 40 keV, cathode current of 20 mA) and X'Celerator detector, located in the Department of Physics & Engineering Physics, University of Saskatchewan (Figure 3.7). The XRD patterns of samples were measured in continuous mode over a range of 0−40° 2θ, with a scan speed of 335 ms/step (3°/min). The powdered samples were placed in a horizontal mode and mounted prior to the test. The identification of diffraction peaks were evaluated using the Powder Diffraction File (PDF) database and relevant literature using Xpert's High Score software.

Figure 3.7. PANalytical Empyrean powder XRD instrument used in this work.

3.6.7 Thermogravimetric analysis (TGA)

TGA is a technique used to verify thermal stability and decomposition temperature of graphene-based materials [211–213]. In this technique the change in the sample weight is measured continuously as the temperature is increased. In this work, TGA of the samples were obtained using a TA Instruments Q50000IR TGA system, located in the College of Arts and Science, University of Saskatchewan. It was operated using ~ 100 mg of sample which is heated from 23 to 500 °C with a heating rate of 5 °C min^{-1} under a nitrogen atmosphere (Figure 3.8).

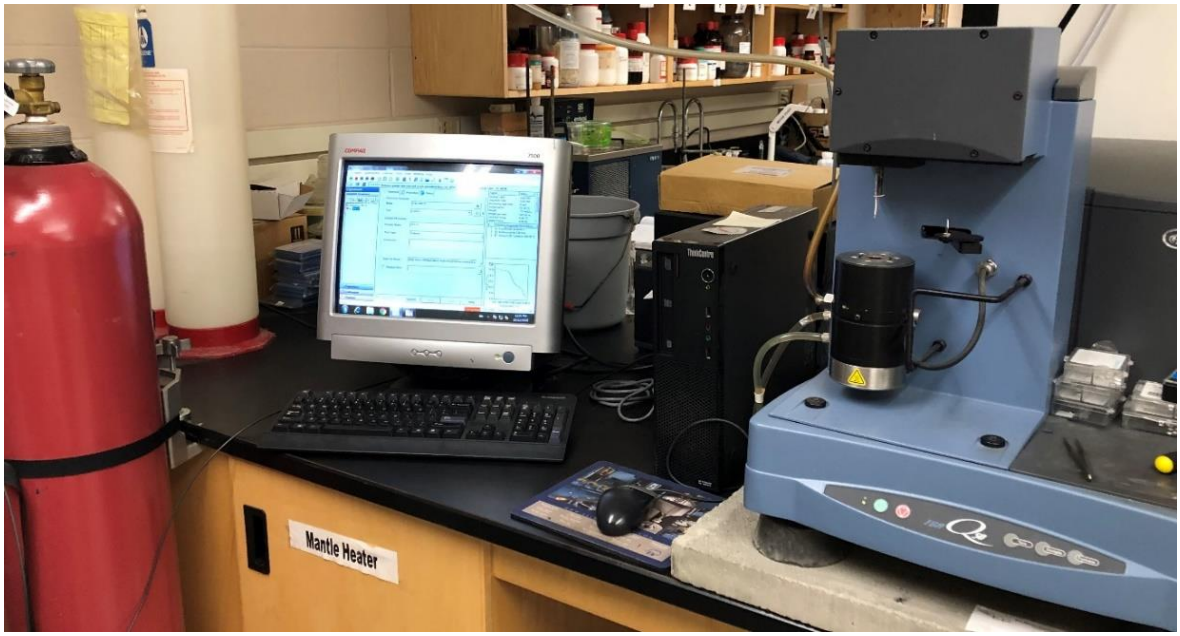

Figure 3.8. TA Instruments Q50000IR TGA instrument used in this work.

3.6.8 Equilibrium swelling properties (solvent swelling properties)

Solvent-based swelling is a key feature of the cross-linked polymer characteristics when it is immersed in a solvent. If the structure of the material network is not broken down in presence of a solvent and only swells, an equilibrium swelling may be reached [214]. In this work, the swelling properties of the samples were studied following ASTM D5229-14 standard [215] by immersing 50 mg of the material in 12 mL millipore water as the solvent and equilibrated in a horizontal shaker (SCILOGEX SK-O330-Pro) for 24 h. The weight of the swollen samples (W_s) was determined by weighing hydrated samples after removing excess surface water with filter paper.

By drying the hydrated samples in an oven at 60 °C, the dry weight (W_d) was obtained and water swelling (S_w) was calculated using equation 3.1.

$$S_w = \frac{(W_s - W_d)}{W_d} \times 100 \quad (3.1)$$

3.7 Dye-based adsorption properties

Dye adsorption using MB offers an effective method for estimation of the SA of graphene-based materials [216,218]. MB used in this research as a model dye exhibited a distinct blue color in aqueous media (chemical structure shown in Figure 3.9). In the case of adsorbates containing chromophores (such as MB), the decrease in the concentration of sorbate (as a result of adsorption by sorbent), can be measured using the optical absorbance properties of the dye adsorbate. The absorption properties of this dye is used to estimate sorption capacity, binding affinity, sorption site accessibility, and SA of the adsorbent phase [217,218].

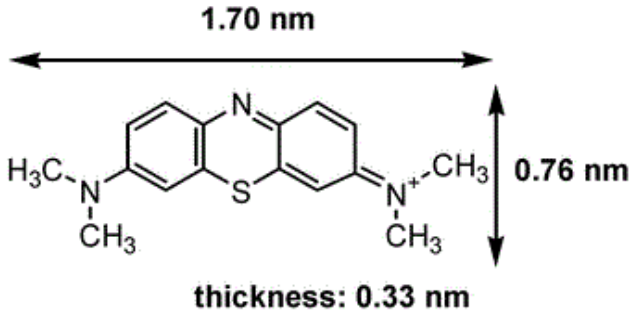

Figure 3.9. Chemical structure of MB [219] .

3.7.1 Equilibrium dye uptake

Adsorption onto solid adsorbents in liquid phase takes place under equilibrium or kinetic conditions. The adsorption process at equilibrium can be studied using a batch technique following ASTM D3860–98 (2014) standard [220]. In this method, the solid adsorbent is immersed into the solution phase containing the adsorbate dye species. The interaction between the adsorbate, solvent, and adsorbent surface occurs until the system reaches equilibrium. At equilibrium, the maximum sorption capacity (Q_m) of sorbent can be evaluated by plotting sorptive uptake capacity (Q_e) vs equilibrium concentration of adsorbate (C_e) in the solution phase, along with analysis of

the isotherm profile using an appropriate isotherm model. Q_e can be estimated using the initial concentration of adsorbate (C_0), equilibrium concentration of adsorbate (C_e), adsorbent mass (m) and volume of solution (V) as given in equation 3.2.

$$Q_e = \frac{C_0 - C_e}{m} * V \quad (3.2)$$

The obtained equilibrium adsorption profiles were analyzed by fitting the adsorption isotherms to various models (Langmuir, Freundlich, and Sips isotherms). After obtaining Q_m values by proper fitting of isotherm profiles, the corresponding SA of the samples in aqueous solution were estimated using equation 3.3.

$$SA = Q_m * N * \delta * Y^{-1} \quad (3.3)$$

In this equation Q_m (mol g^{-1}) is the maximum adsorption capacity at equilibrium per unit mass of sorbent, N (mol^{-1}) is Avogadro's number, δ (m^2) represents the cross-sectional molecular area occupied by MB (δ is 8.72 x 10^{-19} m^2) [221], while the dimensions of the MB are 1.70 x 0.76 nm [221] and Y is the coverage factor (Y = 2.0 for MB) [222].

3.7.2 Kinetic dye uptake

The kinetic adsorption studies also used a dye probe adsorbate, referred herein as the "one-pot" method developed by Mohamed et al. [223] for adsorption processes of nanomaterial sorbents. In this technique, approximately 100 mg of a solid adsorbent is placed into a folded and sealed filter paper (with favourable diffusion processes and negligible adsorption of the barrier material). The filter paper consists of sorbent that is placed into the solution phase containing the adsorbate. Then fixed aliquots of solution are pipetted at variable time intervals. In this condition, the adsorption capacity of the sorbent at variable times (Q_t) can be determined by plotting Q_t vs time and then analyzed using an appropriate kinetic model. Based on a suitable best-fit result, the value of Q_t can be calculated using the initial concentration of adsorbate (C_0), the concentration of sorbate at variable times (C_t), adsorbent mass (m) and volume of solution (V), according to equation 3.4.

$$Q_t = \frac{C_0 - C_t}{m} * V \quad (3.4)$$

The obtained dynamic adsorption profiles were analyzed by fitting the adsorption isotherms to suitable kinetic models (PFO and PSO).

3.7.3 Regeneration study

Regeneration study of an adsorbent is an important consideration for use of a material in wastewater applications because of economic demands and for environmental sustainability [2]. Moreover, facile separation and effective regeneration over multiple adsorption cycles is important adsorbent property for practical applications. The regeneration study of samples was conducted using a mixture of dilute HCl and ethanol (1:1, v/v), to desorb the bound MB dye species. This solvent system represents an inexpensive option for the release of MB and regeneration of sorbent material [224]. The desorption cycle was followed by drying of the material at 40 ℃ for 24 h and repeated adsorption through three cycles of MB adsorption.

3.8 Water vapour adsorption isotherms

The water vapour uptake capacity and SA of the samples were studied by determining the adsorption-desorption isotherms with water vapour. In this work, the Intelligent Gravimetric Analyzer (IGA) system, IGA-002 (Hiden Isochema, UK) (Figure 3.10) located in the thermodynamic laboratory, Department of Mechanical Engineering, University of Saskatchewan was used to investigate water vapour adsorption isotherms. The samples each consisting of 30 mg of the adsorbent was placed in a stainless steel chamber attached to a microbalance under an ultra-high vacuum condition. The reactor temperature was controlled using a water bath. The samples were dried at 60 ˚C in vacuum ($\approx 10^{-8}$ mbar) for 5 h. The IGA system enables a desired partial pressure in the chamber by adjusting the input and output valves. Once the sample mass reached equilibrium at one partial pressure (mbar), the IGA system advanced to a higher partial pressure isotherm in the range of 0 to 30 mbar. The corresponding SA (m^2/g) of the GO-based sorbents in the gas phase was calculated according to the obtained Q_m values of water vapour isotherms by equation 3.5.

$$SA = Q_m * N * \delta * M^{-1} \quad (3.5)$$

Q_m (g/g) is the maximum adsorption capacity at equilibrium per unit mass of sorbent, N (mol^{-1}) represents Avogadro's number, δ (m^2) is the cross-sectional molecular area occupied by water

vapour molecules (δ is 1.08 x 10^{-19} m^2 for a water molecule) and M (g/mol) is the molecular mass (M = 18.01 for water) [225]. The PV of samples was estimated from the amount of gas adsorbed at p/p_o=0.99 where the pores are filled with adsorbed water, and the pores are assumed to be of cylindrical shape.

Figure 3.10. IGA-002 system used for water vapour adsorption analysis.

3.9 Nitrogen adsorption-desorption isotherms

The nitrogen adsorption properties, textural characteristics (e.g., SA and PV) of the samples were determined using nitrogen gas. In this work, a Micromeritics ASAP 2020 (Norcross, GA, USA) instrument (Figure 3.11) located at the College of Arts and Science, University of Saskatchewan was used. All samples were initially degassed at ~100 °C under an evacuation rate of 5 mmHg/s prior to conducting the tests. The SA of samples were obtained from the adsorption isotherm profiles of gaseous molecular nitrogen [226].

3.10 Ion permeability test properties

Ion permeability test characteristics of a membrane is an important consideration for its application in wastewater treatment and water desalination. In this work, the permeability properties of prepared membranes were tested using a 4520 Bench conductivity determination equipped with a glass conductivity probe (Figure 3.12) following ASTM D1125 – 14 standard [227], located in the Department of Chemistry, University of Waterloo, Ontario. The membranes were cut to circular shape with diameters of 25 mm. Prior to the tests, the membranes were soaked in 5 mL NaCl solution for 24 h to ensure the membranes remained stable throughout the test.

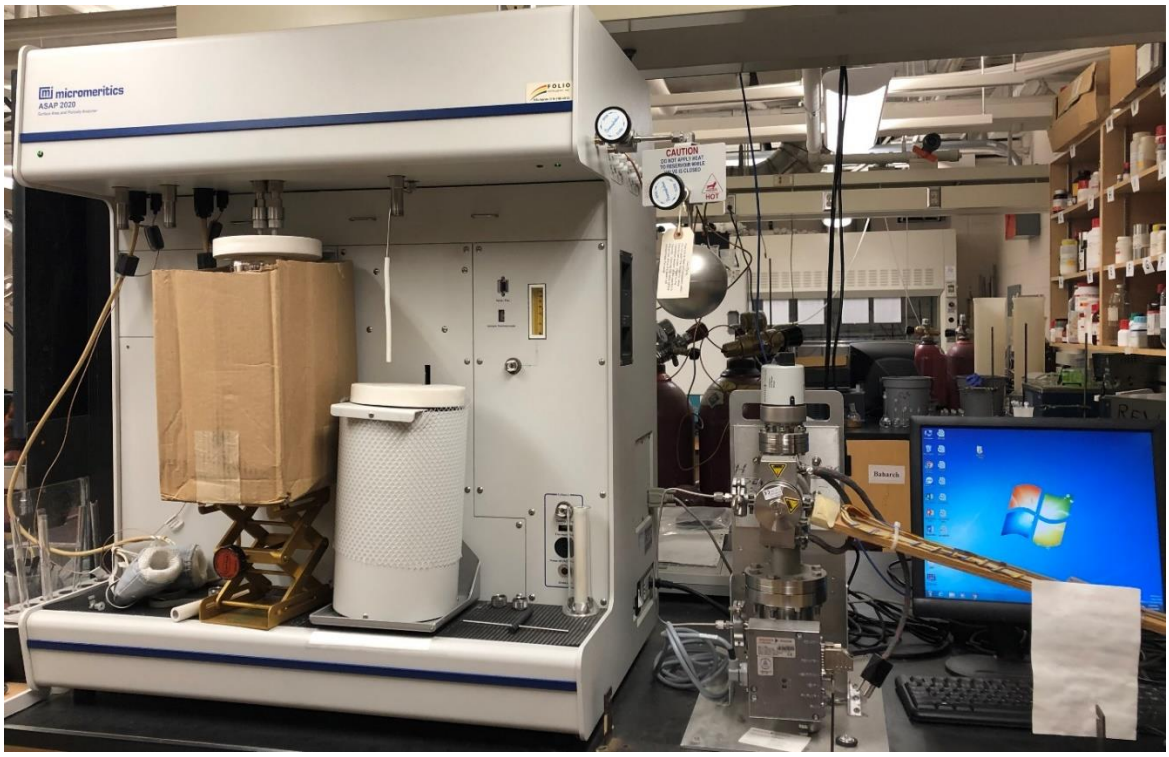

Figure 3.11. Micromeritics ASAP 2020 instrument used for nitrogen adsorption analysis.

The permeation cell is comprised of two reservoirs that are divided by the planar surface upon placement of the prepared membrane in the mid-region of the cell. One of the reservoirs was filled with 5 mL deionized water and the other with either 5 mL of 100 mM NaCl or 100 mM $CaCl_2$ aqueous solutions, respectively. The conductivity of the DI water was measured periodically to observe the increase in its salt concentration as a result of permeation across the membrane over 24 h (1440 minutes). An illustration of the permeation cell is shown schematically in Figure 3.13.

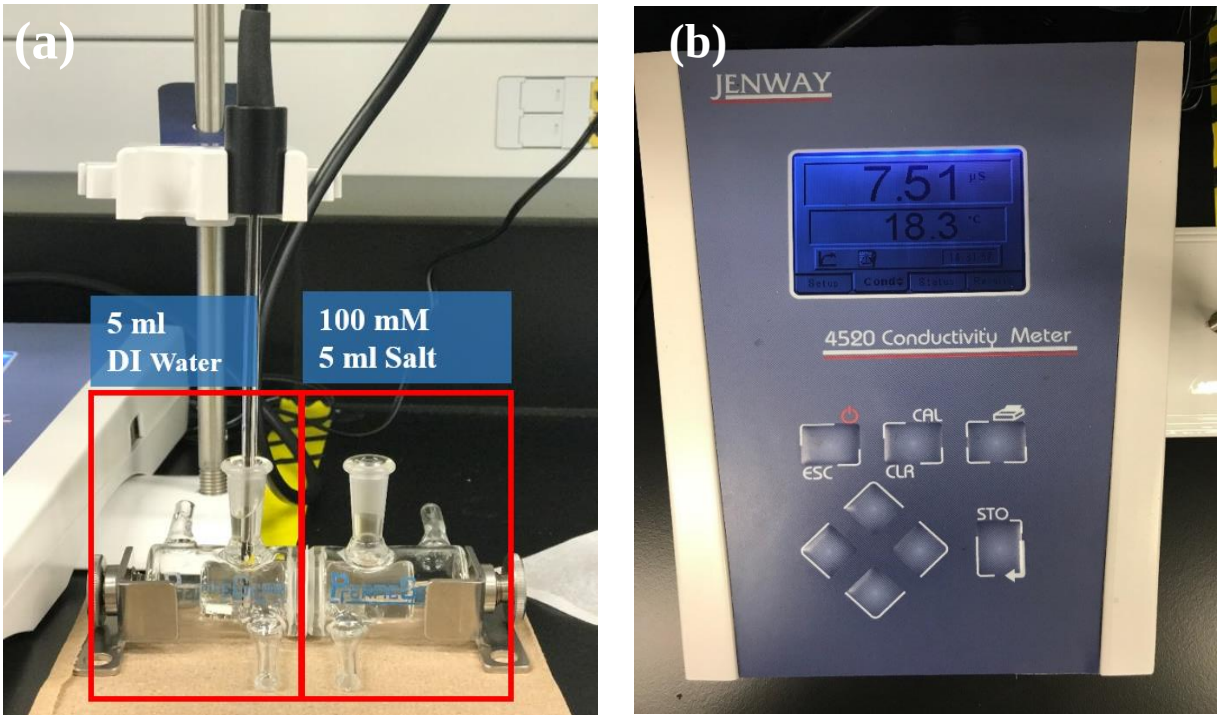

Figure 3.12. (a) Permeability test set up and (b) conductivity meter used for the study of the membrane materials.

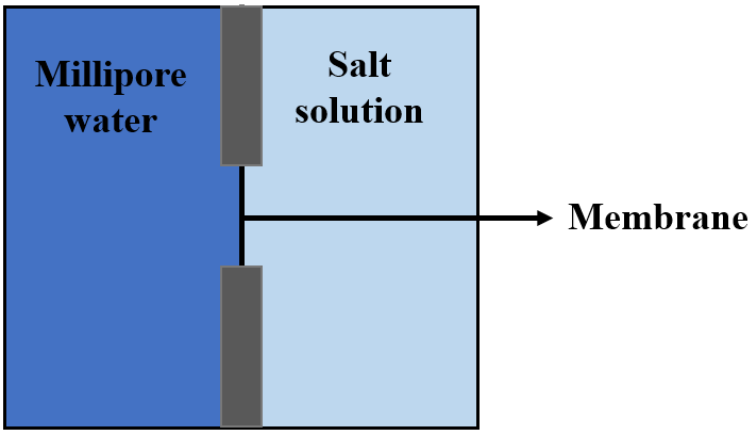

Figure 3.13. Schematic view of the permeation cell used in this work.

3.11 Mechanical properties

Dynamic Mechanical Analysis (DMA) is a technique used to measure the mechanical properties of a wide range of materials. In this work, mechanical properties, such as the tensile strength, tensile modulus and elongation at break of fabricated membranes were analyzed using a DMA instrument Q800, USA (Figure 3.14) located at the Department of Mechanical Engineering at the University of Manitoba. The DMA had a preload of 0.01 N and strain rate of 10^{-5} s^{-1}. The specimens had a gauge length of 16 mm and tested at 295 K with a relative humidity of 40 %. The measurement was repeated three times, and the reported values were the averages of the tests. Rectangular samples with dimensions of 3 mm × 20 mm (width × length) were prepared by compression cutting with a razor blade. The width-to-thickness ratio was controlled to achieve a uniform deformation of the samples.

3.12 Statistical analysis

One-way single factor analysis of variance (ANOVA) [228] was performed to validate the significant statistical differences in measured mechanical properties (including tensile strength, tensile modulus, elongation at break and fracture strength) of GO over GO-based composites with the addition of both Al^{3+} and CTS. The ANOVA F-test calculations were made using Microsoft Excel office 365 2016 with a significance level of 0.05, equal to a confidence level of 95 %. The type of cross-linker (Al^{3+} and CTS) was the variable parameter throughout the measurement. Results assisted to recognize if cross-linking GO with Al^{3+} and CTS can bring a statistical enhancement in mechanical properties.

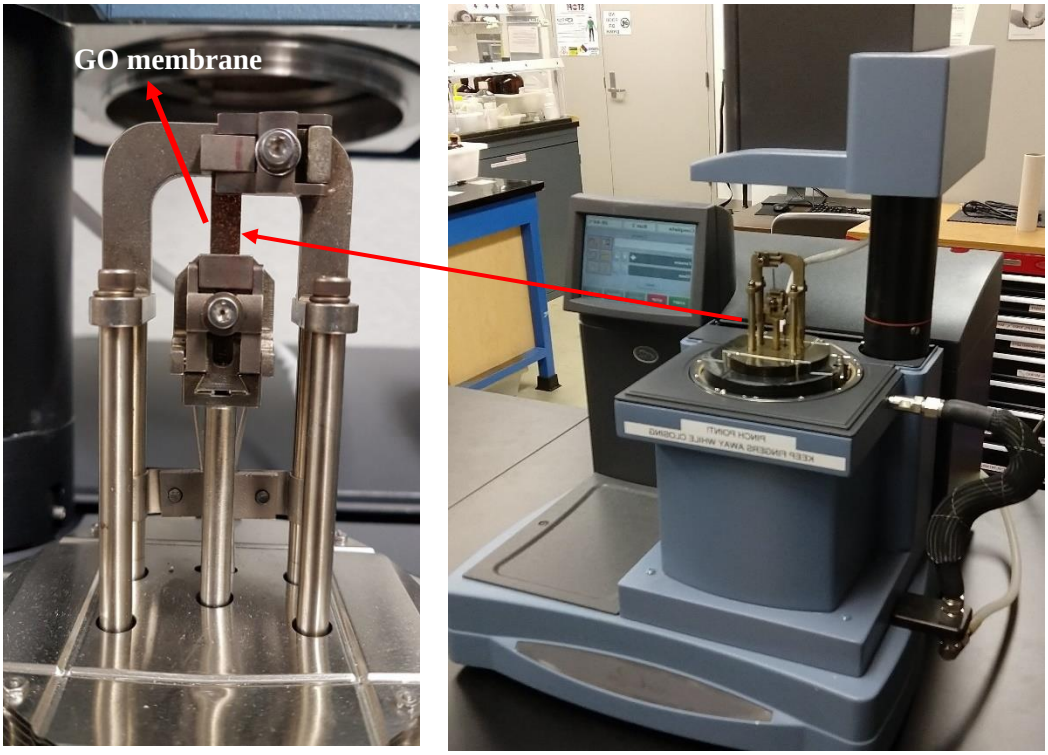

Figure 3.14. DMA analyzer used in this work.

CHAPTER 4: RESULTS AND DISCUSSION

4.1 Overview of chapter 4

In this chapter the characterization results of GO and GO-based composite materials (GO-CTS and GO-AL) prepared from the experimental procedure in chapter 3, are presented. This chapter contains three main sections, where the first part focuses on characterization of prepared materials (structural characterization using spectroscopy techniques and physical characterization). The second part contains results of the adsorption properties of prepared samples in solution and gas media. The third section presents the ion permeability and mechanical properties of samples in the form of membranes. The following chapter has been adopted from either published or submitted manuscripts as the outcome of the current Ph.D. study. For published papers, the copyright permission has been obtained and presented in Appendix B.

4.2 Characterization of GO and GO-based composites

4.2.1 Surface charge (ζ-Potential) measurement

The zeta-potential (ζ) values provide insight toward a greater understanding of the electrostatic attraction between surfaces of a material and other molecules with variable electrostatic potentials. The surface charge of the adsorbent phase (GO and GO-based composites) is likely to influence the adsorption tendency and capacity of the MB cation in solution and gas species with variable polarities (e.g., N_2 vs. H_2O vapour). The surface charge measurement for GO is shown in Figure 4.1 where the ζ-potential of the GO was observed to be highly negative, and this charge decreased continuously with increasing pH from 4 to 10. This observation is consistent with previous literature [229]. The negative surface charge is primarily due to the presence of various functional groups such as −OH and COOH and their ionization state on the GO surface that result from the oxidation process of graphite. Such groups become ionized at higher pH and result in enhanced negative charge [230]. The ionization of carboxylic acid and –OH groups on the GO sheets occurs at pH > pK_a values (pK_a = 4.3) which induce a stable colloidal suspension of GO in polar solvents such as water due to repulsive forces between the GO sheets [229,231]. Accordingly, this will enable individual GO sheets to be readily accessible for cross-linking with different cross-linkers

in aqueous media. Therefore, based on the results, it is recommended to run the cross-linking experiments at any pH above 6. Additionally, it is expected that GO and its cross-linked forms (GO-AL and GO-CTS) will exhibit promising affinity toward cationic species, such as MB, at neutral pH conditions in aqueous media.

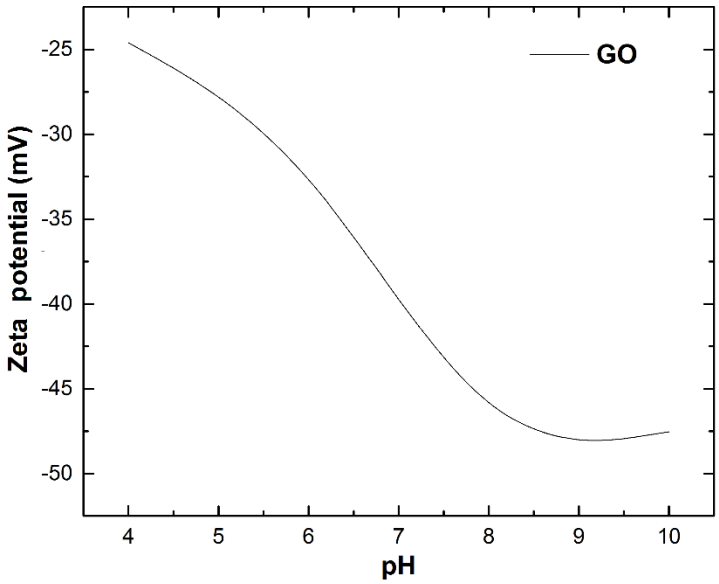

Figure 4.1. The ζ-potential obtained for GO at variable pH.

Figure 4.2 shows the ζ-potential measurement of GO-based composites to further support the formation of the selected composites. While, the surface charge of unmodified GO was negative (-36.5 mV) prior to cross-linking, the ζ-potential of the GO-based composite materials were reduced for GO-CTS (-7.2 mV) and GO-AL (-3.6 mV). The observed variation in ζ-values upon cross-linking of the GO-based composites provided support for the modification of the functional groups on the surface of GO. It has been shown that the formation of electrostatic interactions between the positively charged groups of CTS and negatively charged sheets of GO can decrease the overall surface charge to yield a GO-CTS composite [232,233].

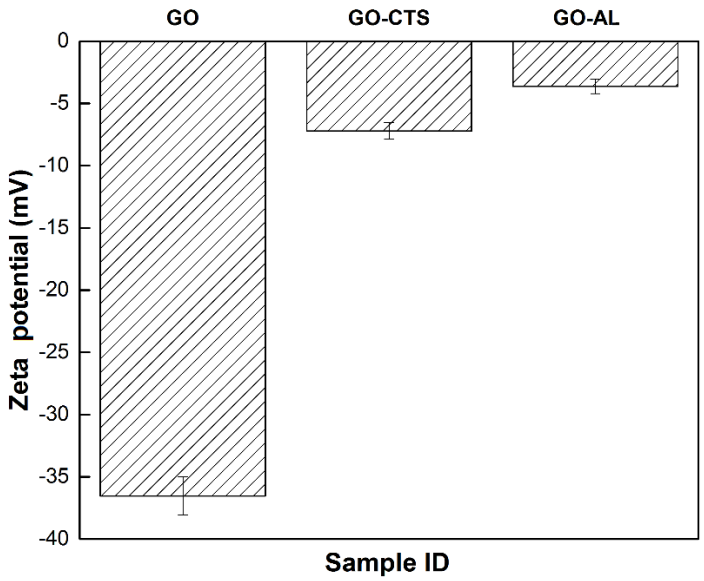

Figure 4.2. The ξ potential obtained for GO and GO-cross-linked composites at ambient pH.

4.2.2 Fourier transform-infrared (FTIR) spectroscopy

Fourier transform infrared (FTIR) spectra were obtained to distinguish the presence of unique chemical bonds and functional groups in GO and to assess changes in these functional groups after cross-linking with CTS and Al^{3+} ions. In Figure 4.3 (a), the FTIR spectra of GO confirmed successful preparation (e.g. oxidation of graphite) by signature IR bands ∼3200−3600 cm^{-1}, ca. 1680-1730 cm^{-1} ca. 1550-1650 cm^{-1}, and ca. 1050-1100 cm^{-1}. These IR bands correspond to the stretching bands of –OH, carbonyls (C=O), C=C vibration of sp^2-carbon skeleton, and C-O-C bond of epoxy groups, respectively [234]. For the IR spectrum of CTS, characteristic bands are centered at 1152 cm^{-1} and 895 cm^{-1} that correspond to IR signatures assigned to the glucopyranose ring unit [235]. Also, the C=O stretching vibration of amide I (NHCO) and amide II (N−H) bending of NH_2 is observed at 1650 cm^{-1} and 1590 cm^{-1}, respectively [236] The presence of the band of both precursors (GO and CTS) is supported by the similar spectral features of cross-linked composite materials. A noteworthy observation for the cross-linked GO composites includes the absence of some bands or changes of intensity when compared to similar IR bands for the unmodified GO. For instance, the CTS glucopyranose band at 895 cm^{-1} was not observed in GO-CTS. The formation of electrostatic interactions between GO and CTS is evidenced by the absence of GO peaks at 1730 cm^{-1}, characteristic of the −COOH moiety of GO, where a greater IR intensity of

the amide II band at 1595 cm^{-1} was observed for cross-linked GO composites [9]. This provides support for electrostatic interactions between GO and CTS, in agreement with a previous report [9]. The cross-linking of GO sheets with Al^{3+} species was further supported by various spectral signatures. A noteworthy observation for the GO-AL composite revealed a reduced C=O band intensity related to C=O groups of GO at 1730 cm^{-1} and epoxy groups at ca.1100 cm^{-1}, when compared to the IR bands of GO described above. This suggests that the functional groups (carboxyl and epoxy) of GO have reacted with Al^{3+} species through a ring-opening reaction. The results concur with corresponding decreases in IR intensity of the bands (ca. 1730 cm^{-1} and 1100 cm^{-1}) in the spectra of GO-AL [11]. The low intensity band at ca. 1380-1410 cm^{-1} is related to the nitrate anion (NO_3^-) signature from aluminum nitrate species, indicating that excess Al^{3+} ions was present to fully coordinate with the COO^- groups of GO. The presence of the nitrate group in the spectra of GO-AL composite suggests the Al^{3+} species were introduced into the GO structure to yield a composite material.

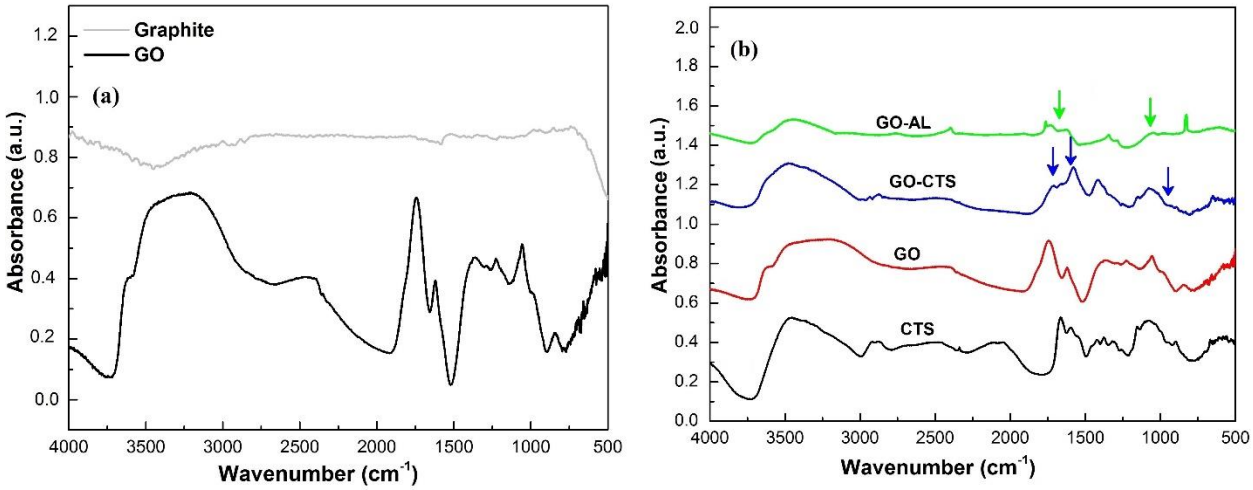

Figure 4.3. FTIR spectra obtained for (a) graphite and GO, and (b) CTS, GO-CTS and GO-AL cross-linked composites.

Figure 4.4 demonstrates structural changes after oxidation of graphite and introduction of oxygen functional groups to the graphitic structure. Changes in the structure of GO after cross-linking with two types of cross-linkers (Al^{3+} ions and CTS) to form a GO-based composite material.

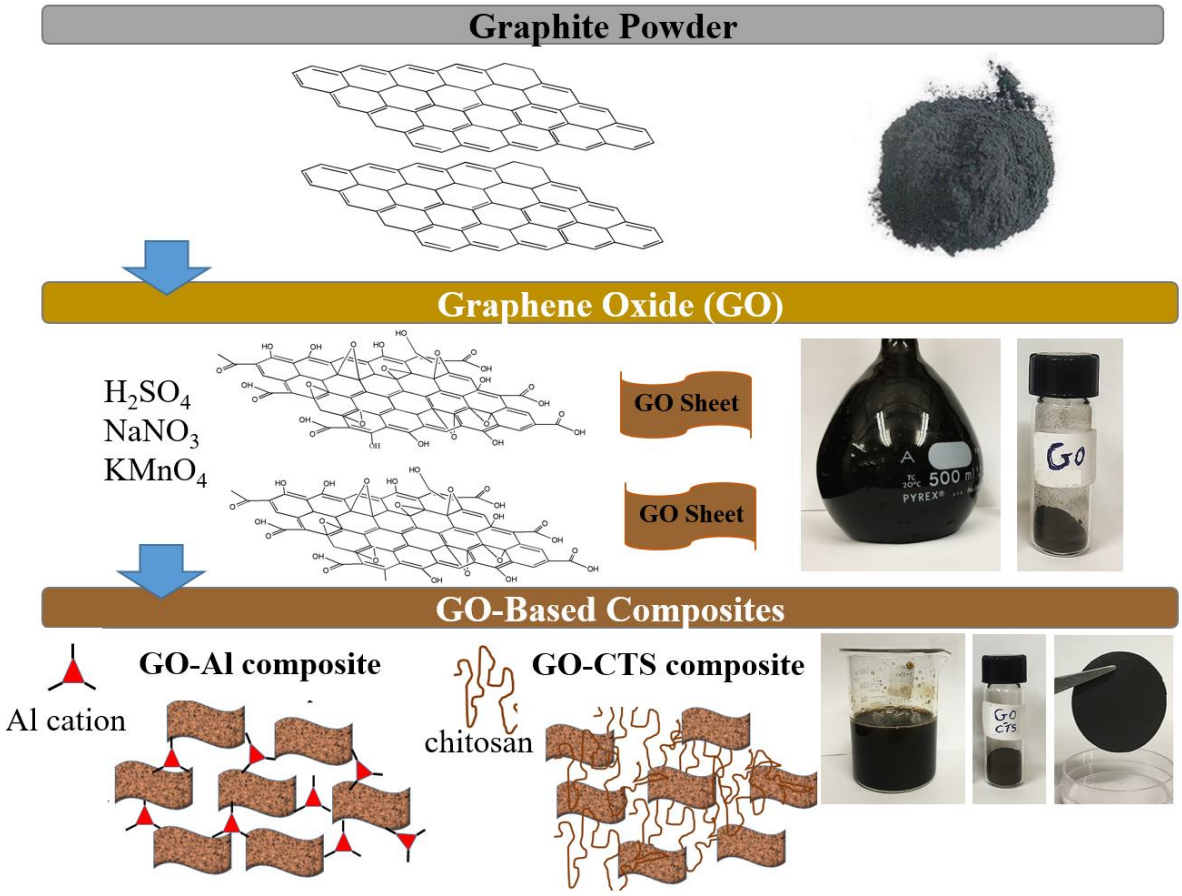

Figure 4.4. Proposed structural changes after oxidation of graphite and after cross-linking of GO with two types of cross-linkers (Al^{3+} ions and CTS) to form GO-based composite materials.

4.2.3 Microstructure

SEM was used to determine changes in the cross-sectional surface morphology and porosity features of graphite, GO and GO-based composites.

SEM micrographs for graphite, GO and its cross-linked form (GO-CTS and GO-AL) powders are shown in Figure 4.5-4.7. As represented in these figures, the SEM images of the graphite (starting material) and the synthesized GO, revealed a densely-layered structure. By comparison, the cross-linked GO composites have wrinkled edges with irregular shapes of dense interconnected layers. The micrographs reveal that cross-linking of GO altered its regular layered morphology according to the cross-linker type. It can be inferred from the SEM results that GO-based composites made

from several two-dimensional GO sheets. The cross-linking of GO sheets with CTS and Al^{3+} ions self-assemble to form a framework structure with higher porosity than either of the precursors.

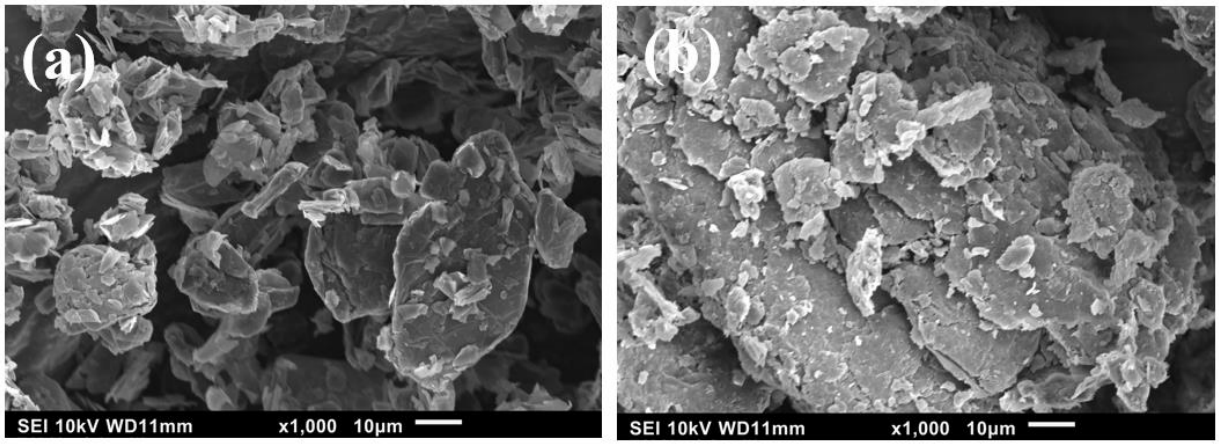

Figure 4.5. SEM micrographs of (a) as-received graphite and (b) synthesized GO.

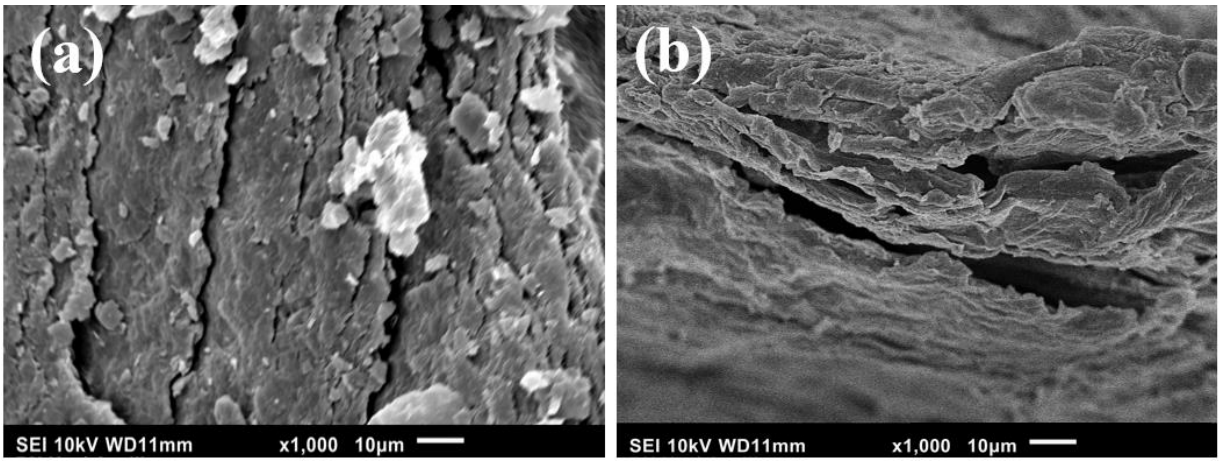

Figure 4.6. SEM micrographs of GO-based materials: (a) GO-CTS and (b) GO-AL.

The cross-sectional morphology of GO and its composites (GO-CTS and GO-AL) in the form of membranes are presented in Figure 4.7. The cross-section of the prepared GO membrane reveals multiple and dense layers of GO sheets stacked in a vertical manner. The cross-sections of both GO-based composites (GO-CTS in Figure 4.7 (b) and GO-AL in Figure 4.7 (c)) somewhat resemble the sheet-like morphology of a GO sheets with some defects and inter-layer spacing. The cross-sections of GO-based composites show an interconnected layered-assembly with wrinkled edges, and layers with irregular shapes. This is probably due to the presence of either CTS or Al (III) species in the 2D plane of the GO sheets. The overall GO sheet thickness and distance between the GO layers increased upon cross-linking, where GO-CTS composites have slightly greater

thickness when compared to a GO-AL composite. The variable morphology and textural changes observed in the GO-based composites provide evidence that cross-linkers (either CTS or Al^{3+} ions) altered the regular inter-layer spacing of GO by inducing void defects or linkages that changed the planar arrangement of GO sheets.

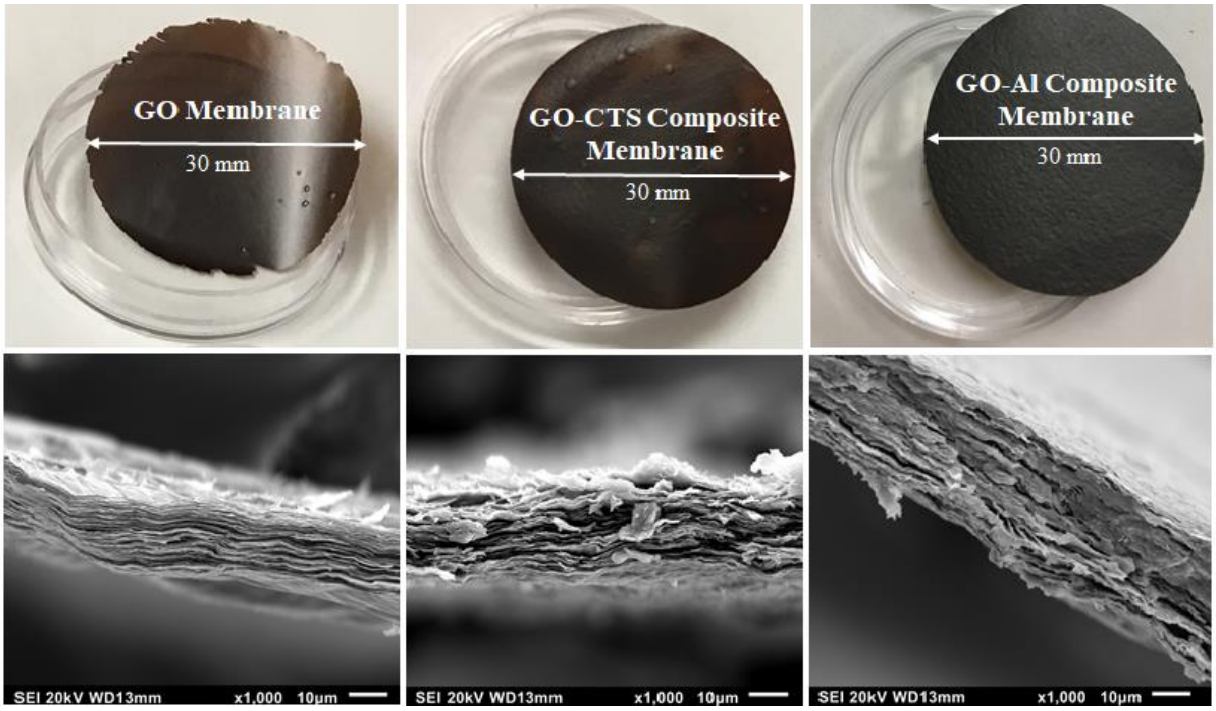

Figure 4.7. SEM micrographs of cross-sections of GO and the GO-based composites membranes: (a) GO (b) GO-CTS and (c) GO-AL.

4.2.4 Raman spectroscopy

The Raman spectra of samples were obtained to monitor changes in the degree of order-disorder of the GO carbon framework structure after oxidation and after cross-linking. The D-band and G-band intensity ratios represent the degree of disorder in the graphene-based structure [237]. The Raman spectrum obtained for GO is shown in Figure 4.8. It consists mainly of D- and G-band signatures at 1350 cm^{-1} and 1580 cm^{-1}, respectively. The G-band is characteristic of sp^2-hybridized carbon networks of graphene sheets, whereas the D-band results are due to structural imperfections created by the attachment of oxygen-based functional groups on the carbon basal plane and its partially disordered structure [238]. In contrast to GO, graphite has almost insignificant D-band because of its highly crystalline structure [239]. Upon cross-linking of GO

with CTS and Al^{3+} species, the intensity of the D-band increased and became broader. Cross-linking of GO led to changes in the D/G band intensity ratio, from 0.98 in GO to 1.16 in GO-based composite with Al^{3+} ions and 1.24 in GO composite with CTS. This variation in the D/G signal intensity ratio corresponds to disruption of the regular GO layer structure upon cross-linking which was greater when GO was cross-linked with CTS than with Al^{3+} species. The greater D/G band intensity ratio could be due to the alteration of the functional groups of GO structure and introduction of defects according to the type of cross-linkers and CTS self-assembly of GO composites [173,240].

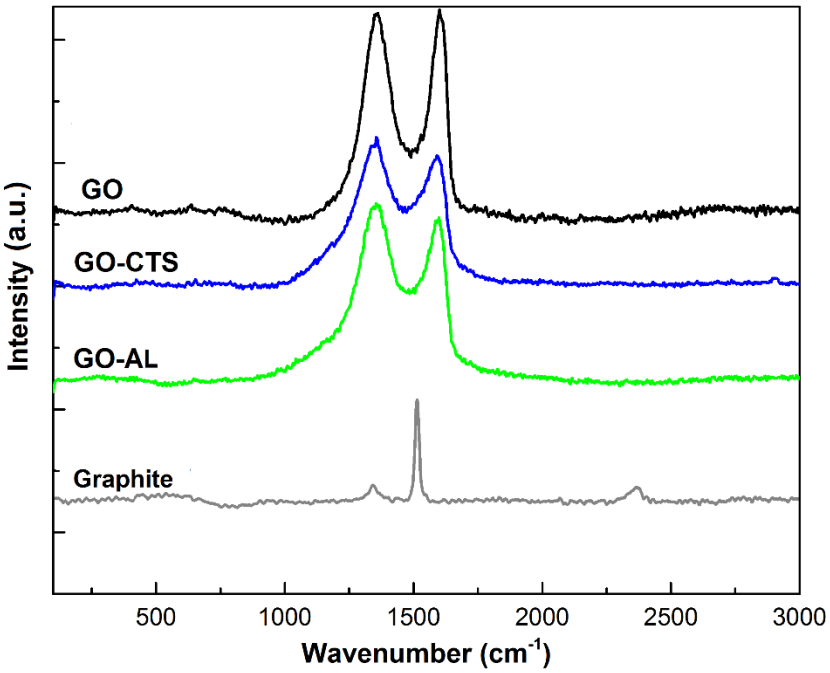

Figure 4.8. Raman spectra obtained for graphite, GO, GO-CTS and GO-AL cross-linked composites.

4.2.5 X-ray diffraction (XRD)

XRD characterization of GO and GO-based composites (after cross-linking of GO with CTS or Al^{3+} species) was used to evaluate the structural order-disorder of the produced samples, as well as monitor changes in the inter-layer spacing of GO after cross-linking. The XRD pattern of graphite given in Figure 4.9 (a) shows a sharp characteristic peak at $2\theta = 31.5°$. After oxidation of graphite and introduction of the oxygen functional groups, the graphitic peak shifts to $2\theta = 13.4°$

as shown in Figure 4.9 (b). The distance between adjacent GO sheets can be calculated according to Bragg's law as 0.77 nm [190,241]. Compared to the GO XRD pattern, GO-based composite materials display a peak shift in the 2θ values of XRD patterns, where 2θ = 10.8 ° and 2θ = 10.4 ° for GO-AL and GO-CTS composites, respectively. Notable shifts in the XRD patterns of GO-based composites imply that d-spacing of GO sheets increased from 0.77 nm in GO to (0.95-0.98) nm. The XRD results provide support that although there is peak broadening in the XRD pattern of GO-based composites with lower crystallinity, the shifting of the XRD band to lower 2θ values indicates an increase in inter-layer spacing of the GO sheets upon cross-linking. This effect provides supporting evidence of intercalation of cross-linkers between the GO sheets upon cross-linking, while maintaining the stacked sheet-like structure of the GO material [104].

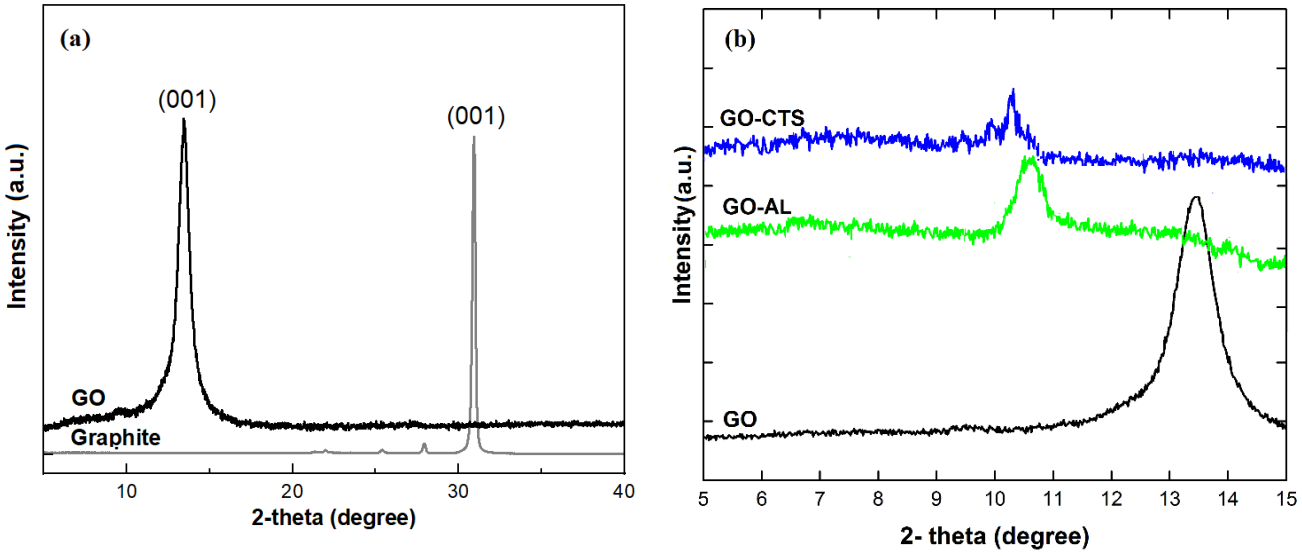

Figure 4.9. XRD patterns of (a) graphite, and (b) GO, GO-CTS and GO-AL cross-linked composites compared with GO.

4.2.6 Thermogravimetric analysis (TGA)

The relative thermal stability and decomposition temperatures of GO and GO-based composites are compared in Figure 4.10. The DTGA curves for GO show a sharp thermal decomposition at ~140 °C. This event is related to decomposition of the GO oxygen functionalities which resulted in a weight loss for the material. Jiang et al. [242] and McAllister et.al. [41] reported that heating GO powder at a heating rate of 1 °C/min generated a considerable amount of heat and gas in the

form of an exothermic reaction which led to the decomposition of the entire GO sample during analysis.

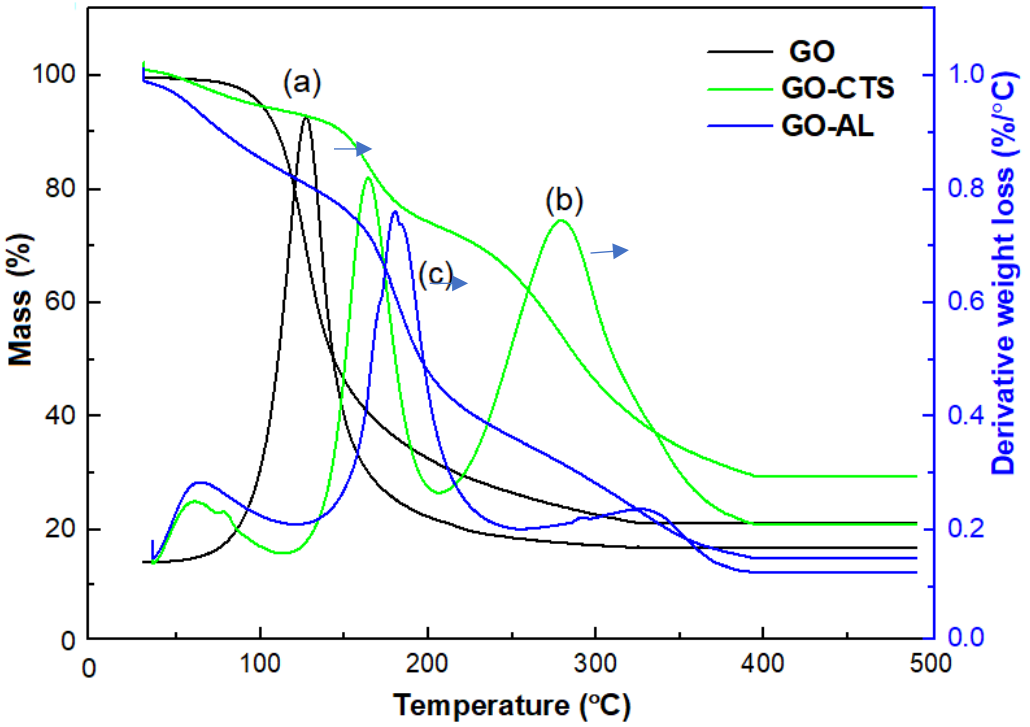

Figure 4.10. TGA and DTGA curves obtained for (a) GO, (b) GO-CTS and (c) GO-AL cross-linked composites from room temperature up to 500 °C.

The TGA curves for GO-based composites show a minor weight loss event between 80-100 °C which relates to the loss of volatiles and/or adsorbed water [243]. The cross-linked GO-CTS material revealed two key thermal events appearing at approximately 155°C and 270°C. These thermal events for the GO-CTS composite are related to the decomposition of GO oxygen functionalities and the CTS backbone [41,244] which yields degradation of the entire GO-CTS framework structure. Furthermore, the GO-AL composite revealed two weight losses which occurred at approximately 200°C and 340 °C due to the decomposition of Al (III) sites along with the GO functional groups resulting in degradation of the GO-AL framework consistent with a previous report on thermal stability of GO-AL composite [11]. The TGA results confirmed the GO-based composite structures (GO-CTS and GO-AL) exhibited a gradual loss profile that started at higher temperatures in accordance with the variable thermal stability due to cross-linking effects. This result suggests the GO-based composite structures had a higher thermal stability than

GO as shown by their higher onset temperatures upon heating to the upper temperature limit (500 °C). GO-CTS and GO-AL composites can be used in applications such as electronic devices and sensors where the temperatures cannot exceed 150 °C.

4.2.7 Equilibrium swelling properties (solvent swelling properties)

Equilibrium swelling and water uptake properties of graphite, GO and the GO-based composite materials were compared in Figure 4.11 and listed in Table 4.1. The material swelling degree (SD) in solvent can be related to the degree of solvent infiltration into the material due to sorption (adsorption and absorption) processes. As represented in Figure 4.11, the GO-based composite membranes were swollen in water but did not dissolve after 72 h under quiescent conditions. The results for GO-based composites (GO-CTS and GO-AL) in Table 4.1 showed reduced SD in water for GO-based composites as compared with pristine GO.

For the GO-CTS composite, this reduction in SD can be related to the reduced number of functional groups (-COOH) on the GO surface due to electrostatic interactions, which is in agreement with the IR spectral results (Figure 4.3). The greater swelling ratio of GO can be attributed to the highly hydrophilic nature of the GO due to its functional groups (e.g., -OH, -COOH, etc.). By contrast, cross-linking GO with CTS decreased the hydrophilic character of CTS, which reduced water penetration. Differences in the hydrophilic character of the GO-CTS and GO network structure accounted for the water swelling of these materials. Similarly, SD was reduced for GO-AL composite materials due to coordination of Al (III) with the GO sheets. In addition, the smaller ionic radius of Al^{3+} versus the CTS biopolymer contributed to variable PV and composite rigidity that tended to affect the SD properties. The greater swelling of composite materials with lower levels of cross-linker (0.3 % w/w versus 0.6 % w/w) are related to the moderate accessibility of functional groups on the surface of the GO sheets (e.g., -OH, -COOH, etc.) that led to greater hydrophilic character. In particular, the SD was reduced for GO-CTS composites and gradually levelled off when the cross-linker content was above 0.3 % w/w. Therefore, greater cross-linking led to reduced swelling [240].

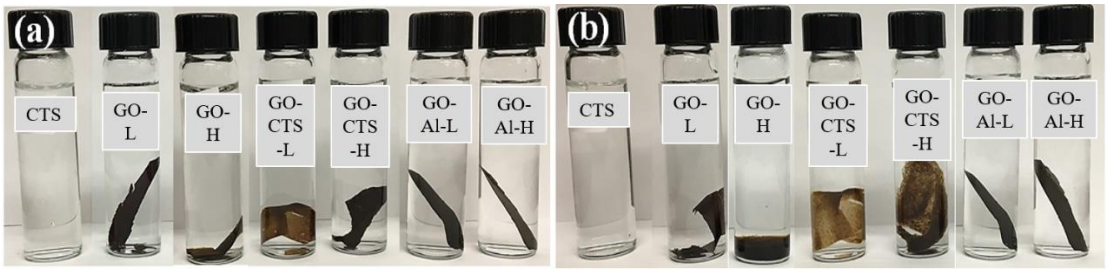

Figure 4.11. Swelling test of GO and GO-based composite materials in water. a) After 24 h, and b) 72 h.

Table 4.1. Water swelling properties of graphite, GO and GO-based composites.

Sample	Swelling %	Comments
Graphite	-	Colloidal solution
CTS	356.5	Colloidal solution
Pure GO	683.3	Partial colloidal solution
GO-CTS-L	394.1	Expanded gel-like
GO-CTS-H	279.2	Expanded gel-like
GO-AL-L	165.4	Stable hydrated film
GO-AL-H	143.2	Stable hydrated film

4.2.8 Equilibrium dye uptake

The adsorption performance and corresponding SA of the samples in aqueous solution were studied by evaluating the MB uptake isotherms at equilibrium and kinetic conditions.

The MB equilibrium optical absorbance properties in solution was used to estimate the uptake properties of GO and GO-based composites, where the greater decolorization of MB solutions during the adsorption process reflected higher MB adsorptive uptake of materials (GO, GO-CTS and GO-AL) at pH ~6. Decolorization of MB solution before and after the sorption process with GO-CTS composites can be observed in Figure 4.13 where a near constant dosage of ~5 mg adsorbent dispersed into 7 mL of MB solution at an incremental initial concentration of MB (100-1000 µM), sample number 1 to 10, respectively. The MB adsorption isotherms and maximum

uptake capacity (Q_m) for the GO and GO-based composites are shown in Figure 4.12. The MB adsorption isotherms were analyzed by fitting the MB uptake results at variable MB concentration at equilibrium. The best-fit sorption parameters were obtained by the Sips model, according to favourable correlation coefficients (adjusted R^2; $0.966 \leq$ adjusted $R^2 \leq 0.978$) listed in Table 4.2. As revealed in Figure 4.12, the materials had an MB adsorption capacity (Q_m) in descending order, as follows: GO-CTS (408.7 mg/g) > GO-AL (351.4 mg/g) > GO (267.1 mg/g). The higher Q_m values of GO-based materials (GO-CTS and GO-AL) over pristine GO can be related to the cross-linking effects where the presence of more adsorption sites favoured adsorption of MB. Cross-linking of GO with CTS and Al^{3+} species contributed to structural changes of the GO framework that enhanced the sorbent-MB interactions. Moreover, the comparative ordering of the MB uptake for GO-based composites can be related to the role of material ζ-values in aqueous media (*cf.* Figure 4.2), where GO-CTS with increased negatively charged surfaces showed a parallel agreement with the trend in Q_m values compared to GO-AL. The higher Q_m values of GO-CTS versus GO-AL are related to the improved interconnected network structure (greater PV) of GO-CTS sheets in the composite, as will be later supported by nitrogen adsorption isotherm results in Figure 4.16. Moreover, CTS as the cross-linking agent was reported to adsorb additional MB in solution via electrostatic interactions [245].

The corresponding SA of the materials was estimated by the Q_m values for MB obtained from the isotherm profiles listed in Table 4.2 (see equation 3.3). GO-based composite materials showed greater SA values compared to pristine GO owing to the effect of cross-linking.

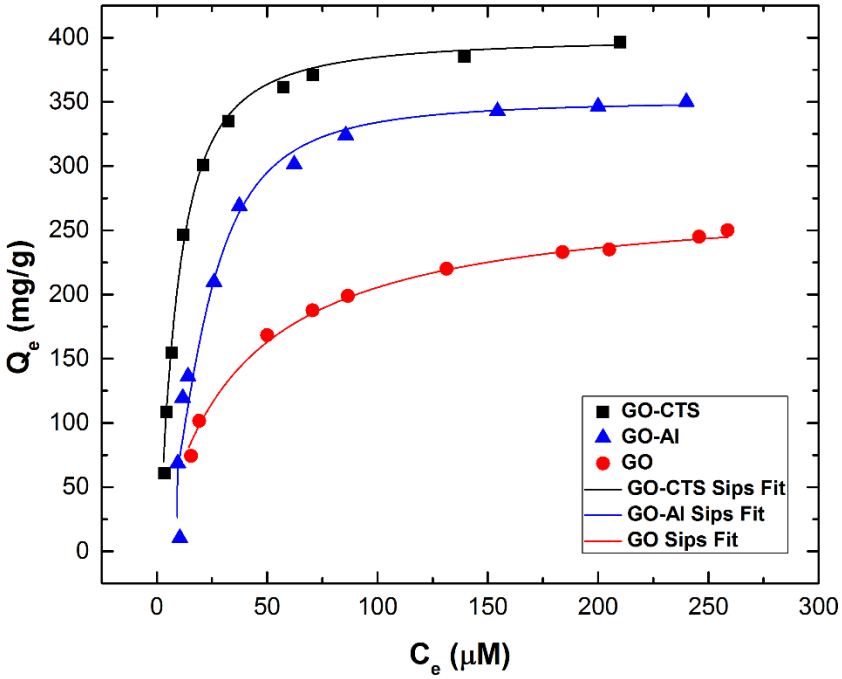

Figure 4.12. Equilibrium isotherm sorption results obtained for MB with GO and GO-based composites, where the solid lines correspond to the best-fit results obtained using the Sips model. [Note: In this plot, Q_e represents sorptive uptake capacity and C_e refers to equilibrium concentration of adsorbate].

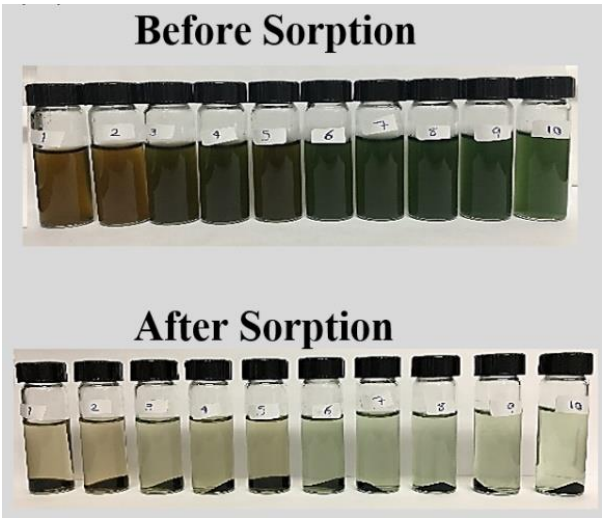

Figure 4.13. Decolorization of MB before and after the sorption process with GO-CTS composite.

The greater MB uptake for GO-CTS and GO-AL versus GO related to the *pillaring effect* of inter-layer spaces between GO sheets [246]. While GO has relatively high SA in its dispersed form, it

is known to undergo aggregation in aqueous solution, lowering the effective MB uptake due to incomplete surface coverage [249]. Cross-linking serves to offset aggregation of GO sheets and stabilizes the GO framework and favours the uptake of MB in aqueous solution.

Table 4.2. The adsorption isotherm parameters obtained from Sips model for GO and GO-based composites with MB.

		Samples		
Adsorbate	Parameter	GO	GO-CTS	GO-AL
MB	Q_m (mg g^{-1})	267.1	408.7	351.4
	K_s (L mg^{-1})	0.028	0.111	0.047
	n_s	1.101	1.341	1.904
	Adjusted R^2	0.966	0.978	0.976
	SA (m^2 g^{-1})	235.7	335.5	288.5

4.2.9 Kinetics of dye uptake

Figure 4.14 represents the kinetic uptake profiles of GO and GO-based composites with MB over a period of 250 min. The results showed an increase in the MB uptake capacity for all materials which occured in the first 40 min. Thereafter, a reduced uptake occurred over an interval of 250 min. The initially higher rate of MB adsorption is attributed to the availability of negatively charged adsorption sites for the dye uptake on the surface of the sorbent materials (GO and GO-based composites). The decreasing rate of uptake after 40 mins relates to the decreasing number of available surface sites as the adsorbent becomes saturated. The GO-CTS contained a more negatively charged surface, in accordance with the ζ-potential values in Figure 4.2 and showed a higher overall MB uptake, while the lower GO-AL uptake is attribute to its less negative ζ-values. The results were analyzed using the pseudo-second-order kinetic model where good agreement with experiments is evidenced by correlation coefficients (Adjusted R^2) near unity ($0.976 \leq$ Adjusted $R^2 \leq 0.994$). According to the best-fit results, the kinetic rate parameters (k_{pso} and Q_e) for GO-CTS and GO-AL materials showed greater MB adsorption over pristine GO. The Q_e (μmol g^{-1}) values for the samples are listed in descending order: GO-CTS (5.54 μmol g^{-1}) > GO-AL (5.05 μmol g^{-1}) > GO (4.17 μmol g^{-1}) where Q_e values increased upon cross-linking. The PSO rate

constant values (k_{pso}; g/µmol. min) followed a similar relative order: GO-CTS (0.015 g/µmol.min) > GO-AL (0.010 g/µmol.min) > GO (0.004 g/µmol.min). The more rapid kinetic uptake of the composite materials provided support that synergistic effects (an effect arising from combination of GO and cross-linkers that yields an effect greater than the individual GO or cross-linker effects) (e.g., higher MB uptake of GO-based composites compared to GO or cross-linkers individually) may occur due to cross-linking between the functional groups of GO and with CTS or Al^{3+}. Cross-linking appears to result in an enhancement of availability of the adsorption sites for uptake of MB, which concurs with greater Q_e values for GO as it undergoes cross-linking. The MB kinetics of the materials provide support that attenuated dye diffusion occurs through the pore network of the framework as the contact time increased, along with a decreased number of available adsorption sites with increasing time.

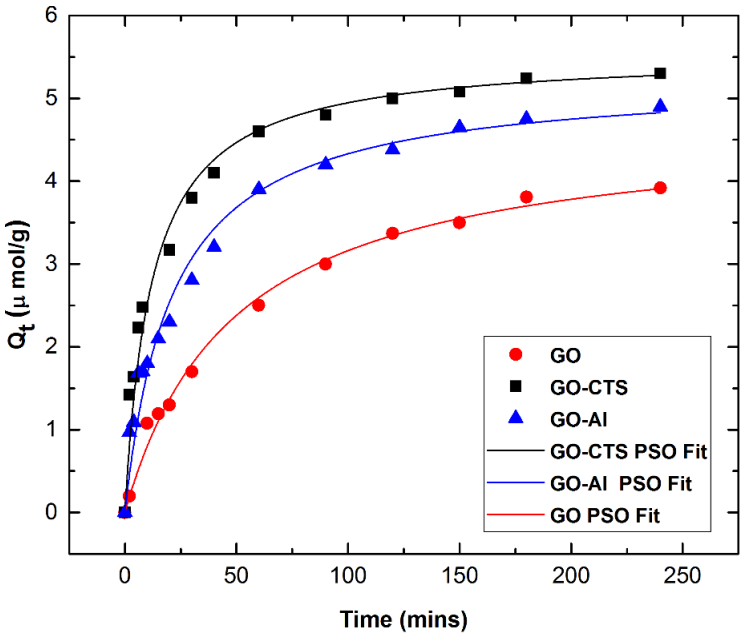

Figure 4.14. Kinetic uptake profile obtained for MB by the GO-based composites, where the fitted lines correspond to the PSO model (see equation 2.5). [Note: In this plot, Q_t represents the sorptive uptake capacity capacities at time t (min)].

Table 4.3. Kinetic parameters for GO-based composites with MB obtained using the PSO model.

Adsorbate	Parameter	Samples		
		GO	GO-CTS	GO-AL
MB	Q_e (μmol g^{-1})	4.170	5.541	5.059
	k_{pso} (g μmol.min^{-1})	0.00435	0.015	0.010
	Adjusted R^2	0.994	0.979	0.976

4.2.10 Regeneration study

As shown in Figure 4.15, the sorbent materials maintained high removal efficiency with MB with a minor decline from the first to the third cycle. After the third cycle, the MB removal (%) is preserved up to a variable extent for the GO-based materials: GO-CTS (88.60 %), GO-AL (86.65 %) and GO (83.85 %). This regeneration study revealed the novel GO-based materials can effectively be regenerated and re-used at least for three adsorption-desorption cycles, in contrast to colloidal GO due to its reduced ease of handling over solid-phase materials in aqueous media.

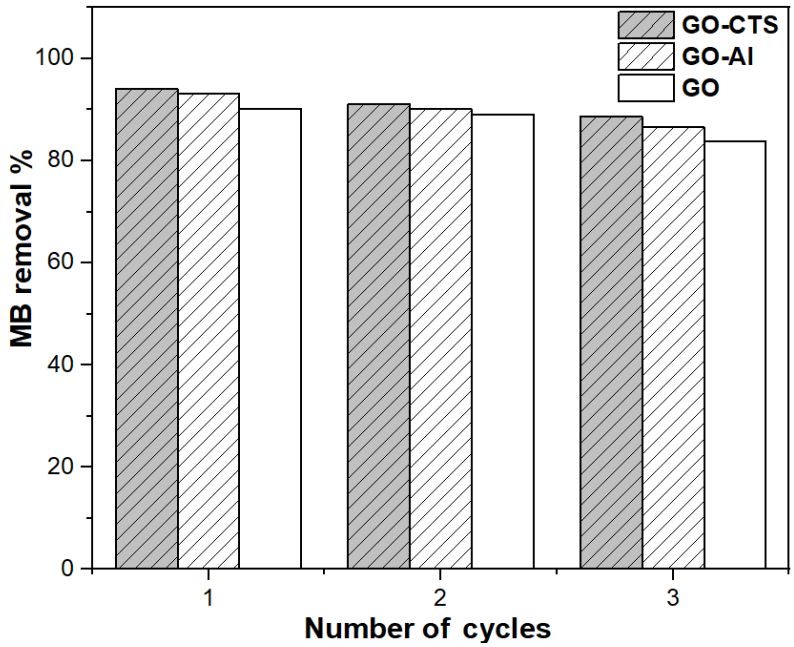

Figure 4.15. Adsorption-desorption cycles obtained for GO and GO-based composites (GO-CTS and GO-AL) for MB systems.

4.2.11 Water vapour adsorption isotherms

The water vapour adsorption-desorption isotherms in Figure 4.16 provide an estimate of the SA and sorption parameters of the GO and GO-based composites are represented as listed in Table 4.4. The GO and GO-based composites displayed a Type II isotherm for the water vapour desorption-adsorption profiles according to the IUPAC classification system [19,250]. The adsorption of water vapour in GO-based composites (GO-CTS and GO-AL) showed similarities related to the composite structure and the role of adsorption sites. In addition, the monolayer saturation adsorption occurred at a low value of $p/p_o \approx 0.3$, where the major amount of vapour uptake occurred at $p/p_o > 0.8$. The water vapour adsorption (w/w %) for the GO and its composites adopted uptake capacities according to the following order: GO-CTS > GO-AL > GO, where it is notable that the GO composites exceeded the pristine GO uptake capacity. This may be attributed to the *pillaring effects* of GO in such framework materials and the presence of cross-linker sites which altered the surface chemistry, and textural properties (surface area and porosity characteristic) versus unmodified GO [246]. It is noted that the water uptake of GO-CTS exceeded GO-AL, which agrees with the higher SA and PV of GO-CTS compared to GO-AL. The enhanced textural properties (PV of GO from 0.53 cm^3/g to 1.97 cm^3/g and 1.33 cm^3/g for GO-CTS and GO-AL, respectively) and presence of sites aided the diffusion of water vapour into the framework structure of GO-CTS more efficiently. The estimated SA and PV of the GO-based composites based on their corresponding vapour uptake exceed that for pure GO, especially for GO-CTS that concur with the adsorption capacity values. However, the estimated SA calculated from vapour isotherms were notably higher than the SA obtained from MB adsorption isotherms. This difference can be related to different surface interactions of each adsorbate with GO and GO-based composite surfaces. MB is a cationic dye likely adsorbed at electron rich domains of the graphene surface via electrostatic interactions. In addition, smaller size of water molecules enables it to access micropore domains of materials that are likely restricted in the case of MB with larger sizes (as shown in Figure 3.15).

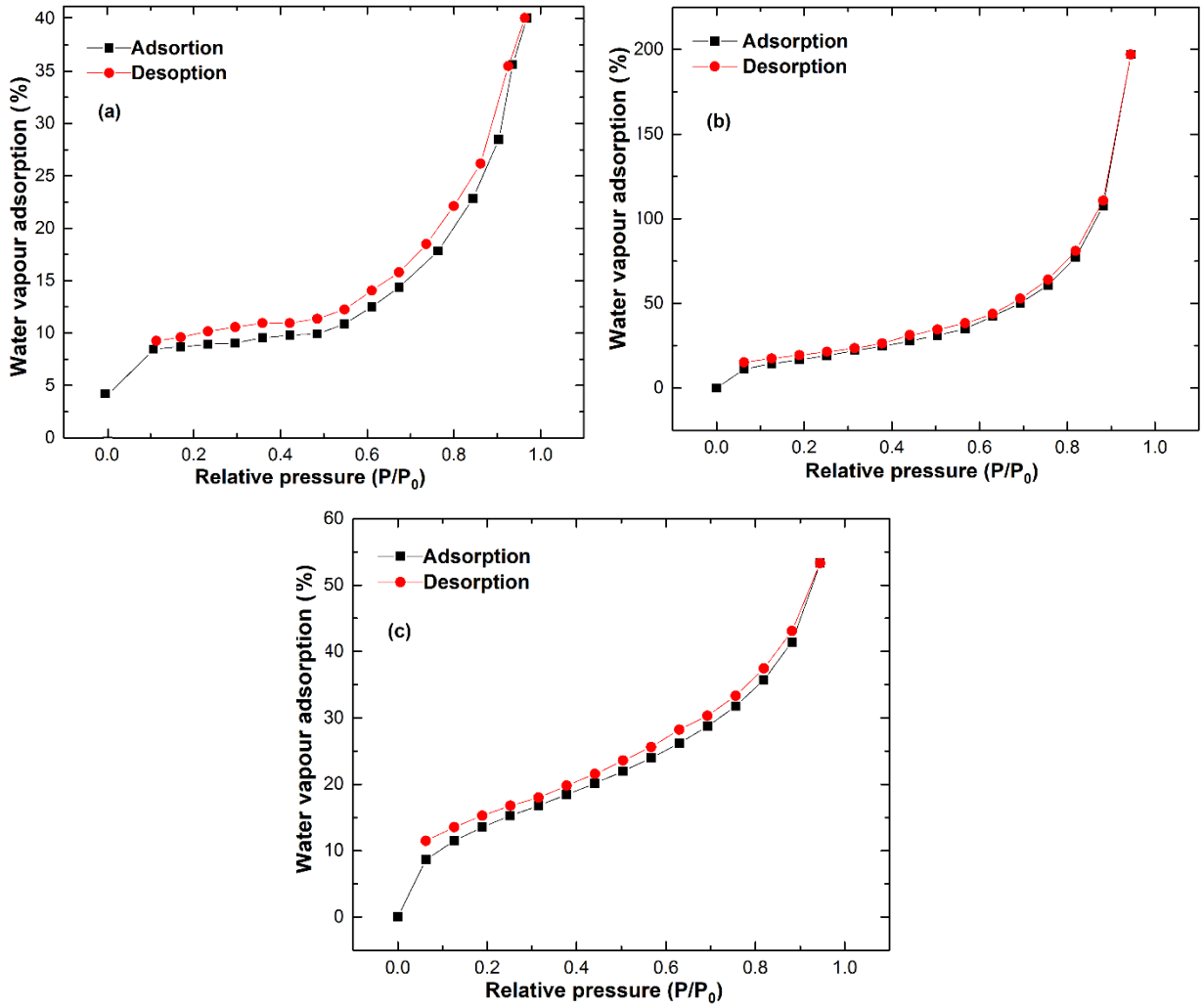

Figure 4.16. Water vapour adsorption isotherms obtained for (a) GO and GO-based composites: (b) GO-CTS, (c) GO-AL. [Note: the solid lines represent a guide to illustrate the adsorption-desorption profile].

The significance of conducting the water-vapour adsorption is to show that the inter-layer distance of GO sheets can be modified using suitable cross-linker for fast transport of water vapour molecules through GO layers. This can be an indication of efficient use of these materials in the field of pervaporation, air dehumidification and desiccant applications. To provide a complementary characterization of GO and GO-based materials toward solution and gas species, the samples were further characterized using a nitrogen adsorption-desorption method.

Table 4.4. Adsorption isotherm parameters for GO and GO-based composites with water vapour.

Adsorbate	Samples			
	Parameter	GO	GO-CTS	GO-AL
Water vapour	Q_m (mg/mg)	11.099	17.539	13.946
	*K_{BET} (L/mg)	0.308	42.925	34.426
	*C_s	1.137	1.273	1.025
	Adjusted R^2	0.993	0.996	0.995
	SA (m^2/g)	408.9	560.9	481.8
	PV (cm^3/g)	0.53	1.97	1.33

*K_{BET} and C_s represent the adsorption constant at equilibrium and adsorbate saturated concentration, respectively.

4.2.12 Nitrogen adsorption-desorption isotherms

The nitrogen adsorption-desorption isotherms of the GO and GO-based composites are shown in Figure 4.17. The SA, PS and PV of the samples obtained from N_2 adsorption isotherms are listed in Table 4.5. The nitrogen adsorption isotherms of GO and GO-based composites follow a Type II isotherm profile [250]. The negligible level of N_2 adsorption by GO provides an indication of the limited inter-layer spacing of GO sheets and densely packed structure of GO which resulted in a reduced PV to the occurrence of adsorption solely at the surface of the powder grains. GO exhibited an increase in N_2 adsorption up to a value for $p/p_o \approx 0.7$ and a hysteresis of $p/p_o > 0.8$. The GO-based composites display a relatively high N_2 uptake where the major adsorption occurred at relatively low values of p/p_o that is characteristic of microporous materials. Cross-linking of GO with CTS or Al^{3+} ions resulted in a composite material with a greater PV and increase in the nitrogen adsorption near a value of $p/p_o \approx 0.8$. Note that the overall uptake of N_2 is much lower than that of MB in aqueous solution or in water vapour. This may relate to the important role of swelling effects of water in vapour or condensed media [251].

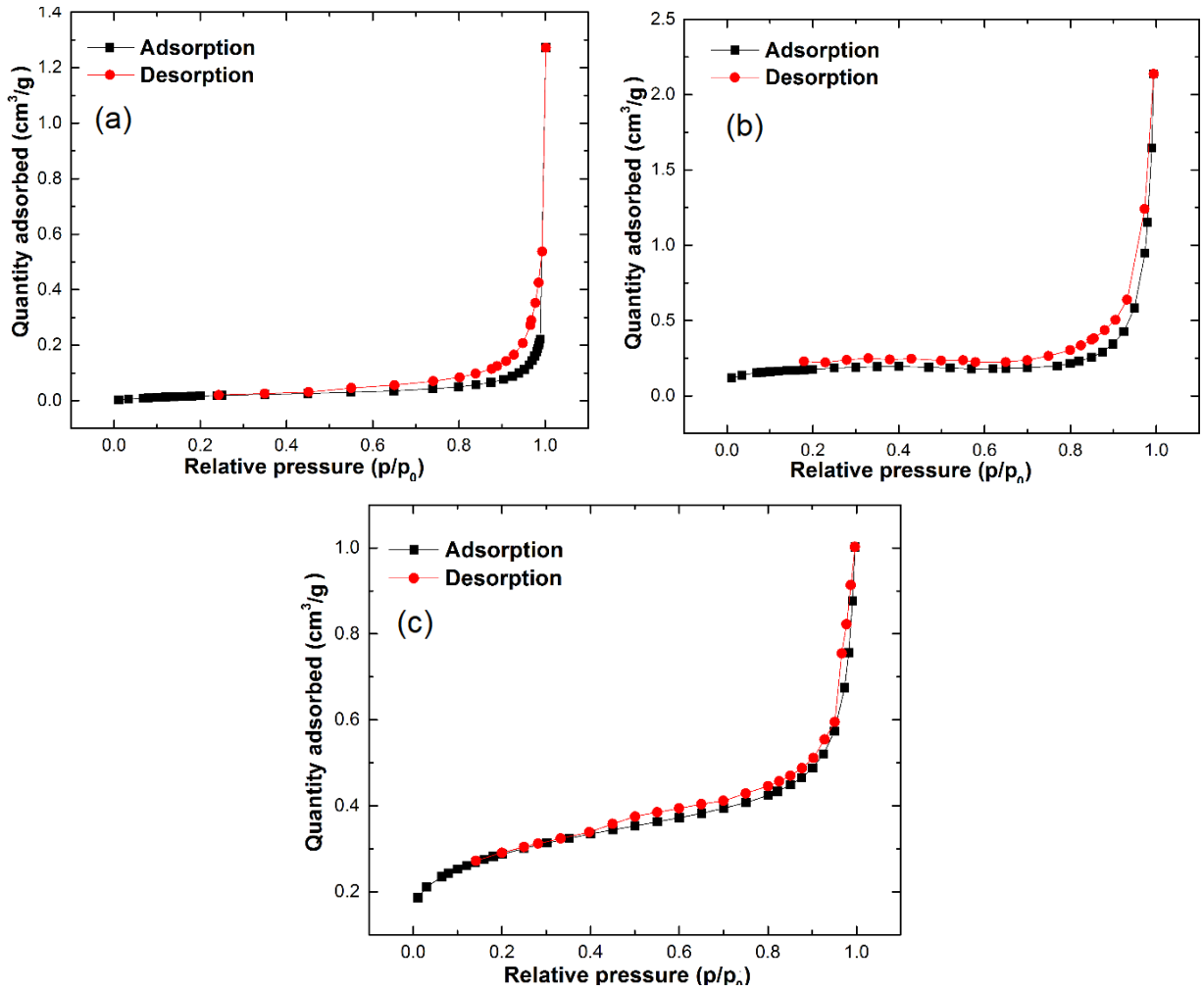

Figure 4.17. Nitrogen adsorption isotherms obtained for (a) GO and GO-based composites: (b) GO-CTS, (c) GO-AL.

The isotherms for GO and its composites revealed differences between cross-linked and pristine GO, as evidenced by differences in the SA, PV and PS. The cross-linked GO samples (GO-CTS and GO-AL) showed greater PV and PS over that of pristine GO. In particular, GO-CTS samples had greater PV and PS. The cross-linked samples of CTS and Al^{3+} cations displayed variable SA (1.24 m^2/g and 1.40 m^2/g, respectively), and variable PS (18.79 nm and 34.90 nm, respectively) values compared to pristine GO. The results agree with the greater PV of cross-linked GO samples (0.83 cm^3/g and 0.76 cm^3/g for GO-CTS and GO-AL, respectively) compared to GO, which are the key parameters for enhanced nitrogen sorption at higher p/p_o values. The high nitrogen adsorption capacities of cross-linked GO samples can be directly correlated to their framework structure with large PV. It is noted that use of CTS as a cross-linker yielded a GO-based composite

with higher porosity (PS and PV) and SA compared to GO-AL. The interconnected network structure between GO sheets in the GO-CTS composite, afforded greater diffusion of adsorbates (MB, water vapour, and N_2).

Table 4.5. Adsorption isotherm parameters for GO and GO-based composites with nitrogen (equation 2.6).

Adsorbate	Samples			
	Parameter	GO	GO-CTS	GO-AL
Nitrogen	SA ($m^{2/}g$)	0.61	1.40	1.24
	PS (nm)	9.66	34.90	18.79
	PV (cm^3/g)	0.19	0.83	0.76

Comparing the SA and sorption capacity of the three samples revealed a greater SA, PV and uptake of cross-linked GO samples. This phenomenon relates the role of cross-linking of GO sheets to provide greater accessibility of active sites in the composites. GO-based materials with tunable SA, PV play a promising role for high pressure adsorption applications in gaseous systems. These trends are in agreement with results observed for MB and water vapour adsorption isotherms for the GO-based materials as shown earlier. This difference in uptake values by other molecules (MB and water vapour) may be attributed to the weak surface interactions of GO and GO-based materials with nitrogen gas.

4.2.13 Membrane ion permeation properties

The GO and GO-based membranes were prepared with different cross-linkers and membrane thicknesses according to the Table 4.6. Prior to the permeation tests, all membranes were soaked in 5 mL NaCl solution for 24 h to ensure the membranes remained stable throughout the diffusion tests. The results shown in Figure 4.18 indicate the pristine GO membranes were not stable, while GO cross-linked composites (GO-CTS and GO-AL) remained stable in the NaCl solutions. According to this observation, the GO-based composite membranes are suitable for further permeation tests. The ion permeation results of NaCl and $CaCl_2$ through GO-based composites are represented in Figure 4.19.

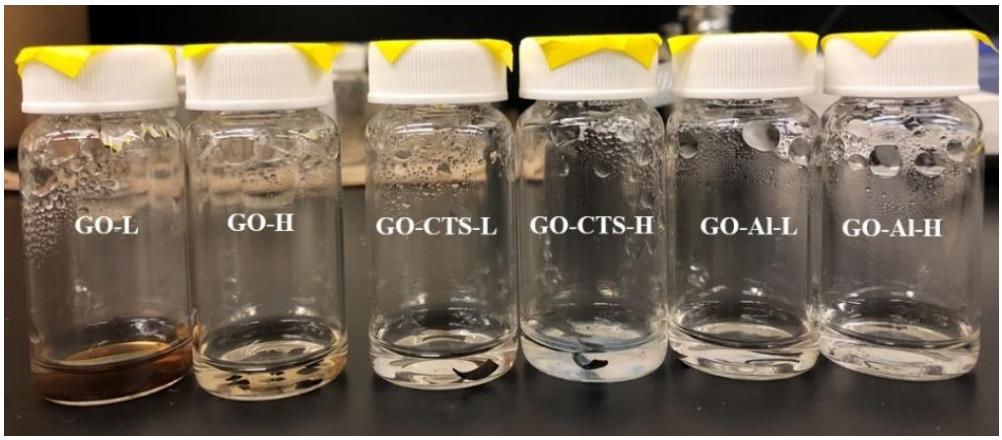

Figure 4.18. Stability tests of GO and GO-based composites.

Table 4.6. Membranes prepared for ion permeation test.

Sample No.	Description	Ave. thickness of composite membranes (μm)
1	Pure GO-L	19.6 ± 1.5
2	Pure GO-H	22.1 ± 1.2
3	GO-CTS-L	29.6 ± 1.6
4	GO-CTS-H	33.7 ± 1.2
5	GO-AL-L	26.1 ± 1.4
6	GO-AL-H	31.2 ± 1.2

Generally, a solution containing electrolyte is remarkably more electrically conducting compared to millipore water at room temperature. Consequently, permeation of ions through the membrane lead to an increase in conductivity of millipore water. Therefore in this test, the increase in the millipore water conductivity due to permeation of the ions across the GO and GO-based composite membranes were monitored. The increase in conductivity of millipore water is proportional to the amount of ions that pass through the membranes. Moreover, it has been shown that ion permeability across a membrane is greatly affected by the existence of free volume (e.g., inter-layer spacing) in the membrane and size of ions that pass through the membrane [252]. According to the change in the inter-layer spacing of GO sheets upon cross-linking with various cross-linkers, it was expected that the cross-linking method could be applied to efficiently control the ion

permeability characteristics of GO membranes. Figures 4.19 (a) and (b) represent the increase in the conductivity of the millipore water for GO-based composite membranes toward NaCl and $CaCl_2$, respectively. According to these results, the ion permeability for both salts (e.g. NaCl and $CaCl_2$) increased gradually for all membranes within 1440 minutes and decreased thereafter due to loss of ion permeability. Specifically, the ion permeability was higher for GO-based samples cross-linked with CTS (GO-CTS-H and GO- CTS-L) which is in agreement with the increased inter-layer spacing of those membranes. GO-based samples cross-linked with Al^{3+} ions (GO-AL-L and GO-AL-H) demonstrated lower ion permeability resulting from reduced ion passage through the membranes. This could be related to reduced inter-layer spacing of GO-AL composite membranes when compared to GO-CTS.

The observed increase in conductivity in the case of $CaCl_2$ was similar for GO-based composite membranes. However, the rise in conductivity for NaCl was higher compared to $CaCl_2$ as a result of higher initial permeation rate for the monovalent ions (e.g., Na^+) attributed to their smaller size compared to Ca^{2+} ions [253]. The cross-linked GO membranes with higher cross-linker content (e.g., GO-CTS-H and GO-AL-H) led to an increase in the permeation rate of ions which can be due to the role of cross-linker type and greater increase in inter-layer spacing of GO sheets. The GO membranes with low Al^{3+} contents showed the lowest ionic conductivity which can be due to the smallest inter-layer spacing between the GO sheets. According to the presented results, the cross-linking method was shown to be a facile technique to effectively control the permeability characteristics of the GO membrane and tailor the properties of these membranes for specific ions for different applications.

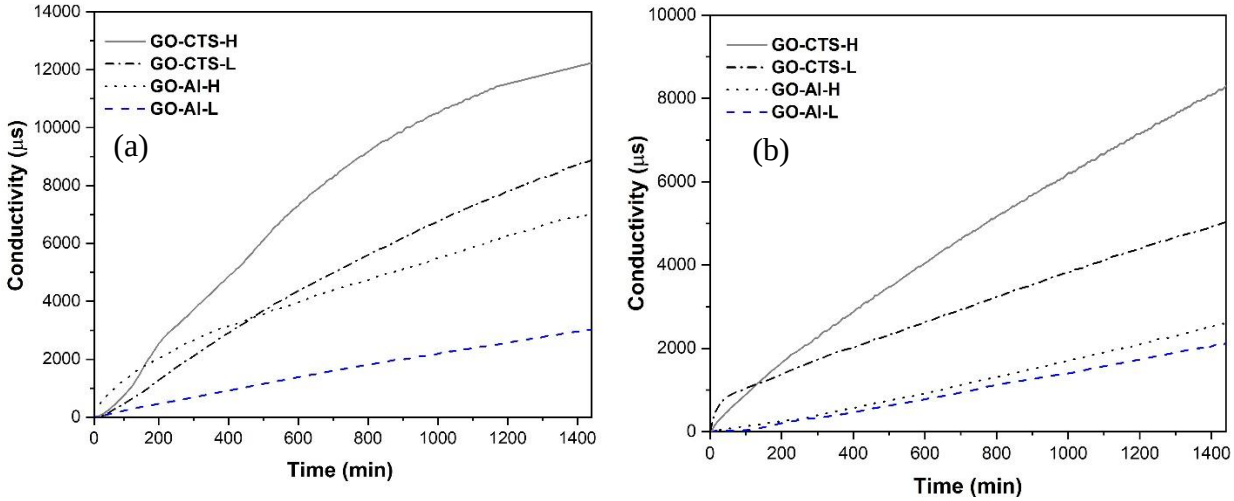

Figure 4.19. Conductivity of water on one side of membrane as a result of permeation of (a) NaCl solution and (b) $CaCl_2$ solution through GO and GO-based composites at room temperature.

4.2.14 Mechanical properties

Although the mechanical properties of GO and GO-based composite membranes have been studied as summarized in Table 4.7, the literature values for GO sheets are wide-ranging for experimental and theoretical estimates. The variability in ion permeability relates to the various fabrication processes and the contents of oxygen-containing groups yielding complex microstructures during GO preparation. Additionally, loading conditions and geometry of the samples may contribute to substantial variations in the measured mechanical properties [254]. The mechanical properties of GO and GO-based composite membranes cross-linked with CTS and Al^{3+} ions were evaluated and compared.

Stress-strain behavior of pristine precursors (GO, CTS) and GO-based composites (GO-CTS and GO-AL) with various cross-linker contents (w/v%) are shown in Figure 4.20 and their corresponding properties (tensile strength and tensile modulus) are shown in Figure 4.21 (a and b).

In Figure 4.20 (a), GO membranes with two thicknesses (GO-L and GO-H) had a tensile strength in the range of 14.76-15.93 MPa and a tensile modulus of 0.37-0.41 GPa. As well, the pure CTS membrane had a tensile strength and modulus of 10.27 MPa and 0.36 GPa, respectively. In Figure 4.20 (b), the GO-based composite membranes revealed higher values of tensile strength, tensile

modulus, elongation at break (ductility) and fracture strength. For instance, the GO-based composites containing 0.3 w/v% CTS had an elongation at break that increased substantially relative to the pristine precursors (GO or CTS). The tensile strength, tensile modulus and elongation at break of the GO-CTS-L are 30.11 MPa, 0.67 GPa, and 1.68 %, respectively. By comparison, the values of GO-AL-L composite are 26.18 MPa, 0.56 GPa, and 0.46 %, respectively. Therefore, with addition of 0.3 w/v% CTS and Al^{3+} ions, the tensile strength of pristine GO membranes increased by 101 % and 74 %, respectively, while the tensile modulus improved by 58 % and 33 %, respectively, as compared to the pristine GO. Moreover, the addition of 0.3 w/v% CTS and Al^{3+} ions had a greater effect on the ductility (elongation % at break) of the GO membrane by 290 % and 7 %, respectively compared to pristine GO.

Table 4.7. Literature comparison of mechanical properties of GO produced in different forms.

Material form	Thickness (µm)	Tensile modulus (GPa)	Tensile strength (MPa)	Measuring technique	Ref
Single-layer GO sheet	0.0007	208	77	Atomic force microscopy (AFM)	[81]
GO papers	1-30	32	15 -133	Dynamic mechanical analyzer (DMA)	[82]
GO films	0.055	695-697	8-11	Nanoindentation	[91]

GO membranes were brittle and tended to disintegrate in aqueous media (*e.g.*, water). However, GO-based composite membranes yielded more stable membranes, where the flexibility and brittleness were amenable for tuning of its properties, according to the relative composition of GO and cross-linker type. This effect provides an indication that the formation of stable interactions occurred between individual GO sheets (via cross-linking) that can significantly change the mechanical behaviour of the GO-based composites at different stress levels. The membrane flexibility and tensile strength of GO was enhanced by the addition of cross-linker. Furthermore, the enhanced tensile strength and fracture strength of GO-based composite membranes are ascribed to the planar structure of graphene sheets which directs the rearrangement of either CTS

and/or Al^{3+} ions during tensile deformation, as illustrated by the structural model in Figure 4.22. The enhancement in properties was observed to depend on the relative cross-linker content. For instance, the introduction of 0.6 w/v% of cross-linkers (CTS or Al^{3+} ions) in the GO led to a tensile strength of 36.99 MPa and 27.34 MPa for GO-CTS-H and GO-AL-H, respectively. This was an enhancement of 146 % and 83 %, respectively, while the modulus increased by 64 % and 41 %, respectively. The greater tensile strength of GO-CTS composite membranes related to the dispersion of CTS in the GO matrix and the bonding between the components. This effect produced a robust interfacial region that enhanced the tensile strength of the GO membranes. On the other hand, GO has hydrophilic groups (e.g., –COOH and –OH) attached to its surface that imparts negative surface charges when dispersed in solvents [104]. This tends to induce a great dispersion of individual GO sheets in water. Cross-linking between GO and CTS can notably increase the mechanical properties, as depicted in the proposed model in Figure 4.22.

In the case of GO-AL composites, the introduction of a metal cation species may result in covalent and/or ionic bonding between the COOH and –OH groups of the GO sheets. This results in a co-dispersion of bonded GO-metal ions, as illustrated in Figure 4.3. GO membranes modified with CTS (GO-CTS) had higher tensile strengths and greater elongation at break compared to GO-AL composite membranes. The elongation at break for GO membranes with 0.6 w/v % CTS increased by about 200 % in comparison with GO, while GO-AL containing 0.6 w/v % AL cross-linker increased by about 15 %. Moreover, the anionic nature of GO and polycationic nature of CTS resulted in favorable electrostatic attraction and reduced chain segmental mobility. This phenomenon which led to enhanced tensile properties is in agreement with other reports on GO composites [104,255].

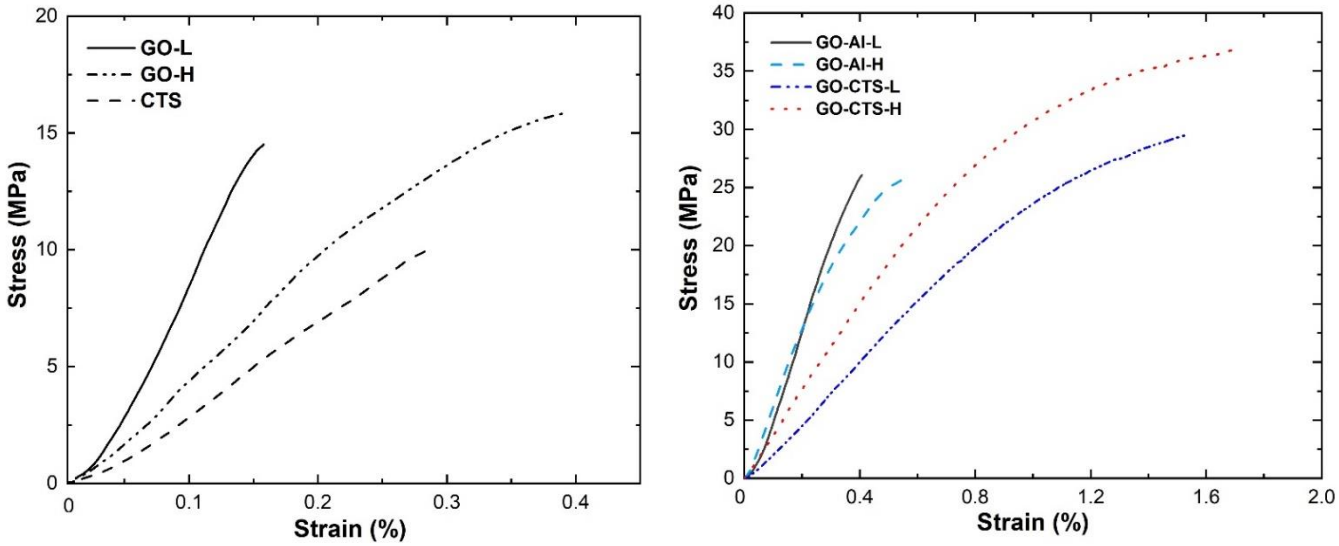

(a) (b)

Figure 4.20. Tensile stress versus strain curves: (a) unmodified synthetic precursors (GO and CTS) and, (b) GO-based composite membranes (GO-AL and GO-CTS).

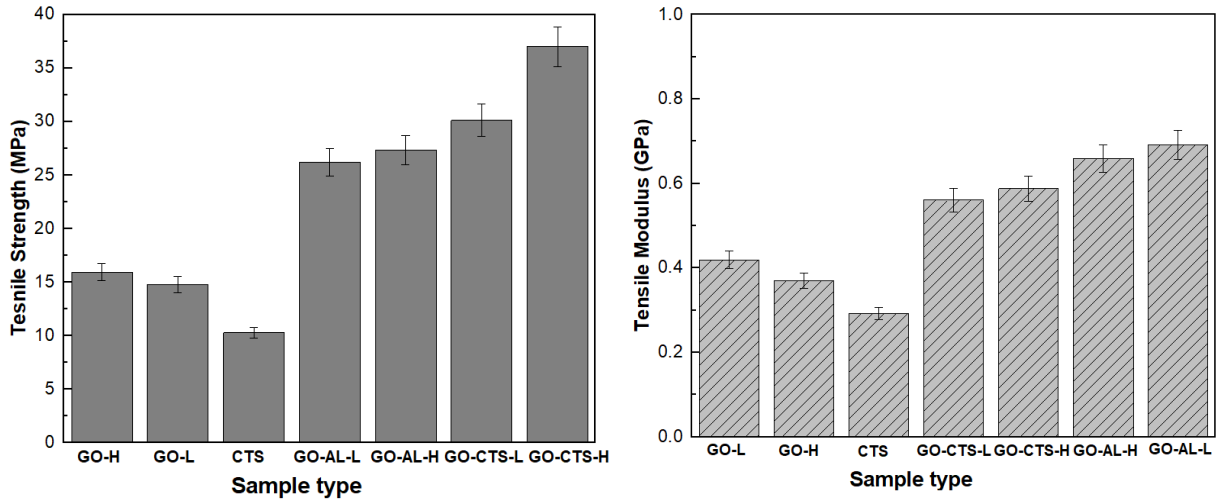

Figure 4.21. a) Tensile strength and b) tensile modulus for GO and GO-based composites.

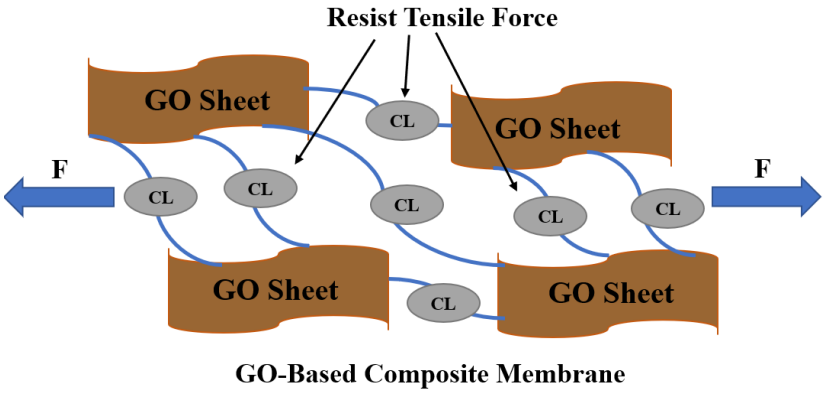

Figure 4.22. A conceptual structural model for GO-based composites upon cross-linking to account for changes in tensile strength. CL indicates cross-linker type (CTS or Al^{3+} ions) and F is the force or load applied to the composite membrane.

4.2.15 Statistical analysis

Tables 4.8 and 4.9 show the results of one-way single factor ANOVA for tensile strength, tensile modulus, elongation at break and fracture strength. The results confirmed if significant changes between groups occurred with addition of two types of cross-linkers (added separately) including Al^{3+} and CTS. According to ANOVA results, if the F value is greater than F_{crit} value, the results are significantly different in mean values. Also, a smaller p value (less than 0.05) verifies that there is greater significant change between the groups of data. The ANOVA performed for all tests and the outcome showed the F-test was greater than F_{crit}. Based on ANOVA results, GO-based composites cross-linked with either Al^{3+} or CTS had statistically significant change in tensile strength, tensile modulus, elongation at break and fracture strength. In general, when the two different type of cross-linker (Al^{3+} and CTS) in two concentrations (low and high) were added to GO, the obtained GO-base composites had important improvement in their mechanical properties.

Table 4.8. ANOVA results at a 0.05 level of significance for tensile strength, tensile modulus, elongation at break and fracture strength based on the addition of CTS in a GO-based composite.

	Source of Variation	SS	df	MS	F	P-value	F_{crit}
Tensile	BG	776.6288	2	388.3144	125.6975	1.27E-05	5.143253
strength	WG	18.53567	6	3.089278	-	-	-
Tensile	BG	0.192769	2	0.096384	10.42568	0.011157	5.143253
modulus	WG	0.055469	6	0.009245	-	-	-
Elongation	BG	3.5402	2	1.7701	17701	4.87E-12	5.143253
at break	WG	0.0006	6	0.0001	-	-	-
Fracture	BG	777.1298	2	388.5649	388.5649	4.5E-07	5.143253
strength	WG	6	6	1	-	-	-

Note: BG, between groups; WG, within groups; SS, sum of squares; df, degree of freedom; MS, mean square; F, F-test statistic; and F_{crit}, critical value.

Table 4.9. ANOVA results at a 0.05 level of significance for tensile strength, tensile modulus, elongation at break and fracture strength based on the addition of Al^{3+} in a GO-based composite.

	Source of Variation	SS	df	MS	F	P-value	Fcrit
Tensile	BG	289.7669	2	144.8834	53.4877	0.00015	5.143253
strength	WG	16.25233	6	2.708722	-	-	-
Tensile	BG	0.084494	2	0.042247	4.41829	0.066138	5.143253
modulus	WG	0.057371	6	0.009562	-	-	-
Elongation	BG	0.1134	2	0.0567	567.3182	1.46E-07	5.143253
at break	WG	0.0006	6	0.0001	-	-	-
Fracture	BG	264.5384	2	132.2692	132.2692	1.09E-05	5.143253
strength	WG	6	6	1	-	-	-

CHAPTER 5: CONCLUSIONS, FUTURE WORK AND CONTRIBUTIONS

5.1 Conclusions

In this Ph.D. research work, GO was synthesized and chemically modified using CTS and Al^{3+} species by a green chemistry approach. The GO was successfully cross-linked with two different cross-linkers at variable weight contents (e.g. 0.3 and 0.6 w/v %) in an effort to improve dye and gas adsorption and mechanical properties which can be used in water treatment applications. The freestanding GO membranes were obtained through a drop cast technique using a polystyrene substrate followed by drying. The chemical structure, physical (thermal and swelling), adsorption properties and mechanical properties of prepared GO-based composites were investigated. The key findings of the experimental studies are concluded as follows:

- The ζ-potential measurement of the GO indicated that GO was highly negative (below -30 mV), however, this negative charge decreased after introduction of either type of cross-linker, respectively. This is attributed to modification of the functional groups on the surface upon cross-linking, where the ζ potential was -7.2 mV and -3.6 mV for GO-CTS and GO-AL, respectively.

- The structural analysis of GO-based composites using FTIR indicated changes in the IR bands of GO before and after modification as a result of coordination of cross-linkers to the GO functional groups and formation of linkages between GO and the cross-linkers.

- SEM observation of GO and GO-based composites in the form of powder and membranes (Figure 4.5-4.7) showed that both types of cross-linkers (CTS or Al^{3+} ions) altered the layered-assembly structure of GO sheets.

- The Raman and XRD investigations suggested that GO-based composites had greater inter-layer spacing and less ordered-structures (lower crystallinity) related to disruption of the regular GO layer structure (Figure 4.4) upon cross-linking and the introduction of defects in the structure of GO.

- The physical investigations of GO-based composites including TGA and swelling test results revealed GO-based composites had major weight losses related to desorption of free water, decomposition of GO oxygen functionalities and cross-linkers. While, the GO framework was decomposed at 80-100 ℃, GO composites were determined to degrade at 155 ℃ (GO-CTS) and 255 ℃ (GO-AL). Also, equilibrium swelling and water uptake results of GO before and after cross-linking showed a decrease in swelling degree for GO-based composites compared to pristine GO due to coordination of cross-linkers with the GO sheets.

- The adsorption properties of GO-based composites were studied in solution using MB as a model dye system to represent cationic species in effluent. The adsorption capacity (mg/g) of the various sorbents adopted the following order: GO-CTS > GO-AL > GO, where the GO composites exceeded the GO uptake capacity (by 22.4 % and 42.13 % for GO-AL and GO-CTS, respectively). The trend relates to the enhancement of accessibility of adsorption sites of GO upon cross-linking, where the prepared sorbents were observed to be able to regenerate for at least three sorption cycles.

- Measurement of the adsorption properties of GO and GO-based composites in gas media toward N_2 and water vapour suggested that cross-linking of GO with other additives alter its porosity (PS and PV) and SA of GO. The SA and PV of GO toward N_2 increased from 0.61 m^2/g to 1.24 m^2/g and 1.40 m^2/g and from 0.19 cm^3/g to 0.76 cm^3/g and 0.83 cm^3/g by addition of Al^{3+} ions and CTS, respectively. Also, for water vapour, the SA and PV of GO increased from 408.9 m^2/g to 481.8 m^2/g and 560.9 m^2/g and 0.53 cm^3/g to 1.33 cm^3/g and 1.97 cm^3/g by addition of the respective cross-linker (Al^{3+} ions and CTS).

- It was observed that chemically cross-linked GO composites displayed different ion permittivity characteristics in response to changes in inter-layer spacing of GO sheets upon cross-linking with various cross-linkers. It was shown that ion diffusion was higher for GO-based samples cross-linked with CTS (GO-CTS) compared to GO-based samples cross-linked with Al ions (GO-AL). This could be related to the smaller inter-layer spacing of GO-AL composite membranes compared to GO-CTS.

- Mechanical properties obtained for GO-based composites were found to be greater than those of pure GO. This enhancement is suggested to be an indication that stable bonds were formed

between individual GO sheets (via cross-linking) which changed the mechanical behaviour at different stress levels.

- The tensile strength and tensile modulus of the GO-CTS and GO-AL composites exceeded those of pristine GO by 74 % and 33 % (for both composites), respectively. As the cross-linker content increased, the tensile strength and modulus increased up to a maximum of 146 % and 64 % (for both composites), respectively.

5.2 Recommendations for future work

- Based on the present Ph.D. research, promising preliminary results for potential removal of positively charged dyes (MB) using GO-based composites were obtained. Additionally, GO has been shown to have high adsorption capacity toward some heavy metals as a result of oxygen-containing functional groups on the GO surfaces. Therefore, additional research would have to be done to evaluate adsorption properties of GO and GO-based composites for potential removal of heavy metals such as Co(II), Cd(II), Cu(II), Ni(II), and Pb(II).

- According to obtained results, it was shown that the GO-based composites membranes can hinder the passage of ions of NaCl and $CaCl_2$ aqueous solutions. Moving forward, work with GO-based composite membranes would have to be focused on determining membrane properties (such as flux and durability over a period of time) under an applied force. Also, the membrane properties can be further modified through changing the GO and cross-linker (e.g. CTS or metal ions) composition (e.g. GO to cross-linker concentration ratio (to above 0.6 w/v %), increasing reaction time, etc.) or using supported membranes onto a suitable porous substrate to afford the required mechanical properties. This may improve mechanial properties, required for membranes under pressure and resolve difficulties of applicability of these materials in practical large-scale desalination processes in the future.

- The results indicated that GO can be effectively cross-linked by means of either CTS or Al^{3+} ions. Future work can focus on further modification of GO which could be done through cross-linking of GO using other types of cross-linkers. This modification would further affect the strength of the GO-based membranes, as well as the permeability of ions through the membrane.

- The results of mechanical properties of GO-based composites were measured in dry-state and found to be greater than that pure GO. It may be beneficial to measure the mechanical properties of these materials in wet-state to obtain some insights for applications which requires strength in wet conditions.

- The results revealed that GO-based composites cross-linked with CTS and/or Al^{3+} ions formed a 3D-framework with greater accessible SA, porosity and gas uptake properties toward nitrogen and water vapour. It may be beneficial to explore gas adsorption properties of these materials toward greenhouse gases (such as CO_2) and a mixture of gases (such as N_2/H_2) to investigate gas selectivity properties of GO-based membranes.

- The results presented in this work provided new information about the microstructure, mechanical and thermal behavior of GO-based composites. The results indicated that these materials have great potential for wastewater treatment applications. Further work can explore other areas of applications such as electronic devices, sensors, hydrogen storage, drug delivery, etc.

5.3 Significance of the thesis results

5.3.1 limitations of current adsorbents/membranes

- The current adsorbents commercially used in industry for wastewater treatment include mineral, organic or biological sorbents. The applicability of these adsorbents has been limited due to their low adsorption capacity, cost and regenerability issues. So, the goal is to replace the current sorbent materials in long term.

- On the other hand, there are various types of membranes available for treatment of wastewater that enables the passage of different species, depending on the relationship between the physical and chemical properties of the species and the membrane. Membranes for treatment of wastewater are classified according to the nature of the material used to fabricate the membrane [1]. The current membranes includes microfiltration (MF), ultrafiltration (UF), and reverse osmosis (RO) as summarized below:

Table 5.1. Current membranes characteristic use for wastewater treatment.

Process	Separation Mechanism	Pore Size (Å)
Microfiltration (MF)	Size Exclusion	500 - 50,000
Ultrafiltration (UF)	Size Exclusion	20 - 500
Reverse Osmosis (RO)	Diffusion	< 10

- Polymer-based membranes such as polyvinylidene fluoride (PVDF), polyacrylonitrile (PAN), and polyethersulfone (PES) are known as the most widely used types of membranes for water treatment according to their good separation performance. However, the applicability of polymeric membranes is restricted by their limited thermal and physiochemical properties and lack of biological degradation [256]. The other issues associated with use of current membranes mainly includes poor stability of water flux in long-term, high cost of membrane replacement and limited size and scaling [257]. Therefore, the success of novel adsorbent/membrane materials required for field conditions seems to be a factor of interdisciplinary research which needs collaboration of chemistry, mechanical engineering and material science using novel composite materials.

5.3.2 Advances of GO-based composites

- GO-based composite membranes fabricated in this research have promise to reduce some of the current membrane limitations and therefore impact on the efficiency of water treatment. These advances include improving the mechanical, physiochemical and thermal stability by processing into large-scale membranes that have limited the application of membrane processes in water treatment.

- In this work, two types of GO-based composites were synthesized by employing a solution-mixing method that was systematically examined using various techniques. The advances in the properties of GO-based composites reported in this thesis contribute new knowledge about these materials and practical applications relevant to chemical separations, nanofiltration, dye removal, etc. This work suggests that when forming GO-based composites from solution, the

formation of cross-links between GO sheets is advantageous for achieving good physiochemical and mechanical properties. Based on the work presented in this thesis, the formation of GO-based composites with chitosan or Al^{3+} revealed significant differences when compared against colloidal GO in aqueous media. The uptake of a model cationic dye (methylene blue; MB) revealed that the sorption properties for GO-CTS and GO-Al composites were superior to that of GO. This indicates that the composites had unique textural properties and surface chemistry that favour uptake of MB over that of GO materials without modification. This improvement in adsorption capacity of GO-based composites over available sorbents can be found in Table 2.1 and 2.2.

- The tensile strength of the GO-based composite membranes achieved in this work compare well with the values reported in the field for advanced materials in wastewater treatment such as polymeric membranes, CTS, and carbon nanotubes (CNTs). The following table highlights the advancement in the improved mechanical properties of GO-based composites (GO-CTS and GO-AL) over currently available membranes.

Table 5.2. Literature comparison of the mechanical properties of available membranes and GO-based composite membranes.

Membrane material	Mechanical test	Tensile strength (MPa)	Tensile modulus (MPa)	Elongation at break (%)	Ref
Polyethylene glycol (PEG)-Carbon nanotubes (CNTs)	Uniaxial tensile test	(7-15)	-	-	[258]
polyvinylidene fluoride (PVDF)	Uniaxial tensile test	(8-11)	-	(20-90)	[259]
PVDF	Uniaxial tensile test	(6-7)	-	(5-118)	[260]
polyacrylonitrile (PAN)	DMA	(10-17)	(60-140)	(20-100)	[261]

PAN	Uniaxial tensile test	(2-4)	(135-205)	(4-14)	[262]
Membrane material	Mechanical test	Tensile strength (MPa)	Tensile modulus (MPa)	Elongation at break (%)	Ref
polyethersulfone (PES)	Uniaxial tensile test	(1-5)	(57-138)	(9-58)	[263]
PES	Uniaxial tensile test	(2-3)	(107-138)	(29-43)	[264]
Polysulfone (PSF)	Uniaxial tensile test	(4-5)	-	(12-20)	[265]
CTS	Uniaxial tensile test	(2-7)	-	(8-23)	[266]
CTS	Uniaxial tensile test	(6-17)	-	-	[267]
GO-PVDF	Uniaxial tensile test	(2-5)	-	(12-92)	[268]
PSF-GO		-	(152-204)	-	[269]
GO-CTS	DMA	(30-36)	(650-690)	(1.6-1.7)	**This Study**
GO-Al	DMA	(26-27)	(560-580)	(0.4-0.6)	

- An additional advantage of the GO-CTS and GO-AL composites over the single component precursor materials (i.e. GO and CTS) is the superior adsorption, thermal and structural stability of this material. The improved properties make it much more suitable for practical applications in the wet-state and under high temperature and pressure (e.g., water flux) for adsorption-related applications as well as other applications such as sensing mechanical deformation and applications at higher hydrostatic pressures.

- One potential area of application for mechanically strong GO-based composite membranes is for the desalination of saline water. As a proof of concept and to show the applicability of GO-based membranes as potential water desalination membranes, a simple conductivity measurement was demonstrated by placing a GO-based composite membrane in between two

stationary reservoirs of fluids and measuring the permeability (and hence ion rejection) performance of the membrane material as it was placed in between a salt solution and water. Despite the intrinsic brittleness and instability of pure GO membranes in a wet state, the GO-based composites membranes undergo more elongation before they break.

- As these materials are solution-processible, this technique may offer advantages from an energy balance perspective and therefore can be potentially used to scale up the fabrication for practical applications.

- Proficiency of GO-based composites in adsorption and removal of MB from water, as a widespread, water soluble cationic dye, along with their mechanical properties in the form of advanced materials as membranes, sorbents, or as a coating layer and other technologies such as wearable sensors, biocompatible actuators, and biodegradable circuits.

- It should be noted that the relevant applicability GO-based composite membranes reported in this study are dependent on the feed water source, pre-treatment, system design and operation conditions at variable pressure, temperature, etc.

5.4 Contributions to original knowledge

The outcomes of this Ph.D. research contribute towards using a stable chemical cross-linking between adjacent GO sheets to obtain thin yet robust GO-based membranes. This approach holds promise for innovative developments of GO-based membranes for adsorption-based applications. New knowledge obtained in this field are listed below.

5.4.1 Synthesis of GO-based composites

- Synthesis of GO-based composites using new weight contents of CTS and Al^{3+} (e.g. 0.3 and 0.6 w/v %) represents novelty that was not reported prior to the completion of this thesis study.

- The process of making freestanding GO and GO-based membranes using polystyrene substrates is novel.

5.4.2 Characterization of GO-based composites membranes

- Characterization of GO-AL composites (using 0.3 and 0.6 w/v %) was novel and had not been reported elsewhere at the completion of this thesis research. This includes surface charge studies, spectroscopy studies (FTIR, Raman and XRD), adsorption measurements (in liquid and gas phases), physical properties (swelling and TGA up to 500 °C), ion permiability and mechanical properties (using DMA).

- The kinetic of adsorption of GO-based composites were investigated for the first time using a novel kinetic adsorption assay using the one-pot method developed at Dr. Wilson's research group [223].

- The swelling properties of GO-based composite membranes in water is yet unreported apart from this research.

- Ion permeability determination of GO-based composites (GO-CTS and GO-AL) toward $CaCl_2$ by conductivity meter was not reported previously and represents a unique contribution.

- The instrument used to measure water vapour adsorption of GO and GO-based composites (i.e., IGA-002 system) signifies novelty and the obtained results were presented for the first time.

- Characterization of GO-based composites using the DMA instrument (with strain rate of 10-5 s^{-1}) was novel.

- The effect of different interface bonding between organic and inorganic materials (CTS and Al^{3+} ions) on the mechanical properties of GO had not yet been systematically compared prior to the completion of this thesis research.

References

[1] Bhatnagar, A., and Minocha, A. K., 2006, "Conventional and Non-Conventional Adsorbents for Removal of Pollutants from Water - A Review" Indian J. Chem. Technol., 13, 203-217.

[2] Chowdhury, S., and Balasubramanian, R., 2014, "Recent Advances in the Use of Graphene-Family Nanoadsorbents for Removal of Toxic Pollutants from Wastewater" Adv. Colloid Interface Sci., 204, 35–56.

[3] Zhu, Y., Murali, S., Cai, W., Li, X., Suk, J. W., Potts, J. R., and Ruoff, R. S., 2010, "Graphene and Graphene Oxide: Synthesis, Properties, and Applications" Adv. Mater., 22, 3906–3924.

[4] Ramesha, G. K., Vijaya Kumara, A., Muralidhara, H. B., and Sampath, S., 2011, "Graphene and Graphene Oxide as Effective Adsorbents toward Anionic and Cationic Dyes" J. Colloid Interface Sci., 361, 270–277.

[5] Joshi, R. K., Alwarappan, S., Yoshimura, M., Sahajwalla, V., and Nishina, Y., 2015, "Graphene Oxide: The New Membrane Material" Appl. Mater. Today, 1, 1-12.

[6] Zhao, G., Li, J., Ren, X., Chen, C., and Wang, X., 2011, "Few-Layered Graphene Oxide Nanosheets as Superior Sorbents for Heavy Metal Ion Pollution Management" Environ. Sci. Technol., 45, 10454-10462.

[7] Yeh, C.-N., Raidongia, K., Shao, J., Yang, Q.-H., and Huang, J., 2014, "On the Origin of the Stability of Graphene Oxide Membranes in Water" Nat. Chem., 7, 166–70.

[8] Park, S., Lee, K.-S., Bozoklu, G., Cai, W., Nguyen, S. T., and Ruoff, R. S., 2008, "Graphene Oxide Papers Modified by Divalent Ions-Enhancing Mechanical Properties via Chemical Cross-Linking" ACS Nano, 2, 572–578.

[9] Zuo, P.-P., Feng, H.-F., Xu, Z.-Z., Zhang, L.-F., Zhang, Y.-L., Xia, W., and Zhang, W.-Q.,

2013, “Fabrication of Biocompatible and Mechanically Reinforced Graphene Oxide-Chitosan Nanocomposite Films” Chem. Cent. J., 7, 39-50.

[10] Yang, L., Yang, B., Zeng, D., Wang, D., Wang, Y., and Zhang, L. M., 2011, “Formation and Properties of a Novel Complex Composed of an Amylose-Grafted Chitosan Derivative and Single-Walled Carbon Nanotubes” Carbohydr. Polym., 85, 845–853.

[11] Turgut, H., Tian, Z. R., Yu, F., and Zhou, W., 2017, “Multivalent Cation Cross-Linking Suppresses Highly Energetic Graphene Oxide’s Flammability” J. Phys. Chem. C., 121, 5829–5835.

[12] Travlou, N. A., Kyzas, G. Z., Lazaridis, N. K., and Deliyanni, E. A., 2013, “Functionalization of Graphite Oxide with Magnetic Chitosan for the Preparation of a Nanocomposite Dye Adsorbent” Langmuir, 29, 1657-1668.

[13] Lim, M. Y., Choi, Y. S., Kim, J., Kim, K., Shin, H., Kim, J. J., Shin, D. M., and Lee, J. C., 2017, “Cross-Linked Graphene Oxide Membrane Having High Ion Selectivity and Antibacterial Activity Prepared Using Tannic Acid-Functionalized Graphene Oxide and Polyethyleneimine” J. Memb. Sci., 521, 1-9.

[14] Rouquerol, J., Rouquerol, F., Llewellyn, P., Maurin, G., and Sing, K. S. W., 2013, "Adsorption by Powders and Porous Solids: Principles, Methodology and Applications", Second Edition. Academic Press.

[15] Smit B, Reimer JA, Oldenburg CM, B. I., 2014, "Introduction to Carbon Capture and Sequestration", World Scientific.

[16] McKay, G., Porter, J. F., and Prasad, G. R., 1999, “The Removal of Dye Colours from Aqueous Solutions by Adsorption on Low- Cost Materials” Water. Air. Soil Pollut., 114, 423-438.

[17] Brunauer, S., Emmett, P. H., and Teller, E., 1938, “Adsorption of Gases in Multimolecular Layers” J. Am. Chem. Soc., 60, 309-319.

[18] Duffus, J. H., 2014, “International Union of Pure and Applied Chemistry,” Encyclopedia of

Toxicology: Third Edition, Elsevier.

[19] Kumar, P., Kim, K.-H., Kwon, E. E., and Szulejko, J. E., 2016, "Metal–Organic Frameworks for the Control and Management of Air Quality: Advances and Future Direction" J. Mater. Chem. A., 4, 345–361.

[20] Langmuir, I., 1918, "The Adsorption of Gases on Plane Surfaces of Glass, Mica and Platinum" J. Am. Chem. Soc., 40, 1361–1403.

[21] Mohsenipour, M., Shahid, S., and Ebrahimi, K., 2015, "Nitrate Adsorption on Clay Kaolin: Batch Tests" J. Chem., 2015, 397–404.

[22] Lagergren, S., 1898, "About the Theory of So-Called Adsorption of Soluble Substances", Sven. Vetenskapsakad. Handingarl, 24, 1–39.

[23] Ho, Y. S., 2006, "Review of Second-Order Models for Adsorption Systems" J. Hazard. Mater., 136, 681-689.

[24] Qiu, H., Lv, L., Pan, B., Zhang, Q., Zhang, W., and Zhang, Q., 2009, "Critical Review in Adsorption Kinetic Models" J. Zhejiang Univ-Sci. A., 10, 716-724.

[25] Linsen, B. G. ", 1970, Physical and Chemical Aspects of Adsorbents and Catalysts, Academic Press.

[26] Tien, C., 1994, Adsorption Calculations and Modeling. Butterworth-Heineman, Academic Press.

[27] Wang, X., Liu, B., Lu, Q., and Qu, Q., 2014, "Graphene-Based Materials: Fabrication and Application for Adsorption in Analytical Chemistry" J. Chromatogr. A., 10, 716-724.

[28] Carmalin Sophia, A., Lima, E. C., Allaudeen, N., and Rajan, S., 2016, "Application of Graphene Based Materials for Adsorption of Pharmaceutical Traces from Water and Wastewater- a Review" Desalin. Water Treat., 57, 27573-27586.

[29] Xu, L., and Wang, J., 2017, "The Application of Graphene-Based Materials for the Removal of Heavy Metals and Radionuclides from Water and Wastewater" Crit. Rev. Environ. Sci.

Technol., 47, 1042–1105.

[30] Perreault, F., Fonseca De Faria, A., and Elimelech, M., 2015, “Environmental Applications of Graphene-Based Nanomaterials” Chem. Soc. Rev., 44, 5861-5896.

[31] Xiang, Q., Yu, J., and Jaroniec, M., 2012, “Graphene-Based Semiconductor Photocatalysts” Chem. Soc. Rev., 41, 782-796.

[32] Hu, Y. J., Jin, J., Zhang, H., Wu, P., and Cai, C. X., 2010, “Graphene: Synthesis, Functionalization and Applications in Chemistry” Acta Phys. Chim. Sin., 26, 2073–2086.

[33] Compton, O. C., and Nguyen, S. T., 2010, “Graphene Oxide, Highly Reduced Graphene Oxide, and Graphene: Versatile Building Blocks for Carbon-Based Materials” Small, 6, 711-723.

[34] Srinivas, G., Burress, J., and Yildirim, T., 2012, “Graphene Oxide Derived Carbons (GODCs): Synthesis and Gas Adsorption Properties” Energy Environ. Sci., 5, 6453-6459.

[35] Liu, Q., Shi, J., Sun, J., Wang, T., Zeng, L., and Jiang, G., 2011, “Graphene and Graphene Oxide Sheets Supported on Silica as Versatile and High-Performance Adsorbents for Solid-Phase Extraction” Angew. Chemie Int. Ed., 50, 5913-5917.

[36] Brodie, B. C., 1859, “On the Atomic Weight of Graphite,” Philos. Trans. R. Soc. London, 149, 249–259.

[37] Staudenmaier, L., 1898, “Verfahren Zur Darstellung Der Graphitsäure,” Berichte der Dtsch. Chem. Gesellschaft, 31, 1481–1487.

[38] Hummers, W. S., and Offeman, R. E., 1958, “Preparation of Graphitic Oxide” J. Am. Chem. Soc., 80, 1339–1339.

[39] Shahriary, L., and Athawale, A. A., 2014, “Graphene Oxide Synthesized by Using Modified Hummers Approach” Int. J. Renew. Energy Environ. Eng., 2, 58-63.

[40] Franklin, R. E., 1951, “The Structure of Graphitic Carbons” Acta Crystallogr, 4, 253-261.

[41] McAllister, M. J., Li, J. L., Adamson, D. H., Schniepp, H. C., Abdala, A. A., Liu, J., Herrera-Alonso, M., Milius, D. L., Car, R., Prud'homme, R. K., and Aksay, I. A., 2007, "Single Sheet Functionalized Graphene by Oxidation and Thermal Expansion of Graphite" Chem. Mater., 19, 4396-4404.

[42] Schniepp, H. C., Li, J. L., McAllister, M. J., Sai, H., Herrera-Alonson, M., Adamson, D. H., Prud'homme, R. K., Car, R., Seville, D. A., and Aksay, I. A., 2006, "Functionalized Single Graphene Sheets Derived from Splitting Graphite Oxide" J. Phys. Chem. B., 110, 8535-8539.

[43] Peng, W., Li, H., Hu, Y., Liu, Y., and Song, S., 2016, "Does Silicate Mineral Impurities in Natural Graphite Affect the Characteristics of Synthesized Graphene?" Mater. Res. Bull. 74, 333-339.

[44] Fan, L., Luo, C., Li, X., Lu, F., Qiu, H., and Sun, M., 2012, "Fabrication of Novel Magnetic Chitosan Grafted with Graphene Oxide to Enhance Adsorption Properties for Methyl Blue" J. Hazard. Mater., 215, 272–279.

[45] Jiao, T., Zhao, H., Zhou, J., Zhang, Q., Luo, X., Hu, J., Peng, Q., and Yan, X., 2015, "Self-Assembly Reduced Graphene Oxide Nanosheet Hydrogel Fabrication by Anchorage of Chitosan/Silver and Its Potential Efficient Application toward Dye Degradation for Wastewater Treatments" ACS Sustain. Chem. Eng., 3, 3130-3139.

[46] Gao, W., Alemany, L. B., Ci, L., and Ajayan, P. M., 2009, "New Insights into the Structure and Reduction of Graphite Oxide" Nat. Chem., 1, 403-409.

[47] Mkhoyan, K. A., Contryman, A. W., Silcox, J., Stewart, D. A., Eda, G., Mattevi, C., Miller, S., and Chhowalla, M., 2009, "Atomic and Electronic Structure of Graphene-Oxide" Nano Lett., 9, 1058-1063.

[48] Wallace, G. G., Kaner, R. B., Muller, M., Gilje, S., Li, D., and Li, D., 2008, "Processable Aqueous Dispersions of Graphene Nanosheets Publication Details Processable Aqueous Dispersions of Graphene Nanosheets" Nat. Nanotechnol., 3, 101–105.

[49] Hu, X., Yu, Y., Hou, W., Zhou, J., and Song, L., 2013, "Effects of Particle Size and PH

Value on the Hydrophilicity of Graphene Oxide" Appl. Surf. Sci., 273, 118-121.

[50] Sheshmani, S., Akhundi Nematzadeh, M., Shokrollahzadeh, S., and Ashori, A., 2015, "Preparation of Graphene Oxide/Chitosan/FeOOH Nanocomposite for the Removal of Pb(II) from Aqueous Solution" Int. J. Biol. Macromol., 80, 475-480.

[51] Dimiev, A., Kosynkin, D. V., Alemany, L. B., Chaguine, P., and Tour, J. M., 2012, "Pristine Graphite Oxide" J. Am. Chem. Soc., 134, 2815-2822.

[52] Parades, J. I., Villar-Rodil, S., Martínez-Alonso, A., and Tascón, J. M. D., 2008, "Graphene Oxide Dispersions in Organic Solvents" Langmuir, 24, 10560-10564.

[53] Sun, L., and Fugetsu, B., 2013, "Mass Production of Graphene Oxide from Expanded Graphite" Mater. Lett., 109, 207-210.

[54] Wu, Z. S., Ren, W., Gao, L., Liu, B., Jiang, C., and Cheng, H. M., 2009, "Synthesis of High-Quality Graphene with a Pre-Determined Number of Layers" Carbon, 47, 493-499.

[55] Krishnamoorthy, K., Veerapandian, M., Yun, K., and Kim, S. J., 2013, "The Chemical and Structural Analysis of Graphene Oxide with Different Degrees of Oxidation" Carbon, 53, 38-49.

[56] Kim, M., Safron, N. S., Han, E., Arnold, M. S., and Gopalan, P., 2010, "Fabrication and Characterization of Large-Area, Semiconducting Nanoperforated Graphene Materials" Nano Lett., 4, 1125-1131.

[57] Abraham, J., Vasu, K. S., Williams, C. D., Gopinadhan, K., Su, Y., Cherian, C. T., Dix, J., Prestat, E., Haigh, S. J., Grigorieva, I. V., Carbone, P., Geim, A. K., and Nair, R. R., 2017, "Tunable Sieving of Ions Using Graphene Oxide Membranes" Nat. Nanotechnol., 12, 546-570.

[58] Chen, B., Jiang, H., Liu, X., and Hu, X., 2017, "Observation and Analysis of Water Transport through Graphene Oxide Interlamination" J. Phys. Chem. C., 121, 1321-1328.

[59] Kim, D., Kim, D. W., Lim, H. K., Jeon, J., Kim, H., Jung, H. T., and Lee, H., 2014,

"Intercalation of Gas Molecules in Graphene Oxide Inter-layer : The Role of Water" J. Phys. Chem. C., 118, 11142-11148.

[60] Nair, R. R., Wu, H. A., Jayaram, P. N., Grigorieva, I. V., and Geim, A. K., 2012, "Unimpeded Permeation of Water Through Helium-Leak-Tight Graphene-Based Membranes" Science, 335, 442–444.

[61] Yang, X., Yang, X., and Liu, S., 2015, "Molecular Dynamics Simulation of Water Transport through Graphene-Based Nanopores: Flow Behavior and Structure Characteristics" Chinese J. Chem. Eng., 23, 1587-1592.

[62] Shen, J., Liu, G., Huang, K., Jin, W., Lee, K. R., and Xu, N., 2015, "Membranes with Fast and Selective Gas-Transport Channels of Laminar Graphene Oxide for Efficient CO_2 Capture" Angew. Chemie - Int. Ed., 54, 578–582.

[63] Yoo, B. M., Shin, J. E., Lee, H. D., and Park, H. B., 2017, "Graphene and Graphene Oxide Membranes for Gas Separation Applications" Curr. Opin. Chem. Eng., 16, 39-47.

[64] Wang, S., Wu, Y., Zhang, N., He, G., Xin, Q., Wu, X., Wu, H., Cao, X., Guiver, M. D., and Jiang, Z., 2016, "A Highly Permeable Graphene Oxide Membrane with Fast and Selective Transport Nanochannels for Efficient Carbon Capture" Energy Environ. Sci., 9, 3107-3112.

[65] Joshi, R. K., Carbone, P., Wang, F. C., Kravets, V. G., Su, Y., Grigorieva, I. V, Wu, H. a, Geim, a K., and Nair, R. R., 2014, "Precise and Ultrafast Molecular Sieving through Graphene Oxide Membranes" Science, 343, 752–4.

[66] Huang, K., Liu, G., and Jin, W., 2017, "Vapor Transport in Graphene Oxide Laminates and Their Application in Pervaporation" Curr. Opin. Chem. Eng., 16, 56-64.

[67] Lian, B., De Luca, S., You, Y., Alwarappan, S., Yoshimura, M., Sahajwalla, V., Smith, S. C., Leslie, G., and Joshi, R. K., 2018, "Extraordinary Water Adsorption Characteristics of Graphene Oxide" Chem. Sci., 9, 5106-5111.

[68] Liu, R., Gong, T., Zhang, K. and Lee, C., 2017, "Graphene Oxide Papers with High Water Adsorption Capacity for Air Dehumidification" Sci. Rep., 7, 9761–9770.

[69] Stampfer, C., Güttinger, J., Molitor, F., Graf, D., Ihn, T., and Ensslin, K., 2008, "Tunable Coulomb Blockade in Nanostructured Graphene" Appl. Phys. Lett., 92, 12101-12105.

[70] Liu, H., Wang, H., and Zhang, X., 2015, "Facile Fabrication of Freestanding Ultrathin Reduced Graphene Oxide Membranes for Water Purification" Adv. Mater., 27, 249-254.

[71] Xiong, W., Liu, J. Z., Ma, M., Xu, Z., Sheridan, J., and Zheng, Q., 2011, "Strain Engineering Water Transport in Graphene Nanochannels" Phys. Rev. E - Stat. Nonlinear, Soft Matter Phys., 84, 56329-56346.

[72] Hu, M., and Mi, B., 2013, "Enabling Graphene Oxide Nanosheets as Water Separation Membranes" Environ. Sci. Technol., 47, 3715–3723.

[73] Dimiev, Ayrat M., and Siegfied Eigler, eds, 2016, Graphene Oxide: Fundamentals and Applications, John Wiley & Sons.

[74] Wang, Y., Li, Z., Wang, J., Li, J., and Lin, Y., 2011, "Graphene and Graphene Oxide: Biofunctionalization and Applications in Biotechnology" Trends Biotechnol., 29, 205–212.

[75] Li, F., Jiang, X., Zhao, J., and Zhang, S., 2015, "Graphene Oxide: A Promising Nanomaterial for Energy and Environmental Applications" Nano Energy, 16, 488-515.

[76] Kuila, T., Bose, S., Mishra, A. K., Khanra, P., Kim, N. H., and Lee, J. H., 2012, "Chemical Functionalization of Graphene and Its Applications" Prog. Mater. Sci., 57, 1061-1105.

[77] Stankovich, S., Dikin, D. A., Dommett, G. H., Kohlhaas, K. M., Zimney, E. J., Stach, E. A., Piner, R. D., Nguyen, S. T., and Ruoff, R. S., 2006, "Graphene-Based Composite Materials" Nature, 442, 282–286.

[78] Park, S., and Ruoff, R. S., 2009, "Chemical Methods for the Production of Graphenes" Nat. Nanotechnol., 4, 217-224.

[79] Singh, V. K., Patra, M. K., Manoth, M., Gowd, G. S., Vadera, S. R., and Kumar, N., 2009, "In Situ Synthesis of Graphene Oxide and Its Composites with Iron Oxide" New Carbon

Mater., 24, 147–152.

[80] Satti, A., Larpent, P., and Gun'Ko, Y., 2010, "Improvement of Mechanical Properties of Graphene Oxide/Poly(Allylamine) Composites by Chemical Crosslinking" Carbon, 48, 3376–3381.

[81] Suk, J. W., Piner, R. D., An, J., and Ruoff, R. S., 2010, "Mechanical Properties of Monolayer Graphene Oxide" ACS Nano, 4, 6557–6564.

[82] Dikin, D. A., Stankovich, S., Zimney, E. J., Piner, R. D., Dommett, G. H. B., Evmenenko, G., Nguyen, S. T., and Ruoff, R. S., 2007, "Preparation and Characterization of Graphene Oxide Paper" Nature, 448, 457–460.

[83] Medhekar, N. V., Ramasubramaniam, A., Ruoff, R. S., and Shenoy, V. B., 2010, "Hydrogen Bond Networks in Graphene Oxide Composite Paper: Structure and Mechanical Properties" ACS Nano., 4, 2300-2306.

[84] Chen, C., Yang, Q. H., Yang, Y., Lv, W., Wen, Y., Hou, P. X., Wang, M., and Cheng, H. M., 2009, "Self-Assembled Free-Standing Graphite Oxide Membrane" Adv. Mater., 21, 3007-3011.

[85] Tian, Z., Xu, C., Li, J., Zhu, G., Shi, Z., and Lin, Y., 2013, "Self-Assembled Free-Standing Graphene Oxide Fibers" ACS Appl. Mater. Interfaces, 5, 1489-1493.

[86] Lee, J., Chae, H. R., Won, Y. J., Lee, K., Lee, C. H., Lee, H. H., Kim, I. C., and Lee, J. min, 2013, "Graphene Oxide Nanoplatelets Composite Membrane with Hydrophilic and Antifouling Properties for Wastewater Treatment" J. Memb. Sci., 448, 223-230.

[87] Paci, J. T., Belytschko, T., and Schatz, G. C., 2007, "Computational Studies of the Structure, Behavior upon Heating and Mechanical Properties of Graphite Oxide" J. Phys. Chem. C., 111, 18099-18111.

[88] Chen, H., Muller, M. B., Gilmore, K. J., Wallace, G. G., and Li, D., 2008, "Mechanically Strong, Electrically Conductive, and Biocompatible Graphene Paper" Adv. Mater., 20, 3557-3561.

[89] Zheng, Q., Geng, Y., Wang, S., Li, Z., and Kim, J. K., 2010, “Effects of Functional Groups on the Mechanical and Wrinkling Properties of Graphene Sheets” Carbon, 15, 4315-4322.

[90] Gao, Y., Liu, L. Q., Zu, S. Z., Peng, K., Zhou, D., Han, B. H., and Zhang, Z., 2011, “The Effect of Inter-layer Adhesion on the Mechanical Behaviors of Macroscopic Graphene Oxide Papers” ACS Nano, 5, 2134–2141.

[91] Kang, S. H., Fang, T. H., Hong, Z. H., and Chuang, C. H., 2013, “Mechanical Properties of Free-Standing Graphene Oxide” Diam. Relat. Mater., 38, 73–78.

[92] Gao, E., Wen, Y., Yuan, Y., Li, C., and Xu, Z., 2017, “Intrinsic Mechanical Properties of Graphene Oxide Films: Strain Characterization and the Gripping Effects” Carbon, 118, 467–474.

[93] Wan, Y. J., Tang, L. C., Gong, L. X., Yan, D., Li, Y. B., Wu, L. Bin, Jiang, J. X., and Lai, G. Q., 2014, “Grafting of Epoxy Chains onto Graphene Oxide for Epoxy Composites with Improved Mechanical and Thermal Properties” Carbon, 69, 467-480.

[94] Han, D., Yan, L., Chen, W., and Li, W., 2011, “Preparation of Chitosan/Graphene Oxide Composite Film with Enhanced Mechanical Strength in the Wet State” Carbohydr. Polym., 83, 653-658.

[95] Dash, M., Chiellini, F., Ottenbrite, R. M., and Chiellini, E., 2011, “Chitosan - A Versatile Semi-Synthetic Polymer in Biomedical Applications” Prog. Polym. Sci., 8, 981-1014.

[96] Bustos-Ramrez, K., Martnez-Herndez, A. L., Martnez-Barrera, G., de Icaza, M., Castao, V. M., and Velasco-Santos, C., 2013, “Covalently Bonded Chitosan on Graphene Oxide via Redox Reaction” Materials, 6, 911–926.

[97] Yuan, H., Meng, L.Y. and Park, S.J., 2016, “A Review: Synthesis and Applications of Graphene/Chitosan Nanocomposites” Carbon Lett., 17, 11–17.

[98] Lu, J.-J., Feng, M., and Zhan, H.-B., 2013, “Preparation of Graghene Oxide/Chitosan Composite Films and Investigations on Their Nonlinear Optical Limiting Effect” Wuli Xuebao/Acta Phys. Sin., 62, 14204-14209.

[99] Akbari, A., Derikvandi, Z., and Mojallali Rostami, S. M., 2015, “Influence of Chitosan Coating on the Separation Performance, Morphology and Anti-Fouling Properties of the Polyamide Nanofiltration Membranes” J. Ind. Eng. Chem., 28, 268-276.

[100] Sadeghi-Kiakhani, M., Gharanjig, K., and Arami, M., 2015, “Grafting of Prepared Chitosan-Poly(Propylene) Imines Dendrimer Hybrid as a Biopolymer onto Cotton and Its, Antimicrobial Property” J. Ind. Eng. Chem., 28, 78-85.

[101] Pan, Y., Wu, T., Bao, H., and Li, L., 2011, “Green Fabrication of Chitosan Films Reinforced with Parallel Aligned Graphene Oxide” Carbohydr. Polym., 83, 1908-1915.

[102] Syuhada, N. I., Huang, N. M., Vijay Kumar, S., Lim, H. N., Rahman, S. A., Thien, G. S. H., Ibrahim, N. A., Ahmad, M., and Moradihamedani, P., 2014, “Enhanced Mechanical Properties of Chitosan/EDTA-Go Nanocomposites Thin Films” Sains Malaysiana., 43, 851-859.

[103] Yan, N., Capezzuto, F., Lavorgna, M., Buonocore, G. G., Tescione, F., Xia, H., and Ambrosio, L., 2016, “Borate Cross-Linked Graphene Oxide-Chitosan as Robust and High Gas Barrier Films” Nanoscale, 8, 10783-10791.

[104] Grande, C. D., Mangadlao, J., Fan, J., De Leon, A., Delgado-Ospina, J., Rojas, J. G., Rodrigues, D. F., and Advincula, R., 2017, “Chitosan Cross-Linked Graphene Oxide Nanocomposite Films with Antimicrobial Activity for Application in Food Industry” Macromol. Symp., 374, 1600114-1600122.

[105] Santos, C. M., Mangadlao, J., Ahmed, F., Leon, A., Advincula, R. C., and Rodrigues, D. F., 2012, “Graphene Nanocomposite for Biomedical Applications: Fabrication, Antimicrobial and Cytotoxic Investigations” Nanotechnology, 23, 395101-395111.

[106] Ahmed, J., Mulla, M., Arfat, Y. A., and Thai T, L. A., 2017, “Mechanical, Thermal, Structural and Barrier Properties of Crab Shell Chitosan/Graphene Oxide Composite Films” Food Hydrocoll., 71, 141–148.

[107] Shao, L., Chang, X., Zhang, Y., Huang, Y., Yao, Y., and Guo, Z., 2013, “Graphene Oxide Cross-Linked Chitosan Nanocomposite Membrane” Appl. Surf. Sci., 280, 989-992.

[108] Zhang, D., Yang, S., Chen, Y., Liu, S., Zhao, H., and Gu, J., 2018, "^{60}Co γ-Ray Irradiation Crosslinking of Chitosan/Graphene Oxide Composite Film: Swelling, Thermal Stability, Mechanical, and Antibacterial Properties" Polymers, 10, 294-308.

[109] Chen, L., Li, Y., Chen, L., Li, N., Dong, C., Chen, Q., Liu, B., Ai, Q., Si, P., Feng, J., Zhang, L., Suhr, J., Lou, J., and Ci, L., 2018, "A Large-Area Free-Standing Graphene Oxide Multilayer Membrane with High Stability for Nanofiltration Applications" Chem. Eng. J., 345, 536-544.

[110] Ji, F., Li, Y. L., Feng, J. M., Su, D., Wen, Y. Y., Feng, Y., and Hou, F., 2009, "Electrochemical Performance of Graphene Nanosheets and Ceramic Composites as Anodes for Lithium Batteries" J. Mater. Chem., 19, 9063-9067.

[111] Wang, J., Wang, L.-Y., Yan, X.-H., Liu, X.-J., and Du, F.-H., 2016, "Advances of Chitosan-Based Active Films in Food Packaging" Jt. Int. Conf. Soc. Sci. Environ. Sci., 1, 269-273.

[112] Zhang, J., Zhang, J., Zhang, F., Yang, H., Huang, X., Liu, H., and Guo, S., 2010, "Graphene Oxide as a Matrix for Enzyme Immobilization" Langmuir, 26, 6083-6085.

[113] Sitko, R., Turek, E., Zawisza, B., Malicka, E., Talik, E., Heimann, J., Gagor, A., Feist, B., and Wrzalik, R., 2013, "Adsorption of Divalent Metal Ions from Aqueous Solutions Using Graphene Oxide" Dalton Trans., 42, 5682–5289.

[114] Peng, W., Li, H., Liu, Y., and Song, S., 2017, "A Review on Heavy Metal Ions Adsorption from Water by Graphene Oxide and Its Composites" J. Mol. Liq., 230, 496-504.

[115] Wang, L., Lee, K., Sun, Y. Y., Lucking, M., Chen, Z., Zhao, J. J., and Zhang, S. B., 2009, "Graphene Oxide as an Ideal Substrate for Hydrogen Storage" ACS Nano, 3, 2995–3000.

[116] Burress, J. W., Gadipelli, S., Ford, J., Simmons, J. M., Zhou, W., and Yildirim, T., 2010, "Graphene Oxide Framework Materials: Theoretical Predictions and Experimental Results" Angew. Chemie - Int. Ed., 49, 8902–8904.

[117] Xiong, X., Ji, N., Song, C., and Liu, Q., 2015, "Preparation Functionalized Graphene Aerogels as Air Cleaner Filter" Procedia Eng., 121, 957-960.

[118] Gadipelli, S., and Guo, Z. X., 2015, “Graphene-Based Materials: Synthesis and Gas Sorption, Storage and Separation” Prog. Mater. Sci., 69, 1-60.

[119] Kim, B. H., Hong, W. G., Yu, H. Y., Han, Y. K., Lee, S. M., Chang, S. J., Moon, H. R., Jun, Y., and Kim, H. J., 2012, “Thermally Modulated Multilayered Graphene Oxide for Hydrogen Storage” Phys. Chem. Chem. Phys., 14, 1480-1484.

[120] Kim, J.M., Hong, W.G., Lee, S.M., Chang, S.J., Jun, Y., Kim, B.H. and Kim, H. J., 2014, “Energy Storage of Thermally Reduced Graphene Oxide” Int. J. Hydrogen Energy, 39, 3799–3804.

[121] Sun, Y., Wu, Q., and Shi, G., 2011, “Graphene Based New Energy Materials” Energy Environ. Sci., 4, 1113-1132.

[122] Srinivas, G., Burress, J. W., Ford, J., and Yildirim, T., 2011, “Porous Graphene Oxide Frameworks: Synthesis and Gas Sorption Properties” J. Mater. Chem., 21, 11321-11330.

[123] Dimitrakakis, G. K., Tylianakis, E., and Froudakis, G. E., 2008, “Pillared Graphene: A New 3-D Network Nanostructure for Enhanced Hydrogen Storage” Nano Lett., 8, 3166–3170.

[124] Salavagione, H. J., Gómez, M. A., and Martínez, G., 2009, “Polymeric Modification of Graphene through Esterification of Graphite Oxide and Poly(Vinyl Alcohol)” Macromolecules, 42, 6331-6334.

[125] Putz, K. W., Compton, O. C., Palmeri, M. J., Nguyen, S. B. T., and Brinson, L. C., 2010, “High-Nanofiller-Content Graphene Oxide-Polymer Nanocomposites via Vacuum-Assisted Self-Assembly” Adv. Funct. Mater., 20, 3322-3329.

[126] Ossonon, B. D., and Bélanger, D., 2017, “Synthesis and Characterization of Sulfophenyl-Functionalized Reduced Graphene Oxide Sheets” RSC Adv., 7, 27224-27234.

[127] Wang, Y., Guan, C., Wang, K., Guo, C. X., and Li, C. M., 2011, “Nitrogen, Hydrogen, Carbon Dioxide, and Water Vapor Sorption Properties of Three-Dimensional Graphene” J. Chem. Eng. Data., 56, 642-645.

[128] Hu, F. P., Shen, P. K., Li, Y. L., Liang, J. Y., Wu, J., Bao, Q. L., Li, C. M., and Wei, Z. D., 2008, "Highly Stable Pd-Based Catalytic Nanoarchitectures for Low Temperature Fuel Cells" Fuel Cells., 8, 429-435.

[129] Srivastava, S., 2013, "Sorption of Divalent Metal Ions from Aqueous Solution by Oxidized Carbon Nanotubes and Nanocages: A Review" Adv. Mater. Lett., 4, 2-8.

[130] Huang, Z. H., Zheng, X., Lv, W., Wang, M., Yang, Q. H., and Kang, F., 2011, "Adsorption of Lead(II) Ions from Aqueous Solution on Low-Temperature Exfoliated Graphene Nanosheets" Langmuir, 27, 7558-7562.

[131] Wu, W., Yang, Y., Zhou, H., Ye, T., Huang, Z., Liu, R., and Kuang, Y., 2013, "Highly Efficient Removal of Cu(II) from Aqueous Solution by Using Graphene Oxide" Water. Air. Soil Pollut., 22, 1-8.

[132] G. Zhao, X. Ren, X. Gao, X. Tan, J. Li, C. Chen, Y. Huang, X. W., 2011, "Removal of Pb(II) Ions from Aqueous Solutions on Few-Layered Graphene Oxide Nanosheets" Dalt. Trans., 40, 10945-10952.

[133] Wang, H., Yuan, X., Wu, Y., Huang, H., Zeng, G., Liu, Y., Wang, X., Lin, N., and Qi, Y., 2013, "Adsorption Characteristics and Behaviors of Graphene Oxide for Zn(II) Removal from Aqueous Solution" Appl. Surf. Sci., 279, 432-440.

[134] Romanchuk, A. Y., Slesarev, A. S., Kalmykov, S. N., Kosynkin, D. V., and Tour, J. M., 2013, "Graphene Oxide for Effective Radionuclide Removal" Phys. Chem. Chem. Phys.,15, 2321-2327.

[135] Liu, L., Liu, S., Zhang, Q., Li, C., Bao, C., Liu, X., and Xiao, P., 2013, "Adsorption of Au(III), Pd(II), and Pt(IV) from Aqueous Solution onto Graphene Oxide" J. Chem. Eng. Data., 58, 209-216.

[136] Liu, L., Li, C., Bao, C., Jia, Q., Xiao, P., Liu, X., and Zhang, Q., 2012, "Preparation and Characterization of Chitosan/Graphene Oxide Composites for the Adsorption of Au(III) and Pd(II)" Talanta., 93, 350-357.

[137] Liu, M., Chen, C., Hu, J., Wu, X., and Wang, X., 2011, "Synthesis of Magnetite/Graphene Oxide Composite and Application for Cobalt(II) Removal" J. Phys. Chem. C., 115, 25234-25240.

[138] Fang, F., Kong, L., Huang, J., Wu, S., Zhang, K., Wang, X., Sun, B., Jin, Z., Wang, J., Huang, X. J., and Liu, J., 2014, "Removal of Cobalt Ions from Aqueous Solution by an Amination Graphene Oxide Nanocomposite" J. Hazard. Mater., 270, 1-10.

[139] Samuel, M. S., Bhattacharya, J., Raj, S., Santhanam, N., Singh, H., and Pradeep Singh, N. D., 2019, "Efficient Removal of Chromium(VI) from Aqueous Solution Using Chitosan Grafted Graphene Oxide (CS-GO) Nanocomposite" Int. J. Biol. Macromol., 121, 285–292.

[140] Yang, S. T., Chang, Y., Wang, H., Liu, G., Chen, S., Wang, Y., Liu, Y., and Cao, A., 2010, "Folding/Aggregation of Graphene Oxide and Its Application in Cu^{2+} removal" J. Colloid Interface Sci., 351, 122-127.

[141] Li, J., Zhang, S., Chen, C., Zhao, G., Yang, X., Li, J., and Wang, X., 2012, "Removal of Cu(II) and Fulvic Acid by Graphene Oxide Nanosheets Decorated with Fe_3O_4 nanoparticles" ACS Appl. Mater. Interfaces., 4, 4991-5000.

[142] Yu, B., Xu, J., Liu, J. H., Yang, S. T., Luo, J., Zhou, Q., Wan, J., Liao, R., Wang, H., and Liu, Y., 2013, "Adsorption Behavior of Copper Ions on Graphene Oxide-Chitosan Aerogel" J. Environ. Chem. Eng., 1, 1044-1050.

[143] Sun, Y., Wang, Q., Chen, C., Tan, X., and Wang, X., 2012, "Interaction between Eu(III) and Graphene Oxide Nanosheets Investigated by Batch and Extended X-Ray Absorption Fine Structure Spectroscopy and by Modeling Techniques" Environ. Sci. Technol., 46, 6020-6027.

[144] Najafi, F., Moradi, O., Rajabi, M., Asif, M., Tyagi, I., Agarwal, S., and Gupta, V. K., 2015, "Thermodynamics of the Adsorption of Nickel Ions from Aqueous Phase Using Graphene Oxide and Glycine Functionalized Graphene Oxide" J. Mol. Liq., 208, 106-113.

[145] Yari, M., Rajabi, M., Moradi, O., Yari, A., Asif, M., Agarwal, S., and Gupta, V. K., 2015, "Kinetics of the Adsorption of Pb(II) Ions from Aqueous Solutions by Graphene Oxide and

Thiol Functionalized Graphene Oxide" J. Mol. Liq., 209, 50-57.

[146] Yang, Y., Xie, Y., Pang, L., Li, M., Song, X., Wen, J., and Zhao, H., 2013, "Preparation of Reduced Graphene Oxide/Poly(Acrylamide) Nanocomposite and Its Adsorption of Pb(II) and Methylene Blue" Langmuir, 29, 10727-10736.

[147] He, Y. Q., Zhang, N. N., and Wang, X. D., 2011, "Adsorption of Graphene Oxide/Chitosan Porous Materials for Metal Ions" Chinese Chem. Lett., 22, 859-862.

[148] Hao, L., Song, H., Zhang, L., Wan, X., Tang, Y., and Lv, Y., 2012, "SiO_2/Graphene Composite for Highly Selective Adsorption of Pb(II) Ion" J. Colloid Interface Sci., 369, 981-1014.

[149] Fan, L., Luo, C., Sun, M., Li, X., and Qiu, H., 2013, "Highly Selective Adsorption of Lead Ions by Water-Dispersible Magnetic Chitosan/Graphene Oxide Composites" Colloids Surfaces B Biointerfaces., 103, 523-529.

[150] Zhang, N., Qiu, H., Si, Y., Wang, W., and Gao, J., 2011, "Fabrication of Highly Porous Biodegradable Monoliths Strengthened by Graphene Oxide and Their Adsorption of Metal Ions," Carbon, 49, 827–837.

[151] Xu, Z., Zhang, Y., Qian, X., Shi, J., Chen, L., Li, B., Niu, J., and Liu, L., 2014, "One Step Synthesis of Polyacrylamide Functionalized Graphene and Its Application in Pb(II) Removal" Appl. Surf. Sci., 316, 308-314.

[152] Zhao, G., Wen, T., Yang, X., Yang, S., Liao, J., Hu, J., Shao, D., and Wang, X., 2012, "Preconcentration of U(vi) Ions on Few-Layered Graphene Oxide Nanosheets from Aqueous Solutions" Dalt. Trans., 41, 6182-6188.

[153] Li, Z., Chen, F., Yuan, L., Liu, Y., Zhao, Y., Chai, Z., and Shi, W., 2012, "Uranium(VI) Adsorption on Graphene Oxide Nanosheets from Aqueous Solutions" Chem. Eng. J., 210, 539-546.

[154] Pan, N., Guan, D., He, T., Wang, R., Wyman, I., Jin, Y., & X., 2013, "Removal of Th^{4+} Ions from Aqueous Solutions by Graphene Oxide" J. Radioanal. Nucl. Chem., 298, 1999–2008.

[155] Li, Y., Du, Q., Liu, T., Peng, X., Wang, J., Sun, J., Wang, Y., Wu, S., Wang, Z., Xia, Y., and Xia, L., 2013, "Comparative Study of Methylene Blue Dye Adsorption onto Activated Carbon, Graphene Oxide, and Carbon Nanotubes" Chem. Eng. Res. Des., 91, 361–368.

[156] Gao, Y., Li, Y., Zhang, L., Huang, H., Hu, J., Shah, S. M., and Su, X., 2012, "Adsorption and Removal of Tetracycline Antibiotics from Aqueous Solution by Graphene Oxide" J. Colloid Interface Sci., 368, 540-546.

[157] Yang, X., Li, J., Wen, T., Ren, X., Huang, Y., and Wang, X., 2013, "Adsorption of Naphthalene and Its Derivatives on Magnetic Graphene Composites and the Mechanism Investigation" Colloids Surfaces A Physicochem. Eng. Asp., 442, 118-125.

[158] Zhang, Y., Cheng, Y., Chen, N., Zhou, Y., Li, B., Gu, W., Shi, X., and Xian, Y., 2014, "Recyclable Removal of Bisphenol A from Aqueous Solution by Reduced Graphene Oxide-Magnetic Nanoparticles: Adsorption and Desorption" J. Colloid Interface Sci., 421, 85-92.

[159] Yao, Y., Miao, S., Yu, S., Ping Ma, L., Sun, H., and Wang, S., 2012, "Fabrication of Fe_3O_4/SiO_2core/Shell Nanoparticles Attached to Graphene Oxide and Its Use as an Adsorbent" J. Colloid Interface Sci., 379, 20–26.

[160] Ma, T., Chang, P. R., Zheng, P., Zhao, F., and Ma, X., 2014, "Fabrication of Ultra-Light Graphene-Based Gels and Their Adsorption of Methylene Blue" Chem. Eng. J., 240, 595-600.

[161] Fan, L., Luo, C., Sun, M., Li, X., Lu, F., and Qiu, H., 2012, "Preparation of Novel Magnetic Chitosan/Graphene Oxide Composite as Effective Adsorbents toward Methylene Blue" Bioresour. Technol., 114, 703-706.

[162] Fan, L., Luo, C., Sun, M., Qiu, H., and Li, X., 2013, "Synthesis of Magnetic β-Cyclodextrin-Chitosan/Graphene Oxide as Nanoadsorbent and Its Application in Dye Adsorption and Removal" Colloids Surf B Biointerfaces., 103, 601–607.

[163] Li, Y., Du, Q., Liu, T., Sun, J., Wang, Y., Wu, S., Wang, Z., Xia, Y., and Xia, L., 2013, "Methylene Blue Adsorption on Graphene Oxide/Calcium Alginate Composites" Carbohydr. Polym., 95, 501-507.

[164] Zhang, C., Wu, L., Cai, D., Zhang, C., Wang, N., Zhang, J., and Wu, Z., 2013, "Adsorption of Polycyclic Aromatic Hydrocarbons (Fluoranthene and Anthracenemethanol) by Functional Graphene Oxide and Removal by PH and Temperature-Sensitive Coagulation" ACS Appl. Mater. Interfaces., 5, 4783-4790.

[165] Dong, Z., Wang, D., Liu, X., Pei, X., Chen, L., and Jin, J., 2014, "Bio-Inspired Surface-Functionalization of Graphene Oxide for the Adsorption of Organic Dyes and Heavy Metal Ions with a Superhigh Capacity" J. Mater. Chem. A., 2, 5034-5040.

[166] Chowdhury, R., Adhikari, S., Rees, P., Wilks, S. P., and Scarpa, F., 2011, "Graphene-Based Biosensor Using Transport Properties" Phys. Rev. B - Condens. Matter Mater. Phys., 83, 7322-7340.

[167] Sabzevari, M., Cree, D. E., and Wilson, L. D., 2018, "Graphene Oxide–Chitosan Composite Material for Treatment of a Model Dye Effluent" ACS Omega, 3, 13045–13054.

[168] Dreyer, D. R., Todd, A. D., and Bielawski, C. W., 2014, "Harnessing the Chemistry of Graphene Oxide" Chem. Soc. Rev., 43, 5288–5301.

[169] Li, J., Zeng, X., Ren, T., and van der Heide, E., 2014, "The Preparation of Graphene Oxide and Its Derivatives and Their Application in Bio-Tribological Systems" Lubricants., 2, 137-161.

[170] Liu, Z. B., Xu, Y. F., Zhang, X. Y., Zhang, X. L., Chen, Y. S., and Tian, J. G., 2009, "Porphyrin and Fullerene Covalently Functionalized Graphene Hybrid Materials with Large Nonlinear Optical Properties" J. Phys. Chem. B., 113, 9681-9686.

[171] Fan, Z., Wang, K., Wei, T., Yan, J., Song, L., and Shao, B., 2010, "An Environmentally Friendly and Efficient Route for the Reduction of Graphene Oxide by Aluminum Powder" Carbon., 48, 1686–1689.

[172] Park, S., Dikin, D. A., Nguyen, S. T., and Ruoff, R. S., 2009, "Graphene Oxide Sheets Chemically Cross-Linked by Polyallylamine" J. Phys. Chem. C., 113, 15801–15804.

[173] Fan, Z., Wang, K., Wei, T., Yan, J., Song, L., and Shao, B., 2010, "An Environmentally

Friendly and Efficient Route for the Reduction of Graphene Oxide by Aluminum Powder" Carbon., 48, 1686–1689.

[174] An, Z., Compton, O. C., Putz, K. W., Brinson, L. C., and Nguyen, S. T., 2011, "Bio-Inspired Borate Cross-Linking in Ultra-Stiff Graphene Oxide Thin Films" Adv. Mater., 23, 3842-3846.

[175] Huang, T., Zhang, L., Chen, H., and Gao, C., 2015, "A Cross-Linking Graphene Oxide-Polyethyleneimine Hybrid Film Containing Ciprofloxacin: One-Step Preparation, Controlled Drug Release and Antibacterial Performance" J. Mater. Chem. B., 3, 1605-1611.

[176] Zhang, P., Gong, J. L., Zeng, G. M., Deng, C. H., Yang, H. C., Liu, H. Y., and Huan, S. Y., 2017, "Cross-Linking to Prepare Composite Graphene Oxide-Framework Membranes with High-Flux for Dyes and Heavy Metal Ions Removal" Chem. Eng. J., 322, 657-666.

[177] Kim, S., Lin, X., Ou, R., Liu, H., Zhang, X., Simon, G. P., Easton, C. D., and Wang, H., 2017, "Highly Crosslinked, Chlorine Tolerant Polymer Network Entwined Graphene Oxide Membrane for Water Desalination" J. Mater. Chem. A., 5, 1533-1540.

[178] Bai, H., Li, C., Wang, X., and Shi, G., 2011, "On the Gelation of Graphene Oxide" J. Phys. Chem. C., 115, 5545-5551.

[179] Szabó, T., Szeri, A., and Dékány, I., 2005, "Composite Graphitic Nanolayers Prepared by Self-Assembly between Finely Dispersed Graphite Oxide and a Cationic Polymer" Carbon, 43, 87-94.

[180] Hung, W. S., Tsou, C. H., De Guzman, M., An, Q. F., Liu, Y. L., Zhang, Y. M., Hu, C. C., Lee, K. R., and Lai, J. Y., 2014, "Cross-Linking with Diamine Monomers to Prepare Composite Graphene Oxide-Framework Membranes with Varying d-Spacing" Chem. Mater., 26, 2983–2990.

[181] Qian, Y., Zhou, C., and Huang, A., 2018, "Cross-Linking Modification with Diamine Monomers to Enhance Desalination Performance of Graphene Oxide Membranes" Carbon, 136, 28–37.

[182] Feng, B., Xu, K., and Huang, A., 2016, “Covalent Synthesis of Three-Dimensional Graphene Oxide Framework (GOF) Membrane for Seawater Desalination” Desalination, 394, 123-130.

[183] Hu, K., Gupta, M. K., Kulkarni, D. D., and Tsukruk, V. V., 2013, “Ultra-Robust Graphene Oxide-Silk Fibroin Nanocomposite Membranes” Adv. Mater., 25, 2301-2307.

[184] Goh, K., Setiawan, L., Wei, L., Si, R., Fane, A. G., Wang, R., and Chen, Y., 2015, “Graphene Oxide as Effective Selective Barriers on a Hollow Fiber Membrane for Water Treatment Process” J. Memb. Sci., 474, 244-253.

[185] Hu, M., and Mi, B., 2014, “Layer-by-Layer Assembly of Graphene Oxide Membranes via Electrostatic Interaction” J. Memb. Sci., 469, 80-87.

[186] Chithra, P., Varghese, R., Divya, K. P., and Ajayaghosh, A., 2008, “Solvent-Induced Aggregation and Cation-Controlled Self-Assembly of Tripodal Squaraine Dyes: Optical, Chiroptical and Morphological Properties” Chem. An Asian J., 3, 1365-1373.

[187] Yu, W., Yu, T., and Graham, N., 2017, “Development of a Stable Cation Modified Graphene Oxide Membrane for Water Treatment” 2D Mater., 4, 45006-45020.

[188] Mathesh, M., Liu, J., Nam, N. D., Lam, S. K. H., Zheng, R., Barrow, C. J., and Yang, W., 2013, “Facile Synthesis of Graphene Oxide Hybrids Bridged by Copper Ions for Increased Conductivity” J. Mater. Chem. C., 1, 3084-3090.

[189] Venkatesan, J., and Kim, S. K., 2010, “Chitosan Composites for Bone Tissue Engineering - An Overview” Mar. Drugs., 8, 2252-2266.

[190] Chen, Y., Chen, L., Bai, H., and Li, L., 2013, “Graphene Oxide–chitosan Composite Hydrogels as Broad-Spectrum Adsorbents for Water Purification” J. Mater. Chem. A., 1, 1992–2001.

[191] Liu, Y., Park, M., Shin, H. K., Pant, B., Choi, J., Park, Y. W., Lee, J. Y., Park, S. J., and Kim, H. Y., 2014, “Facile Preparation and Characterization of Poly(Vinyl Alcohol)/Chitosan/Graphene Oxide Biocomposite Nanofibers” J. Ind. Eng. Chem., 20,

4415-4420.

[192] Shamekhi, M. A., Mirzadeh, H., Mahdavi, H., Rabiee, A., Mohebbi-Kalhori, D., and Baghaban Eslaminejad, M., 2019, "Graphene Oxide Containing Chitosan Scaffolds for Cartilage Tissue Engineering" Int. J. Biol. Macromol., 127, 396–405.

[193] Han, D., and Yan, L., 2014, "Supramolecular Hydrogel of Chitosan in the Presence of Graphene Oxide Nanosheets as 2D Cross-Linkers" ACS Sustain. Chem. Eng., 2, 296–300.

[194] Hao, P., Zhao, Z., Leng, Y., Tian, J., Sang, Y., Boughton, R. I., Wong, C. P., Liu, H., and Yang, B., 2015, "Graphene-Based Nitrogen Self-Doped Hierarchical Porous Carbon Aerogels Derived from Chitosan for High Performance Supercapacitors" Nano Energy., 15, 9-23.

[195] Wang, Y., Xia, G., Wu, C., Sun, J., Song, R., and Huang, W., 2015, "Porous Chitosan Doped with Graphene Oxide as Highly Effective Adsorbent for Methyl Orange and Amido Black 10B" Carbohydr. Polym., 115, 686-693.

[196] Travlou, N. A., Kyzas, G. Z., Lazaridis, N. K., and Deliyanni, E. A., 2013, "Graphite Oxide/Chitosan Composite for Reactive Dye Removal" Chem. Eng. J., 217, 256–265.

[197] Kyzas, G. Z., Travlou, N. A., and Deliyanni, E. A., 2014, "The Role of Chitosan as Nanofiller of Graphite Oxide for the Removal of Toxic Mercury Ions" Colloids Surfaces B Biointerfaces., 113, 467-576.

[198] Hegab, H. M., and Zou, L., 2015, "Graphene Oxide-Assisted Membranes: Fabrication and Potential Applications in Desalination and Water Purification" J. Memb. Sci., 484, 95-106.

[199] Sun, P., Zhu, M., Wang, K., Zhong, M., Wei, J., Wu, D., Xu, Z., and Zhu, H., 2013, "Selective Ion Penetration of Graphene Oxide Membranes" ACS Nano, 7, 428–437.

[200] Zhao, X., Su, Y., Liu, Y., Li, Y., and Jiang, Z., 2016, "Free-Standing Graphene Oxide-Palygorskite Nanohybrid Membrane for Oil/Water Separation" ACS Appl. Mater. Interfaces., 8, 8247-8256.

[201] Kim, H. W., Yoon, H. W., Yoon, S.-M., Yoo, B. M., Ahn, B. K., Cho, Y. H., Shin, H. J., Yang, H., Paik, U., Kwon, S., Choi, J.-Y., and Park, H. B., 2013, "Selective Gas Transport through Few-Layered Graphene and Graphene Oxide Membranes" Science, 342, 91–5.

[202] Ma, J., Ping, D., and Dong, X., 2017, "Recent Developments of Graphene Oxide-Based Membranes: A Review" Membranes, 7, 52-81.

[203] He, Y., Wang, J., Zhang, H., Zhang, T., Zhang, B., Cao, S., and Liu, J., 2014, "Polydopamine-Modified Graphene Oxide Nanocomposite Membrane for Proton Exchange Membrane Fuel Cell under Anhydrous Conditions" J. Mater. Chem. A., 2, 9548-9558.

[204] Sarkar, G., Saha, N. R., Roy, I., Bhattacharyya, A., Adhikari, A., Rana, D., Bhowmik, M., Bose, M., Mishra, R., and Chattopadhyay, D., 2016, "Cross-Linked Methyl Cellulose/Graphene Oxide Rate Controlling Membranes for: In Vitro and Ex Vivo Permeation Studies of Diltiazem Hydrochloride" RSC Adv., 6, 36136-16145.

[205] Gharib, A., Fard, L. V., Pesyan, N. N., and Roshani, M., 2015, "A New Application of Nano - Graphene Oxide (NGO) as a Heterogeneous Catalyst in Oxidation of Alcohols Types" Chem. J., 144, 358-361.

[206] Oh, J., Lee, J. H., Koo, J. C., Choi, H. R., Lee, Y., Kim, T., Luong, N. D., and Nam, J. Do, 2010, "Graphene Oxide Porous Paper from Amine-Functionalized Poly (Glycidyl Methacrylate)/Graphene Oxide Core-Shell Microspheres" J. Mater. Chem., 20, 9200-9204.

[207] Lv, S., Zhang, J., Zhu, L., and Jia, C., 2016, "Preparation of Cement Composites with Ordered Microstructures via Doping with Graphene Oxide Nanosheets and an Investigation of Their Strength and Durability" Materials, 9, 924-936.

[208] Dakshinamoorthy, P., and Vaithilingam, S., 2017, "Platinum-Copper Doped Poly(Sulfonyldiphenol/Cyclophosphazene/Benzidine)-Graphene Oxide Composite as an Electrode Material for Single Stack Direct Alcohol Alkaline Fuel Cells" RSC Adv., 7, 34922-34932.

[209] Perumbilavil, S., Sankar, P., Priya Rose, T., and Philip, R., 2015, "White Light Z-Scan Measurements of Ultrafast Optical Nonlinearity in Reduced Graphene Oxide Nanosheets in

the 400-700 Nm Region" Appl. Phys. Lett., 107, 51104-51109.

[210] Jasim, D. A., Lozano, N., and Kostarelos, K., 2016, "Synthesis of Few-Layered, High-Purity Graphene Oxide Sheets from Different Graphite Sources for Biology" 2D Mater., 3, 14006-14023.

[210] Johra, F. T., Lee, J. W., and Jung, W. G., 2014, "Facile and Safe Graphene Preparation on Solution Based Platform" J. Ind. Eng. Chem., 20, 2883-2887.

[211] Wu, T., Wang, X., Qiu, H., Gao, J., Wang, W., and Liu, Y., 2012, "Graphene Oxide Reduced and Modified by Soft Nanoparticles and its Catalysis of the Knoevenagel Condensation" J. Mater. Chem., 22, 4772-4780.

[212] Zhang, C., Chen, M., Xu, X., Zhang, L., Zhang, L., Xia, F., Li, X., Liu, Y., Hu, W., and Gao, J., 2014, "Graphene Oxide Reduced and Modified by Environmentally Friendly Glycylglycine and Its Excellent Catalytic Performance" Nanotechnology, 25, 135707-135719.

[213] Şinoforoğlu, M., Gür, B., Arik, M., Onganer, Y., and Meral, K., 2013, "Graphene Oxide Sheets as a Template for Dye Assembly: Graphene Oxide Sheets Induce H-Aggregates of Pyronin (Y) Dye" RSC Adv., 3, 11832-11838.

[214] Pal, K., Paulson, A. T., and Rousseau, D., 2009, "Biopolymers in Controlled-Release Delivery Systems" Modern Biopolymer Sci., 1, 519-557.

[215] ASTM D5229-14, 2014, Standard Test Method for Moisture Absorption Properties and Equilibrium Conditioning of Polymer Matrix Composite Materials, ASTM International, West Conshohocken, PA.

[216] Wang, X., Jiao, L., Sheng, K., Li, C., Dai, L., and Shi, G., 2013, "Solution-Processable Graphene Nanomeshes with Controlled Pore Structures" Sci. Rep., 3, 1996-2001.

[217] Kipling, J.J. and Wilson, R. B., 1960, "Adsorption of Methylene Blue in the Determination of Surface Areas" J. Appl. Chem.,10, 109–113.

[218] Voudrias, E., Fytianos, K., and Bozani, E., 2002, “Sorption - Desorption Isotherms of Dyes from Aqueous Solutions and Wastewaters with Different Sorbent Materials” Glob. Nest, Int. J., 4, 75-83.

[219] Umemura, Y., Shinohara, E., and Schoonheydt, R. A., 2009, “Preparation of Langmuir-Blodgett Films of Aligned Sepiolite Fibers and Orientation of Methylene Blue Molecules Adsorbed on the Film” Phys. Chem. Chem. Phys., 11, 9804-9810.

[220] ASTM D3860-98, 2014, Standard Practice for Determination of Adsorptive Capacity of Activated Carbon by Aqueous Phase Isotherm Technique, ASTM International, West Conshohocken, PA.

[221] Macedo, J. D. S., Bezerra, N., Almeida, L. E., Fragoso, E., Cestari, A. R., Gimenez, I. D. F., Lênin, N., Carreño, V., and Barreto, L. S., 2006, “Kinetic and Calorimetric Study of the Adsorption of Dyes on Mesoporous Activated Carbon Prepared from Coconut Coir Dust” J. Colloid Interface Sci., 298, 515–522.

[222] Inel, O., and Tumsek, F., 2000, “The Measurement of Surface Areas of Some Silicates by Solution Adsorption” Turkish J. Chem., 24, 9–20.

[223] Mohamed, M. H., and Wilson, L. D., 2015, “Kinetic Uptake Studies of Powdered Materials in Solution” Nanomaterials, 5, 969–980.

[224] Bach, L. G., Van Tran, T., Nguyen, T. D., Van Pham, T., and Do, S. T., 2018, “Enhanced Adsorption of Methylene Blue onto Graphene Oxide-Doped XFe2O4(X = Co, Mn, Ni) Nanocomposites: Kinetic, Isothermal, Thermodynamic and Recyclability Studies” Res. Chem. Intermed., 44, 1661–1687.

[225] Ciesla, J., Sokołowska, Z., Witkowska-Walczak, B., and Skic, K., 2018, “Adsorption of Water Vapour and the Specific Surface Area of Arctic Zone Soils” Int. Agrophysics., 32, 19–27.

[226] Sing, K., 2001, “The Use of Nitrogen Adsorption for the Characterisation of Porous Materials” Colloids Surf A Physicochem Eng Asp., 187, 3-9.

[227] ASTM D1125-14, 2014, Standard Test Methods for Electrical Conductivity and Resistivity of Water, ASTM International, West Conshohocken, PA.

[228] Fisher, R. A., 2006, "Statistical Methods for Research Workers" Genesis Pub. Pvt Ltd

[229] Konkena, B., and Vasudevan, S., 2012, "Understanding Aqueous Dispersibility of Graphene Oxide and Reduced Graphene Oxide through pKa Measurements" J. Phys. Chem. Lett., 3, 867–872.

[230] Sears, K., Dumee, L., Schütz, J., She, M., Huynh, C., Hawkins, S., Duke, M., and Gray, S., 2010, "Recent Developments in Carbon Nanotube Membranes for Water Purification and Gas Separation" Materials, 3, 127–149.

[231] Chen, J.-T., Fu, Y.-J., An, Q.-F., Lo, S.-C., Huang, S.-H., Hung, W.-S., Hu, C.-C., Lee, K.-R., and Lai, J.-Y., 2013, "Tuning Nanostructure of Graphene Oxide/Polyelectrolyte LbL Assemblies by Controlling PH of GO Suspension to Fabricate Transparent and Super Gas Barrier Films" Nanoscale, 5, 9081–8.

[232] Yan, T., Zhang, H., Huang, D., Feng, S., Fujita, M., and Gao, X.-D., 2017, "Chitosan-Functionalized Graphene Oxide as a Potential Immunoadjuvant" Nanomaterials, 7, 59-69.

[233] Emadi, F., Amini, A., Gholami, A., and Ghasemi, Y., 2017, "Functionalized Graphene Oxide with Chitosan for Protein Nanocarriers to Protect against Enzymatic Cleavage and Retain Collagenase Activity" Sci. Rep., 7, 42258-42271.

[234] He, D., Peng, Z., Gong, W., Luo, Y., Zhao, P., and Kong, L., 2015, "Mechanism of a Green Graphene Oxide Reduction with Reusable Potassium Carbonate," RSC Adv., 5, 11966–11972.

[235] Romainor, A. N. B., Chin, S. F., Pang, S. C., and Bilung, L. M., 2014, "Preparation and Characterization of Chitosan Nanoparticles-Doped Cellulose Films with Antimicrobial Property," J. Nanomater., 2014, 130–141.

[236] Mekahlia, S., and Bouzid, B., 2009, "Chitosan-Copper (II) Complex as Antibacterial Agent: Synthesis, Characterization and Coordinating Bond- Activity Correlation Study," Phys.

Procedia, 2, 1045–1053.

[237] Yang, D., Velamakanni, A., Park, S., Stoller, M., Piner, D., Stankovich, S., Jung, I., Field, D., Ventrice, A., Ruoff, S., Bozoklu, G., Ventrice, C., 2009, "Chemical Analysis of Graphene Oxide Films after Heat and Chemical Treatments by X-Ray Photoelectron and Micro-Raman Spectroscopy" Carbon, 47, 145–152.

[238] Wu, J. Bin, Lin, M. L., Cong, X., Liu, H. N., and Tan, P. H., 2018, "Raman Spectroscopy of Graphene-Based Materials and Its Applications in Related Devices," Chem. Soc. Rev., 47, 1822–1873.

[239] Kudin, K. N., Ozbas, B., Schniepp, H. C., Prud'homme, R. K., Aksay, I. A., and Car, R., 2008, "Raman Spectra of Graphite Oxide and Functionalized Graphene Sheets" Nano Lett., 8, 36–41.

[240] Zhao, H., Jiao, T., Zhang, L., Zhou, J., Zhang, Q., Peng, Q., and Yan, X., 2015, "Preparation and Adsorption Capacity Evaluation of Graphene Oxide-Chitosan Composite Hydrogels" Sci. China Mater., 58, 811–818.

[241] Yang S., Xiaosheng T., E. P. and J. X., 2013, "Graphene Oxide Based Fluorescent Nanocomposites for Cellular Imaging" J. Mater. Chem. B, 1, 512–521.

[242] Jiang, Z., Wang, J., Meng, L., Huang, Y., and Liu, L., 2011, "A Highly Efficient Chemical Sensor Material for Ethanol: Al2O3/Graphene Nanocomposites Fabricated from Graphene Oxide" Chem. Commun., 47, 6350-6352.

[243] Omorogie, M. O., Babalola, J. O., Unuabonah, E. I., and Gong, J. R., 2014, "Solid Phase Extraction of Hazardous Metals from Aqua System by Nanoparticle-Modified Agrowaste Composite Adsorbents," J. Environ. Chem. Eng., 2, 675–684.

[244] Lim, B. Y., Poh, C. S., Voon, C. H., and Salmah, H., 2015, "Rheological and Thermal Study of Chitosan Filled Thermoplastic Elastomer Composites," Appl. Mech. Mater., 754, 34–38.

[245] Crini, G., and Badot, P.-M., 2008, "Application of Chitosan, a Natural Aminopolysaccharide, for Dye Removal from Aqueous Solutions by Adsorption Processes

Using Batch Studies: A Review of Recent Literature" Prog. Polym. Sci., 33, 399–447.

[246] Udoetok, I. A., Wilson, L. D., and Headley, J. V, 2018, " 'Pillaring Effects ' in Cross-Linked Cellulose Biopolymers : A Study of Structure and Properties," Int. J. Polym. Sci., 2018, 1-13.

[247] Udoetok, I. A., Dimmick, R. M., Wilson, L. D., and Headley, J. V., 2016, "Adsorption Properties of Cross-Linked Cellulose-Epichlorohydrin Polymers in Aqueous Solution" Carbohydr. Polym., 136, 329-340.

[248] Mohamed, M. H., Udoetok, I. A., Wilson, L. D., and Headley, J. V., 2015, "Fractionation of Carboxylate Anions from Aqueous Solution Using Chitosan Cross-Linked Sorbent Materials" RSC Adv., 5, 82065-82077.

[249] Montes-navajas, P., Asenjo, N. G., and Corma, A., 2013, "Surface Area Measurement of Graphene Oxide in Aqueous Solutions" Langmuir, 29, 13443–13448.

[250] Sing, K. S. W., 1985, "Reporting Physisorption Data for Gas/Solid Systems with Special Reference to the Determination of Surface Area and Porosity (Recommendations 1984)" Pure Appl. Chem., 54, 2201-2218.

[251] Wilson, L. D., Mohamed, M. H., and Headley, J. V., 2011, "Surface Area and Pore Structure Properties of Urethane-Based Copolymers Containing β-Cyclodextrin" J. Colloid Interface Sci., 357, 215-222.

[252] Sint, K., Wang, B., and Kral, P., 2008, "Selective Ion Passage through Functionalized Graphene Nanopores" J. Am. Chem. Soc., 130, 16448–16449.

[253] Nightingale, E. R., 1959, "Phenomenological Theory of Ion Solvation. Effective Radii of Hydrated Ions" J. Phys. Chem., 63, 1381-1387.

[254] Liu, L., Zhang, J., Zhao, J., and Liu, F., 2012, "Mechanical Properties of Graphene Oxides" Nanoscale, 4, 5910–5916.

[255] Abolhassani, M., Griggs, C. S., Gurtowski, L. A., Mattei-Sosa, J. A., Nevins, M., Medina,

V. F., Morgan, T. A., and Greenlee, L. F., 2017, “Scalable Chitosan-Graphene Oxide Membranes: The Effect of GO Size on Properties and Cross-Flow Filtration Performance” ACS Omega, 2, 8751–8759.

[256] Rossignol, N., Vandanjon, L., Jaouen, P., and Quéméneur, F., 1999, “Membrane Technology for the Continuous Separation Microalgae/Culture Medium: Compared Performances of Cross-Flow Microfiltration and Ultrafiltration” Aquac. Eng., 20, 91–208.

[257] Takht Ravanchi, M., Kaghazchi, T., and Kargari, A., 2009, “Application of Membrane Separation Processes in Petrochemical Industry: A Review” Desalination, 235, 199–244.

[258] Choi, J. H., Jegal, J., and Kim, W. N., 2006, “Fabrication and Characterization of Multi-Walled Carbon Nanotubes/Polymer Blend Membranes” J. Memb. Sci., 284, 406–415.

[259] Zhang, X., Xiao, C., Hu, X., and Bai, Q., 2013, “Preparation and Properties of Homogeneous-Reinforced Polyvinylidene Fluoride Hollow Fiber Membrane” Appl. Surf. Sci., 264, 801–810.

[260] Zhu, X., Loo, H. E., and Bai, R., 2013, “A Novel Membrane Showing Both Hydrophilic and Oleophobic Surface Properties and Its Non-Fouling Performances for Potential Water Treatment Applications” J. Memb. Sci., 436, 47–56.

[261] Bui, N. N., and McCutcheon, J. R., 2013, “Hydrophilic Nanofibers as New Supports for Thin Film Composite Membranes for Engineered Osmosis” Environ. Sci. Technol., 47, 1761–1769.

[262] Zhang, S., Fu, F., and Chung, T. S., 2013, “Substrate Modifications and Alcohol Treatment on Thin Film Composite Membranes for Osmotic Power” Chem. Eng. Sci., 87, 40–50.

[263] Wang, R., Shi, L., Tang, C. Y., Chou, S., Qiu, C., and Fane, A. G., 2010, “Characterization of Novel Forward Osmosis Hollow Fiber Membranes” J. Memb. Sci., 355, 158–167.

[264] Qin, J., and Chung, T. S., 1999, “Effect of Dope Flow Rate on the Morphology, Separation Performance, Thermal and Mechanical Properties of Ultrafiltration Hollow Fibre Membranes” J. Memb. Sci., 157, 35–51.

[265] Ma, Y., Shi, F., Zhao, W., Wu, M., Zhang, J., Ma, J., and Gao, C., 2012, "Preparation and Characterization of PSF/Clay Nanocomposite Membranes with LiCl as a Pore Forming Additive" Desalination, 286,131–137.

[266] Boricha, A. G., and Murthy, Z. V. P., 2010, "Preparation of N,O-Carboxymethyl Chitosan/Cellulose Acetate Blend Nanofiltration Membrane and Testing Its Performance in Treating Industrial Wastewater" Chem. Eng. J., 157, 393–400.

[267] Tang, C., Zhang, Q., Wang, K., Fu, Q., and Zhang, C., 2009, "Water Transport Behavior of Chitosan Porous Membranes Containing Multi-Walled Carbon Nanotubes (MWNTs)" J. Memb. Sci., 337, 240–247.

[268] Wang, Z., Yu, H., Xia, J., Zhang, F., Li, F., Xia, Y., and Li, Y., 2012, "Novel GO-Blended PVDF Ultrafiltration Membranes" Desalination, 299, 50–54.

[269] Lee, J., Chae, H. R., Won, Y. J., Lee, K., Lee, C. H., Lee, H. H., Kim, I. C., and Lee, J. min, 2013, "Graphene Oxide Nanoplatelets Composite Membrane with Hydrophilic and Antifouling Properties for Wastewater Treatment" J. Memb. Sci., 448, 223-230.

APPENDIX A

Copyright permissions for the figures presented in chapter 2 and 3.

Copyright Clearance Center

Note: Copyright.com supplies permissions but not the copyrighted content itself.

1 PAYMENT 2 REVIEW 3 CONFIRMATION

Step 3: Order Confirmation

Thank you for your order! A confirmation for your order will be sent to your account email address. If you have questions about your order, you can call us 24 hrs/day, M-F at +1.855.239.3415 Toll Free, or write to us at info@copyright.com. This is not an invoice.

Confirmation Number: 11794542
Order Date: 02/27/2019

If you paid by credit card, your order will be finalized and your card will be charged within 24 hours. If you choose to be invoiced, you can change or cancel your order until the invoice is generated.

Payment Information

Mina Sabzevari
mina.sab@usask.ca
+1 (306) 966-3244
Payment Method: n/a

Order Details

Journal of materials chemistry. A, Materials for energy and sustainability

Order detail ID:	71827928
Order License Id:	4537380509242
ISSN:	2050-7496
Publication Type:	e-Journal
Volume:	
Issue:	
Start page:	
Publisher:	Royal Society of Chemistry
Author/Editor:	Royal Society of Chemistry (Great Britain)

Permission Status: Granted

Permission type: Republish or display content
Type of use: Thesis/Dissertation

Requestor type	Academic institution
Format	Print, Electronic
Portion	chart/graph/table/figure
Number of charts/graphs/tables/figures	1
The requesting person/organization	Mina Sabzevari/University of Saskatchewan
Title or numeric reference of the portion(s)	Fig. 3 IUPAC report (1985) (A) classification of adsorption isotherm
Title of the article or chapter the portion is from	Metal–organic frameworks for the control and management of air quality: advances and future direction

Editor of portion(s)	N/A
Author of portion(s)	Kumar, Pawan, et al.
Volume of serial or monograph	4
Issue, if republishing an article from a serial	2
Page range of portion	345-361
Publication date of portion	2016
Rights for	Main product
Duration of use	Life of current edition
Creation of copies for the disabled	no
With minor editing privileges	no
For distribution to	Worldwide
In the following language(s)	Original language of publication
With incidental promotional use	no
Lifetime unit quantity of new product	Up to 499
Title	PREPARATION AND CHARACTERIZATION OF CROSS-LINKED GRAPHENE OXIDE-BASED COMPOSITES FOR ADSORPTION-BASED APPLICATIONS
Institution name	University of Saskatchewan
Expected presentation date	Mar 2019

Note: This item will be invoiced or charged separately through CCC's **RightsLink** service. More info **$ 0.00**

This is not an invoice.

Copyright Clearance Center

Note: Copyright.com supplies permissions but not the copyrighted content itself.

1 PAYMENT 2 REVIEW 3 CONFIRMATION

Step 3: Order Confirmation

Thank you for your order! A confirmation for your order will be sent to your account email address. If you have questions about your order, you can call us 24 hrs/day, M-F at +1.855.239.3415 Toll Free, or write to us at info@copyright.com. This is not an invoice.

Confirmation Number: 11794553
Order Date: 02/27/2019

If you paid by credit card, your order will be finalized and your card will be charged within 24 hours. If you choose to be invoiced, you can change or cancel your order until the invoice is generated.

Payment Information

Mina Sabzevari
mina.sab@usask.ca
+1 (306) 966-3244
Payment Method: n/a

Order Details

Nature chemistry

Order detail ID:	71827997
Order License Id:	4537391450503
ISSN:	1755-4349
Publication Type:	e-Journal
Volume:	
Issue:	
Start page:	
Publisher:	Nature Publishing Group
Author/Editor:	Nature Publishing Group

Permission Status: Granted

Permission type: Republish or display content
Type of use: Thesis/Dissertation

Requestor type	Academic institution
Format	Print, Electronic
Portion	chart/graph/table/figure
Number of charts/graphs/tables/figures	1
The requesting person/organization	Mina Sabzevari/University of Saskatchewan
Title or numeric reference of the portion(s)	Figure 1 AFM image and structural model of the graphite oxide (GO) sheets
Title of the article or chapter the portion is from	New insights into the structure and reduction of graphite oxide
Editor of portion(s)	N/A

Author of portion(s)	Gao, Wei, et al.
Volume of serial or monograph	1
Issue, if republishing an article from a serial	5
Page range of portion	403-409
Publication date of portion	2009
Rights for	Main product
Duration of use	Life of current edition
Creation of copies for the disabled	no
With minor editing privileges	no
For distribution to	Worldwide
In the following language(s)	Original language of publication
With incidental promotional use	no
Lifetime unit quantity of new product	Up to 499
Title	PREPARATION AND CHARACTERIZATION OF CROSS-LINKED GRAPHENE OXIDE-BASED COMPOSITES FOR ADSORPTION-BASED APPLICATIONS
Institution name	University of Saskatchewan
Expected presentation date	Mar 2019

Note: This item will be invoiced or charged separately through CCC's **RightsLink** service. More info **$ 0.00**

This is not an invoice.

Total order items: 1 **Order Total: 0.00 USD**

Copyright Clearance Center

Note: Copyright.com supplies permissions but not the copyrighted content itself.

1 PAYMENT 2 REVIEW 3 CONFIRMATION

Step 3: Order Confirmation

Thank you for your order! A confirmation for your order will be sent to your account email address. If you have questions about your order, you can call us 24 hrs/day, M-F at +1.855.239.3415 Toll Free, or write to us at info@copyright.com. This is not an invoice.

Confirmation Number: 11794554
Order Date: 02/27/2019

If you paid by credit card, your order will be finalized and your card will be charged within 24 hours. If you choose to be invoiced, you can change or cancel your order until the invoice is generated.

Payment Information

Mina Sabzevari
mina.sab@usask.ca
+1 (306) 966-3244
Payment Method: n/a

Order Details

Science

Order detail ID:	71828004
Order License Id:	4537400435262
ISSN:	1095-9203
Publication Type:	e-Journal
Volume:	
Issue:	
Start page:	
Publisher:	AMERICAN ASSOCIATION FOR THE ADVANCEMENT OF SCIENCE
Author/Editor:	American Association for the Advancement of Science

Permission Status: Granted

Permission type:	Republish or display content
Type of use:	Republish in a thesis/dissertation
Requestor type	Academic institution
Format	Print, Electronic
Portion	chart/graph/table/figure
Number of charts/graphs/tables/figures	1
The requesting person/organization	Mina Sabzevari/University of Saskatchewan
Title or numeric reference of the portion(s)	Fig. 1. Schematic view for possible permeation through the laminates. Typical L/d is ~1000.
Title of the article or chapter the portion is from	Unimpeded Permeation of Water Through Helium-Leak–Tight Graphene-Based Membranes

Editor of portion(s)	N/A
Author of portion(s)	Nair, R. R., et al.
Volume of serial or monograph	335
Issue, if republishing an article from a serial	6067
Page range of portion	442-444
Publication date of portion	2012
Rights for	Main product
Duration of use	Life of current edition
Creation of copies for the disabled	no
With minor editing privileges	no
For distribution to	Worldwide
In the following language(s)	Original language of publication
With incidental promotional use	no
Lifetime unit quantity of new product	Up to 499
Title	PREPARATION AND CHARACTERIZATION OF CROSS-LINKED GRAPHENE OXIDE-BASED COMPOSITES FOR ADSORPTION-BASED APPLICATIONS
Institution name	University of Saskatchewan
Expected presentation date	Mar 2019

Note: This item will be invoiced or charged separately through CCC's **RightsLink** service. More info **$ 0.00**

This is not an invoice.

Copyright Clearance Center

Note: Copyright.com supplies permissions but not the copyrighted content itself.

1 PAYMENT 2 REVIEW 3 CONFIRMATION

Step 3: Order Confirmation

Thank you for your order! A confirmation for your order will be sent to your account email address. If you have questions about your order, you can call us 24 hrs/day, M-F at +1.855.239.3415 Toll Free, or write to us at info@copyright.com. This is not an invoice.

Confirmation Number: 11794564
Order Date: 02/28/2019

If you paid by credit card, your order will be finalized and your card will be charged within 24 hours. If you choose to be invoiced, you can change or cancel your order until the invoice is generated.

Payment Information

Mina Sabzevari
mina.sab@usask.ca
+1 (306) 966-3244
Payment Method: n/a

Order Details

Journal of molecular liquids

Order detail ID:	71828058
Order License Id:	4537431179872
ISSN:	0167-7322
Publication Type:	Journal
Volume:	
Issue:	
Start page:	
Publisher:	ELSEVIER BV

Permission Status: Granted

Permission type: Republish or display content
Type of use: Thesis/Dissertation

Requestor type	Academic institution
Format	Print, Electronic
Portion	chart/graph/table/figure
Number of charts/graphs/tables/figures	1
The requesting person/organization	Mina Sabzevari/University of Saskatchewan
Title or numeric reference of the portion(s)	Fig. 3. Structure of GO (a) and its interaction with heavy metal cations (b).
Title of the article or chapter the portion is from	A review on heavy metal ions adsorption from water by graphene oxide and its composites

Editor of portion(s)	N/A
Author of portion(s)	Peng, Weijun, et al.
Volume of serial or monograph	230
Page range of portion	96-504
Publication date of portion	2017
Rights for	Main product
Duration of use	Life of current edition
Creation of copies for the disabled	no
With minor editing privileges	no
For distribution to	Worldwide
In the following language(s)	Original language of publication
With incidental promotional use	no
Lifetime unit quantity of new product	Up to 499
Title	PREPARATION AND CHARACTERIZATION OF CROSS-LINKED GRAPHENE OXIDE-BASED COMPOSITES FOR ADSORPTION-BASED APPLICATIONS
Institution name	University of Saskatchewan
Expected presentation date	Mar 2019

Note: This item will be invoiced or charged separately through CCC's **RightsLink** service. More info **$ 0.00**

This is not an invoice.

Total order items: 1 **Order Total: 0.00 USD**

Copyright Clearance Center

Note: Copyright.com supplies permissions but not the copyrighted content itself.

1 PAYMENT 2 REVIEW 3 CONFIRMATION

Step 3: Order Confirmation

Thank you for your order! A confirmation for your order will be sent to your account email address. If you have questions about your order, you can call us 24 hrs/day, M-F at +1.855.239.3415 Toll Free, or write to us at info@copyright.com. This is not an invoice.

Confirmation Number: 11798923
Order Date: 03/14/2019

If you paid by credit card, your order will be finalized and your card will be charged within 24 hours. If you choose to be invoiced, you can change or cancel your order until the invoice is generated.

Payment Information

Payment Method: n/a

Order Details

Physical chemistry chemical physics : PCCP

Order detail ID:	71852719
Order License Id:	4547830907632
ISSN:	1463-9076
Publication Type:	Journal
Volume:	
Issue:	
Start page:	
Publisher:	ROYAL SOCIETY OF CHEMISTRY
Author/Editor:	Società chimica italiana ; et al

Permission Status: Granted

Permission type: Republish or display content
Type of use: Thesis/Dissertation

Requestor type	Academic institution
Format	Print, Electronic
Portion	chart/graph/table/figure
Number of charts/graphs/tables/figures	1
The requesting person/organization	Mina Sabzevari/University of Saskatchewan
Title or numeric reference of the portion(s)	Fig. 9 Molecular structures of (a) methylene blue cation (MB+)
Title of the article or chapter the portion is from	Preparation of Langmuir–Blodgett films of aligned sepiolite fibers and orientation of methylene blue molecules adsorbed on the film

Editor of portion(s)	N/A
Author of portion(s)	Umemura, Yasushi, Emi Shinohara, and Robert A. Schoonheydt.
Volume of serial or monograph	11
Issue, if republishing an article from a serial	42
Page range of portion	9804-9810
Publication date of portion	2009
Rights for	Main product
Duration of use	Current edition and up to 5 years
Creation of copies for the disabled	no
With minor editing privileges	no
For distribution to	Worldwide
In the following language(s)	Original language of publication
With incidental promotional use	no
Lifetime unit quantity of new product	Up to 499
Title	PREPARATION AND CHARACTERIZATION OF CROSS-LINKED GRAPHENE OXIDE-BASED COMPOSITES FOR ADSORPTION-BASED APPLICATIONS
Institution name	University of Saskatchewan
Expected presentation date	Mar 2019

Note: This item will be invoiced or charged separately through CCC's **RightsLink** service. More info **$ 0.00**

APPENDIX B

ACS Author Choice License terms of use and Elsevier's Author Rights for content presented in chapter 3 and 4.

Standard ACS AuthorChoice/Editors' Choice Usage Agreement

This ACS article is provided to You under the terms of this Standard *ACS AuthorChoice/Editors' Choice* usage agreement between You and the American Chemical Society ("ACS"), a federally-chartered nonprofit located at 1155 16th Street NW, Washington DC 20036. Your access and use of this ACS article means that you have accepted and agreed to the Terms and Conditions of this Agreement. ACS and You are collectively referred to in this Agreement as "the Parties").

1. SCOPE OF GRANT

ACS grants You non-exclusive and nontransferable permission to access and use this ACS article subject to the terms and conditions set forth in this Agreement.

2. PERMITTED USES

a. For non-commercial research and education purposes only, You may access, download, copy, display and redistribute articles as well as adapt, translate, text and data mine content contained in articles, subject to the following conditions:

i. The authors' moral right to the integrity of their work under the Berne Convention (Article 6bis) is not compromised.

ii. Where content in the article is identified as belonging to a third party, it is your responsibility to ensure that any reuse complies with copyright policies of the owner.

iii. Copyright notices or the display of unique Digital Object Identifiers (DOI's), ACS or journal logos, bibliographic (e.g. authors, journal, article title, volume, issue, page numbers) or other references to ACS journal titles, web links, and any other journal-specific "branding" or notices that are included in the article or that are provided by the ACS with instructions that such should accompany its display, should not be removed or tampered with in any way. The display of *ACS AuthorChoice* or *ACS Editors' Choice* articles on non-ACS websites must be accompanied by prominently displayed links to the definitive published versions of those articles on the ACS website.

iv. Any adaptations for non-commercial purposes must prominently link to the definitive published version on the ACS website and prominently display the statement: "This is an unofficial adaptation of an article that appeared in an ACS publication. ACS has not endorsed the content of this adaptation or the context of its use."

v. Any translations for non-commercial purposes, for which a prior translation agreement with ACS has not been established, must prominently link to the definitive published version on the ACS website and prominently display the statement: "This is an unofficial translation of an article that appeared in an ACS publication. ACS has not endorsed the content of this translation or the context of its use."

b. Each time You distribute this ACS article or an adaptation, ACS offers to the recipient a license to this ACS article on the same terms and conditions as the license granted to You under this License.

c. For permission to use ACS copyrighted articles beyond that permitted here, visit: http://pubs.acs.org/copyright/permissions.html

3. PROHIBITED USES

a. Use of this ACS article for commercial purposes is prohibited. Examples of such prohibited commercial purposes include but are not limited to:

i. Copying or downloading of articles, or linking to such postings, for further distribution, sale or licensing, for a fee;

ii. Copying, downloading or posting by a site or service that incorporates advertising with such content;

iii. The inclusion or incorporation of article content in other works or services (other than normal quotations with an appropriate citation) that is then available for sale or licensing, for a fee;

iv. Use of articles or article content (other than normal quotations with appropriate citation) by a for-profit organizations for promotional purposes, whether for a fee or otherwise;

v. Sale of translated versions of the article that have not been authorized by license or other permission from the ACS

4. TERMINATION

ACS reserves the right to limit, suspend, or terminate your access to and use of the ACS Publications Division website and/or all ACS articles immediately upon detecting a breach of this License.

5. COPYRIGHTS; OTHER INTELLECTUAL PROPERTY RIGHTS

6. DISCLAIMER OF WARRANTIES; LIMITATION OF LIABILITY

ACS warrants that it is entitled to grant this Agreement.

EXCEPT AS SET FORTH IN THE PRECEDING SENTENCE, ACS MAKES NO WARRANTY OR REPRESENTATION OF ANY KIND, EXPRESS OR IMPLIED, WITH RESPECT TO THIS ACS ARTICLE INCLUDING, BUT NOT LIMITED TO WARRANTIES AS TO THE ACCURACY OR COMPLETENESS OF THE ACS ARTICLE, ITS QUALITY, ORIGINALITY, SUITABILITY, SEARCHABILITY, OPERATION, PERFORMANCE, COMPLIANCE WITH ANY COMPUTATIONAL PROCESS, MERCHANTABILITY OR FITNESS FOR A PARTICULAR PURPOSE.

ACS SHALL NOT BE LIABLE FOR: EXEMPLARY, SPECIAL, INDIRECT, INCIDENTAL, CONSEQUENTIAL OR OTHER DAMAGES ARISING OUT OF OR IN CONNECTION WITH THE AGREEMENT GRANTED HEREUNDER, THE USE OR INABILITY TO USE ANY ACS PRODUCT, ACS'S PERFORMANCE UNDER THIS AGREEMENT, TERMINATION OF THIS AGREEMENT BY ACS OR THE LOSS OF DATA, BUSINESS OR GOODWILL EVEN IF ACS IS ADVISED OR AWARE OF THE POSSIBILITY OF SUCH DAMAGES. IN NO EVENT SHALL THE TOTAL AGGREGATE LIABILITY OF ACS OUT OF ANY BREACH OR TERMINATION OF THIS AGREEMENT EXCEED THE TOTAL AMOUNT PAID BY YOU TO ACS FOR ACCESS TO THIS ACS ARTICLE FOR THE CURRENT YEAR IN WHICH SUCH CLAIM, LOSS OR DAMAGE OCCURRED, WHETHER IN CONTRACT, TORT OR OTHERWISE, INCLUDING, WITHOUT LIMITATION, DUE TO NEGLIGENCE.

The foregoing limitations and exclusions of certain damages shall apply regardless of the success or effectiveness of other remedies. No claim may be made against ACS unless suit is filed within one (1) year after the event giving rise to the claim.

7. GENERAL

This Agreement sets forth the entire understanding of the Parties. The validity, construction and performance of this Agreement shall be governed by and construed in accordance with the laws of the District of Columbia, USA without reference to its conflicts of laws principles. You acknowledge that the delivery of the ACS article will occur in the District of Columbia, USA. You shall pay any taxes lawfully due from it, other than taxes on ACS's net income, arising out of your use of this ACS article and/or other rights granted under this Agreement. You may not assign or transfer its rights under this Agreement without the express written consent of ACS.

8. ACCEPTANCE

You warrant that You have read, understand, and accept the terms and conditions of this Agreement. ACS reserves the right to modify this Agreement at any time by posting the modified terms and conditions on the ACS Publications Web site. Any use of this ACS article after such posting shall constitute acceptance of the terms and conditions as modified.

Back to ACS Publishing Policies

Posted: 03/06/2014